

© Copyright by Mohammad Sarraf Joshaghani 2014

All Rights Reserved

**TESTING AND MODELING
OF AXIAL AND LATERAL SLIDING AND
MITIGATION OF DEEPWATER OIL PIPELINES**

A Thesis
Presented to
the Faculty of the Department of Civil and Environmental Engineering
Cullen College of Engineering
University of Houston

In Partial Fulfillment
of the Requirements for the Degree of
Master of Science
in Civil Engineering

by
Mohammad Sarraf Josaghani
August 2014

TESTING AND MODELING OF AXIAL AND LATERAL SLIDING AND MITIGATION OF DEEPWATER OIL PIPELINES

Mohammad Sarraf Joshaghani

Approved:

Chairman of the Committee
C. Vipulanandan, Professor,
Civil and Environmental Engineering

Committee Members:

Kalyana Nakshatrala, Assistant Professor,
Civil and Environmental Engineering

Gino J. Lim, Associate Professor,
Industrial Engineering
Department Chair

Suresh K. Khator, Associate Dean,
Cullen College of Engineering

Kaspar Willam, Professor, Interim Chair,
Civil and Environmental Engineering

**TESTING AND MODELING
OF AXIAL AND LATERAL SLIDING AND
MITIGATION OF DEEPWATER OIL PIPELINES**

An Abstract
of a
Thesis
Presented to
the Faculty of the Department of Civil and Environmental Engineering
Cullen College of Engineering
University of Houston

In Partial Fulfillment
of the Requirements for the Degree of
Master of Science
in Civil Engineering

by
Mohammad Sarraf Joshaghani
August 2014

ABSTRACT

During the service life, network of oil and gas pipelines that connect the floating platforms to the subsea wells in deepwater undergo significant changes in temperature and pressure resulting in high shears, strains, and movement. These pipelines laid on the very soft seabed become susceptible to large movement and lateral buckling resulting in global instability of the entire system. Hence it has become critical to address the issues through combined numerical modeling and experimental study of various conditions in the field.

Several full-scale models have been designed and constructed to investigate the behavior of various types of pipes (steel, plastic) on the simulated clayey sea bed (undrained shear strength ranged from 0.01 kPa to 0.11 kPa). Axial and lateral pipe soil interaction characterized and appropriate mitigation solutions proposed. Also the pipe-soil behavior was numerically modeled using the Coupled Eulerian Lagrangian (CEL) and Arbitrary-Lagrangian-Eulerian (ALE) formulations.

TABLE OF CONTENTS

| | Page |
|---|------|
| ABSTRACT | vi |
| TABLE OF CONTENT | vii |
| LIST OF FIGURES | x |
| LIST OF TABLES | xvi |
| CHAPTER 1. INTRODUCTION | 1 |
| 1.2 GENERAL | 1 |
| 1.3 OBJECTIVES | 2 |
| 1.4 ORGANIZATION..... | 2 |
| CHAPTER 2. BACKGROUND AND LITERATURE REVIEW | 5 |
| 2.1 DEEPWATER SITE INVESTIGATION | 5 |
| 2.2 OFFSHORE SOIL SAMPLING | 5 |
| 2.2.1 High Quality Soil Sampling..... | 5 |
| 2.2.2 Offshore seabed soil corer | 7 |
| 2.3 OFFSHORE IN-SITU TESTING | 11 |
| 2.3.1 Piezocone | 13 |
| 2.3.2 Vane | 15 |
| 2.3.3 Full-flow penetrometer | 16 |
| 2.3.4 FUGRO SMARTPIPE® | 18 |
| 2.4 SUBSEA PIPELINE..... | 20 |
| 2.4.1 Plasticity solutions: | 23 |

| | | |
|--|---|-----|
| 2.4.2 | Numerical analysis..... | 25 |
| 2.4.3 | Arbitrary Lagrangian Eulerian (ALE) Formulation..... | 28 |
| 2.4.4 | Experimental Model Tests | 31 |
| 2.4.5 | Design Practice | 36 |
| 2.4.6 | DNV-RP-F105 | 39 |
| 2.4.7 | SAFEHOOK..... | 39 |
| 2.5 | MITIGATION METHODS | 40 |
| 2.5.1 | Axial walking mitigation | 41 |
| 2.5.2 | Lateral Buckling Mitigation..... | 43 |
| CHAPTER 3. MATERIALS AND METHODS | | 46 |
| 3.1 | PREPARATION OF SOIL | 46 |
| 3.2 | EQUIPMENT..... | 47 |
| 3.2.1 | Medium-scale soil box with viewing sides..... | 47 |
| 3.2.2 | Full-scale soil box | 49 |
| 3.2.3 | Soil strength Assessment Tool: Vane shear..... | 54 |
| 3.2.4 | CIGMAT Reflective Gridding and Remote Gridding Systems | 55 |
| 3.3 | MODEL PIPES | 58 |
| 3.4 | SUMMARY..... | 78 |
| CHAPTER 4. AXIAL PIPE SOIL INTERACTION | | 80 |
| 4.1 | EXPERIMENTAL..... | 80 |
| 4.1.1 | Parametric study..... | 80 |
| 4.1.2 | Modeling | 97 |
| 4.2 | FINITE ELEMENT ANALYSIS | 106 |

| | | |
|---|--|------------|
| 4.2.1 | Introduction..... | 106 |
| 4.2.2 | Finite element model..... | 107 |
| 4.2.3 | Finite Element Procedures | 112 |
| 4.2.4 | Parametric study..... | 118 |
| 4.3 | SUMMARY..... | 120 |
| CHAPTER 5. LATERAL PIPE SOIL INTERACTION | | 122 |
| 5.1 | INTRODUCTION | 122 |
| 5.2 | FIX-END AND FREE-END LATERAL LOADING | 122 |
| 5.3 | EFFECT OF PIPELINE MATERIAL..... | 126 |
| 5.4 | SOIL STRENGTH..... | 128 |
| 5.5 | RATE OF LOADING | 131 |
| 5.6 | EFFECT OF PIPE SIZE | 133 |
| 5.7 | INFLUENCED AREA OF SOIL | 134 |
| 5.8 | SUMMARY..... | 136 |
| CHAPTER 6. MITIGATION METHODS | | 137 |
| 6.1 | INTRODUCTION | 137 |
| 6.2 | AXIAL MITIGATION | 139 |
| 6.2.1 | Application of Axial Resistors..... | 139 |
| 6.3 | PRE-SNAKING | 149 |
| 6.4 | LATERAL MITIGATION | 151 |
| 6.4.1 | Application of Buoyancy Sections..... | 151 |
| 6.5 | SUMMARY..... | 160 |

| | |
|--|-----|
| CHAPTER 7. CONCLUSIONS AND RECOMMENDATIONS | 161 |
| REFERENCES | 164 |
| APPENDIX I | 173 |

LIST OF FIGURES

| | |
|---|----|
| Figure 2.1: (a) IOS box corer (double spade), (b) Box corer with single-spade and tripod frame (www.wikipedia.org) | 8 |
| Figure 2.2: Kullenberg type gravity piston corer after triggering at the seabed (Weaver 1990) | 9 |
| Figure 2.3 STARCO® Stationary Piston Corer (Wong 2008) | 10 |
| Figure 2.4: Cone penetrometer measurements including different pore pressure transducer location | 14 |
| Figure 2.5: Vane shear test facility | 15 |
| Figure 2.6 T-Bar, ball penetrometer, 33 cm^2 and 15 cm^2 piezocone penetrometer (Mccorraon 2011) | 17 |
| Figure 2.7 FUGRO SMART PIPE in situ facility (Ballard 2013) | 18 |
| Figure 2.8: Severe mesh distortion by applying pure Lagrangian approach: (a) vertical penetration of pipe in soft soil (b) vertical penetration of rigid footing in a very soft soil (Sarraf, 2013). | 27 |
| Figure 2.9: Application of CEL approach in penetration of subsea pipe in very soft soil (Sarraf, 2013) | 28 |
| Figure 2.10: Applying ALE formulation (a) pipe soil interaction (b) exaggerated foundation soil interaction (M. V. Sarraf 2013). | 29 |
| Figure 2.11: Full scale testing facility at University of Hong Kong..... | 32 |
| Figure 2.12 Centrifuge model test facilities..... | 33 |
| Figure 2.13 General view of soil tank assembled at IPT facilities | 33 |
| Figure 2.14 Details of Testbed within the (Small-Scale) mini-drum centrifuge .. | 34 |

| | |
|--|----|
| Figure 2.15: Medium size soil tank at CiGMAT laboratory..... | 35 |
| Figure 2.16: Full-scale soil tank at CIGMAT facilities | 35 |
| Figure 2.17: Simplified mechanism for lateral pipe soil interaction (DNV-RP-F109) | 38 |
| Figure 2.18: Pipeline networks and associated infrastructure (Randolph, 2011) . | 41 |
| Figure 2.19: Pipeline anchor with stab and hinge over system..... | 42 |
| Figure 2.20 Anchor and chain restraint for pipeline (Prinet 2006)..... | 42 |
| Figure 2.21 Buoyancy Modules used in Canapu Field (sun, 2012)..... | 44 |
| Figure 2.22 Sleeper system | 44 |
| Figure 2.23 snake lay mitigation solution..... | 45 |
| Figure 3.1 Medium-size soil box at CIGMAT laboratory | 48 |
| Figure 3.2 Schematic of the medium-size test setup for axial and lateral displacement study (Vipulanandan, 2013)..... | 49 |
| Figure 3.3 Axial pipe soil interaction testing facility at CIGMAT (Center for Innovative Grouting Materials and Technology)..... | 50 |
| Figure 3.4 Lateral pipe soil interaction testing facility at CIGMAT (Center for Innovative Grouting Materials and Technology)..... | 50 |
| Figure 3.5 Schematic of the axial sliding testing setup | 51 |
| Figure 3.6 Schematic of the lateral loading testing setup | 51 |
| Figure 3.7 Schematic of loading frame in lateral movement..... | 53 |
| Figure 3.8 Loading mechanism in lateral setup | 53 |
| Figure 3.9: Place of vane shear test measurements in the full-scale soil box | 54 |

| | |
|---|----|
| Figure 3.10: Change in gridlines configuration before and after lateral displacement | 55 |
| Figure 3.11: Interpretation of deformed gridline from plan view..... | 56 |
| Figure 4.1: Axial pipe sliding in CIGMAT full scale soil tank | 80 |
| Figure 4.2: Force-displacement responses for steel and plastic pipes | 82 |
| Figure 4.3: Pipe-soil interaction responses for steel and plastic pipes | 82 |
| Figure 4.4: Schematic of soil contact with steel and plastic pipes during axial sliding..... | 83 |
| Figure 4.5: Effect of undrained shear strength on pipe soil interaction..... | 84 |
| Figure 4.6: Axial force-displacement responses for two pipes with different vertical load laid on the same soil..... | 85 |
| Figure 4.7: Effect of vertical force (weight of pipe) on the axial pipe soil interaction | 86 |
| Figure 4.8 Effect of pipe size (diameter) on the axial pipe soil interation..... | 87 |
| Figure 4.9: Schematic of soil deformation path during axial cyclic loading for small ($D=2.4\text{in}$) and large ($D=8.5\text{in}$) pipe | 88 |
| Figure 4.10: Axial force-displacement responses for different rate of loading | 89 |
| Figure 4.11: Effect of rate of loading on axial pipe soil interaction responses | 89 |
| Figure 4.12: Pipeline embedment for the first three axial cycles | 91 |
| Figure 4.13: Axial pipe soil interaction after axial cyclic loading..... | 91 |
| Figure 4.14: Effects of different boundary length was investigated on axial pipe soil interaction responses | 93 |
| Figure 4.15: Effect of boundary length on axial pipe soil interaction | 94 |

| | |
|---|-----|
| Figure 4.16: Excess pore water pressure development during axial loading with different boundary lengths | 95 |
| Figure 4.17: Effect of initial embedment on axial force-displacement responses | 96 |
| Figure 4.18: Horizontal-vertical displacement for pipes with different initial embedment..... | 96 |
| Figure 4.19: Comparison of the measured and predicted breakout resistance calculated from Equation 4.2..... | 98 |
| Figure 4.20: Comparison of the measured and predicted breakout resistance from different projects | 99 |
| Figure 4.21: Comparison of the measured and predicted residual resistance calculated from equation 4-2 | 100 |
| Figure 4.22: Comparison of the measured and predicted residual resistance from different projects | 100 |
| Figure 4.23: The effect of strain rate on vertical penetration of pipe rested on soft soil..... | 109 |
| Figure 4.24: Coupled Eulerian Lagrangian (CEL) model used in ABAQUS.... | 111 |
| Figure 4.25: Arbitrary Lagrangian Eulerian (ALE) mesh configuration used for vertical penetration of pipe in very soft soil | 112 |
| Figure 4.26: Application of geostatic step at ALE analysis..... | 113 |
| Figure 4.27: laboratory tests and finite elements analyses during vertical penetration of plastic pipe on very soft soil | 114 |
| Figure 4.28: Severe mesh distortion by applying Pure Lagrangian approach in vertical penetration of Pipe in soft soil | 115 |

| | |
|--|-----|
| Figure 4.29: ALE approach was employed in vertical penetration of pipe on soft soil..... | 115 |
| Figure 4.30: CEL approach was used in ABAQUS to model vertical penetration of pipe in soft soil | 116 |
| Figure 4.31: New mesh configuration formed for axial pipe sliding..... | 117 |
| Figure 4.32: Axial force displacement responses for pipe sliding on soil with undrained shear strength of 0.11 kPa..... | 117 |
| Figure 4.33: Axial force displacement responses for pipe sliding on soil with undrained shear strength of 0.03 kPa..... | 118 |
| Figure 4.34: Comparison of the breakout resistance calculated from equation 4-2 and from ALE finite element analyses..... | 119 |
| Figure 4.35: Comparison of the residual resistance calculated from equation 4-3 and from ALE finite element analyses..... | 120 |
| Figure 5.1: Specific lateral loading frame was implemented which is capable of controlling pipe ends fixity | 123 |
| Figure 5.2: Primary penetration of plastic pipe after laying | 124 |
| Figure 5.3: Secondary (long-term) penetration of plastic pipe | 124 |
| Figure 5.4: Vertical penetration of plastic pipe during lateral loading for both cases of fixed-end and free-end boundaries..... | 125 |
| Figure 5.5: Effect of boundary condition on lateral pipe soil interaction | 126 |
| Figure 5.6: Effect of pipeline material on lateral pipe soil interaction of plastic pipe..... | 127 |

| | |
|--|-------|
| Figure 5.7: Vertical penetration of plastic pipe during lateral loading with free-end | 129 |
| | |
| Figure 5.8: Vertical penetration of plastic pipe during lateral loading with fixed-... | |
| end boundaries | 129 |
| Figure 5.9 : Effect soil shear strength on lateral pipe soil interaction with free end | |
| boundaries | 130 |
| Figure 5.10: Effect of soil shear strength on lateral pipe soil interaction with fixed | |
| end boundaries | 131 |
| Figure 5.11: Effect of rate of loading on lateral pipe soil interaction with free end | |
| boundaries | 132 |
| Figure 5.12: Variation of excess pore water pressure during lateral movement | |
| with different rate of loading | 133 |
| Figure 5.13: Effect of pipe size on lateral pipe soil interaction with free end | |
| boundaries | 134 |
| Figure 5.14: Gradual increase in the area of influenced (disturbed) soil during | |
| lateral loading of pipe | 136 |
| Figure 6.1: Effective axial force for a range of friction in a straight pipeline | |
| (Burton,2008)..... | 138 |
| Figure 6.2: Effective axial force in a short pipeline with lateral buckles (Burton, | |
| 2008)..... | 139 |
| Figure 6.3: Axial mitigation methods in medium-sized soil box..... | 141 |
| Figure 6.4: Single-resistor mitigation for the first cycle the axial sliding | 143 |
| Figure 6.5: Single resistor mitigation method was tested in full-scale soil box . | 143 |

| | |
|--|-----|
| Figure 6.6: Double resistors mitigation method was tested in full-scale soil box | 144 |
| Figure 6.7: Effect of different axial mitigations on normalized force-displacement responses | 147 |
| Figure 6.8: Normalized force-displacement responses for different type of double resistors during axial sliding | 148 |
| Figure 6.9: Comparison in axial responses of pre-snaked (Snaked Lay) and straight pipe (small pipe) | 150 |
| Figure 6.10: Comparison in axial responses of pre-snaked (Snaked Lay) and straight pipe (big pipe) | 151 |
| Figure 6.11: Pipe equipped with single buoyancy section tested in medium-sized soil box..... | 152 |
| Figure 6.12: Application of buoyancy section significantly decreased lateral resistance..... | 154 |
| Figure 6.13: Lateral movement of plastic in full-scale soil box: (a) no mitigation, (b) single buoyancy section | 155 |
| Figure 6.14: Effect of single buoyancy section in lateral pipe soil interaction... | 155 |
| Figure 6.15: Lateral buoyancy sections were tested in full-scale soil box for cases of fixed and rolling sections..... | 156 |
| Figure 6.16: Effect of fixed and rolling buoyancy sections on the lateral pipe soil . interaction | 157 |
| Figure 6.17: Separated buoyancy sections was modeled using finite element analysis..... | 158 |

Figure 6.18: Lateral responses of a pipe employed rolling buoyancy sections .. 159

Figure 6.19: Lateral responses of a pipe employed fixed buoyancy sections..... 159

LIST OF TABLES

| | |
|--|----|
| Table 2.1: Testing standards for the field vane shear test..... | 16 |
| Table 2.2: Offshore in situ testing..... | 19 |
| Table 3.1: RGS was utilized to investigate berm formation during axial movement of pipe and the grids were transferred to mathematical coordinates. The gridlines are differentiated from the rest of photo by broken lines..... | 57 |
| Table 3.2 Summary of Pipe Models | 59 |
| Table 3.3 Details of Slim Axial Pipe | 60 |
| Table 3.4 Details of Short Axial Pipe | 61 |
| Table 3.5: Details of Frequent PVC Pipe..... | 62 |
| Table 3.6 Details of Frequent Large PVC Pipe | 63 |
| Table 3.7 Details of Frequent Metal Pipe | 64 |
| Table 3.8 Details of Perforated Axial Resistors..... | 65 |
| Table 3.9 Details of Single Axial Resistors | 66 |
| Table 3.10 Details of Double Axial Resistors | 67 |
| Table 3.11 Details of Short Axial Resistors..... | 68 |
| Table 3.12 Details of Double Axial Resistors with Compressive Springs | 69 |
| Table 3.13 Details of Double Axial Resistors with Tensile Springs | 70 |
| Table 3.14 Details of pipe anchored to other pipe | 71 |
| Table 3.15 Details of Separated Buoyancy Sections | 72 |
| Table 3.16 Details of Global Buoyancy Sections | 73 |

| | |
|---|-----|
| Table 3.17 Details of Short Buoyancy Sections | 74 |
| Table 3.18 Details of Single Buoyancy Sections..... | 75 |
| Table 3.19 Details of Medium Snake Lay Pipe | 76 |
| Table 3.20 Details of Slight Snake Lay | 77 |
| Table 3.21 Details of Severe Snake Lay | 78 |
| Table 4.1: Axial force-displacement responses for the first three cycles | 92 |
| Table 4.2: Original model normalized stress-strain relationship prediction..... | 103 |
| Table 4.3 : Parameter chosen for ALE analysis..... | 119 |
| Table 5.1: Surface displacement of Soil particles during cyclic lateral loading. | 135 |
| Table 6.1: Axial mitigation solutions tested in medium-sized soil box..... | 141 |
| Table 6.2: Normalized force-displacement responses for the first three cycles of axial sliding when double resistors mitigation was employed..... | 145 |
| Table 6.3: Types of double resistors | 148 |
| Table 6.4: snaked lay (pre-snaked) pipe tested in medium-size soil box | 149 |

Chapter 1. INTRODUCTION

1.2 General

With the expansion of the deeper water oil and gas production, the pipelines needed for the operation represent a significant part of the facility cost. Deepwater pipelines laid on the seabed, partially penetrate into the soil based on the submerged self-weight of the pipelines and strength of the seabed soil. During operations these pipes are required to operate at high cycling temperature and pressure conditions causing axial and lateral movements in the pipes which in turn produce high stresses and finally result in local and global buckling. The axial and lateral resistance of the pipes partially embedded in a very soft soil for undrained shear strength ranging from 0.01 kPa to 0.2 kPa is not well understood. The complexity of the issues posed by the High Pressure/ High Temperature (HP/HT) condition is much greater with increase in water depth. In deep water, where severe conditions lead to changes in product dynamics, changing temperature and maintaining flow make pipeline design very complex. Hence it has become critical to address the issues through advanced engineering and research with experimental and numerical study of various conditions in the field.

In this research, we have performed large-scale experiments as well as numerical modeling. Several full-scale models have been designed and constructed to investigate the behavior of various types of pipes (steel, plastic) on the simulated clayey sea bed (undrained shear strength ranged from 0.01 kPa to 0.2 kPa). Axial and lateral pipe soil interactions have been characterized, and appropriate mitigation solutions for axial walking and lateral buckling have been proposed.

On the numerical modeling front, the pipe-soil behavior is simulated using the Coupled Eulerian Lagrangian (CEL) and Arbitrary-Lagrangian-Eulerian (ALE) formulations. First, FEM

models were developed in python syntax and different user-defined subroutines such as UMAT (to define material properties), SIGINI (to define initial stress field), DISP (to define prescribed boundary condition), DLOAD (to define non-uniform distributed loads) and UPOREP (to define initial pore pressure) programed in FORTRAN. Finally, the python scripts and FORTRAN subroutines combined and executed in ABAQUS/CAE for different cases.

1.3 Objectives

1. Develop an authentic full scale model test to study the behavior of plastic and metal pipe on simulated seabed.
2. Advice a remote photogrammetry system to study soil displacement field and trace possible berms formation at vicinity of pipe.
3. Perform parametric study on the axial and lateral pipe soil interaction, considering the effect of pipeline material, rate of loading, initial embedment; boundary length and soil shear strength.
4. Propose new axial and lateral mitigation methods to stop pipeline walking and lateral buckling.
5. Determine axial force displacement responses using different large displacement finite element model.

1.4 Organization

Chapter 1 is an introductory chapter outlining the motivation for the research and chapter 2 provides a review of current literature in the pipe soil interaction. In Chapter 3 experimental methodology including test protocol, soil preparation, soil boxes' instrumentation, sensors' installation, camera correlation, Remote Gridding System and photogrammetry techniques are explained.

Chapter 4 starts with parametric study based on 35 cyclic axial sliding laboratory tests. Based on these tests, 9 sets of equations for axial sliding resistance, breakout resistance and steady-state resistance of plastic pipe proposed which incorporate the effects of soil strength, loading rate, initial penetration, pipe weight and pipe size. Different boundary conditions imposed to our tests and the effects of boundary conditions on excess pore pressure development and pipe soil interaction studied. In the numerical side, pipe-soil interaction during vertical embedment and then axial sliding for 66 different cases of pipelines on the seabed was studied using simple Tresca soil model which was modified to incorporate the effect of strain rate. Both vertical penetration and axial sliding are modeled using Coupled Eulerian Lagrangian (CEL) and approach Arbitrary Lagrangian Eulerian (ALE) approach. The large deformation finite element method is validated by comparing the results with data from our full scale model test.

Chapter 5 contains a study based on 42 partially embedded pipe soil interaction tests which incorporates the effects of soil strength, loading rate, initial penetration, pipe weight and pipe size on the lateral resistance. In order to capture the displacement of soil particles and berms during lateral movement, a couple of photogrammetry techniques applied.

Chapter 6 was focused on investigating and quantifying the effects of various mitigation methods on axial and lateral pipe soil interaction. Mitigation methods studied in this chapter include resistors, pre-snaking and parallel anchoring for axial sliding and buoyancy sections for lateral movements. In lateral mitigation the objective is set to initiate global Flowlines buckling in a controlled manner so to release the effective axial load and to avoid the excessive expansion and pipe bending at other locations. Recommendations are given in term of application of resistors and buoyancy sections for different pipeline design and installation conditions. In the numerical front, the effect of fixed and rolling buoyancy sections were investigated on lateral

force (resistance) and displacement responses using Coupled Eulerian Lagrangian (CEL) approach. In the last chapter, concluding remarks based on the research in this thesis are presented.

Chapter 2. BACKGROUND AND LITERATURE REVIEW

2.1 Deepwater Site Investigation

The design of subsea pipeline similar to floating structures, anchoring systems and offshore foundations requires geotechnical design parameters for soil at depths ranging from right below the pipe invert to a few meters below the seabed. These design parameters are commonly collected by implementing laboratory test on soil samples recovered from the seabed and by in-situ tests such as vane shear test and cone penetrometer test.

In the following section, the existing offshore soil sampling techniques and in-situ testing for soil characterization at deepwater is reviewed. The offshore design is dominated by assessment of capacity or ultimate limit state, rather than deformations and serviceability. Therefore, the review will mainly focus on the current techniques for determining shear strength of soft seabed sediments commonplace in deepwater sites.

2.2 Offshore soil sampling

2.2.1 High Quality Soil Sampling

Soil samples collected from the seabed should have contained high quality with acceptable mechanical sampling disturbance that preserves the in-situ stratigraphy. Minimum disturbance is of high importance for geotechnical characterization of seabed soil properties and maintaining the sample stratigraphy is important for oceanography and sedimentology studies. All such information is important for economic and safe geotechnical design of offshore facilities and for assessment of geohazard that may lead to damage of offshore infrastructures (Hossain, 2008).

In the recent years, substantial studies have been performed to better understand and identify sources and factors that incorporate to sample disturbance and its induced effect on the measured engineering properties and behaviors of normally consolidated fine-grained soils. All of these studies have been performed on onshore sites and sampling techniques proposed by Lune (2006) and Long (2009) on Norwegian clay; Hieght (1992) on Bothkennar clay and Long (2006) Irish varied clay. Based on the understanding gained from these studies, Lunne (2007) concluded that sample disturbance in offshore sampling may be caused by:

1. Stress relief when the soil sample is removed from the seabed.
2. Extrusion.
3. Mechanical disturbance due to sampling tube and retrieval.
4. Techniques used to retrieve sample onto the ship deck.
5. Transportation
6. Sample storage environment
7. Specimen preparation for laboratory testing

In normally consolidated highly plastic clays, sample disturbance causes a reduction in the measured peak shear strength, pre-failure stiffness, yield stress and compression index, yet causes an increase in the measured strain to recompression index. Briefly, application of low quality soil samples for laboratory tests would give misleading results that are in big difference from real in situ behavior. The discrepancy in the measured behavior is a function of stress history, gas concentration in solution and plasticity (i.e., soil composition) of the soil, the sampling method and equipment, and the sample handling procedure (High, 2001). In any study based on mere laboratory tests, the soil parameters determined from soil samples could lead to

conservative or expensive design of subsea pipeline. This issue could be effectively addressed by introducing realistic disturbance factors.

2.2.2 Offshore seabed soil corer

The offshore seabed soil corer was first introduced in 1960's. Since then they have been widely used by the oceanographic community to recover soil samples from the seabed for marine geological studies. Researches performed by Silva (2000) and Young (2000) evaluated soil corer performance in recovering soil samples of sufficient quality and quantity for geotechnical characterization.

This section summarizes a review of the performance of various long seabed cores commonly used to recover soft soil samples from deepwater sites for geotechnical studies and recent developments of new seabed corers (Hossain, 2008).

2.2.2.1 Box Corer

Box corers have been used to provide a simple means of recovering high quality very soft soil for the upper 0.5 m of the seabed. The box corer normally consists of a square box with a cross-sectional area up to 0.25 m^2 and with a length generally less than 1.2 m (Weaver, 1990).

In order to collect a soil sample from the seabed, the box corer is either penetrated into seabed under its own weight and dynamic force or is pushed into the seabed using seabed frame. Prior to pull out, the bottom part of corer is locked by single or double spade lever arm system. The top of the box corer is usually closed to ensure an undisturbed sediment-water interface. The quality of the measured geotechnical properties in a box core was found generally precise than those measured in a gravity core at a very shallow depths. Hence, It is highly reported that, for accurate geotechnical characterization of near seabed sediments (upper 0.5 to 1 of the seabed), the box corer is the best available option (Randolph, 2007).

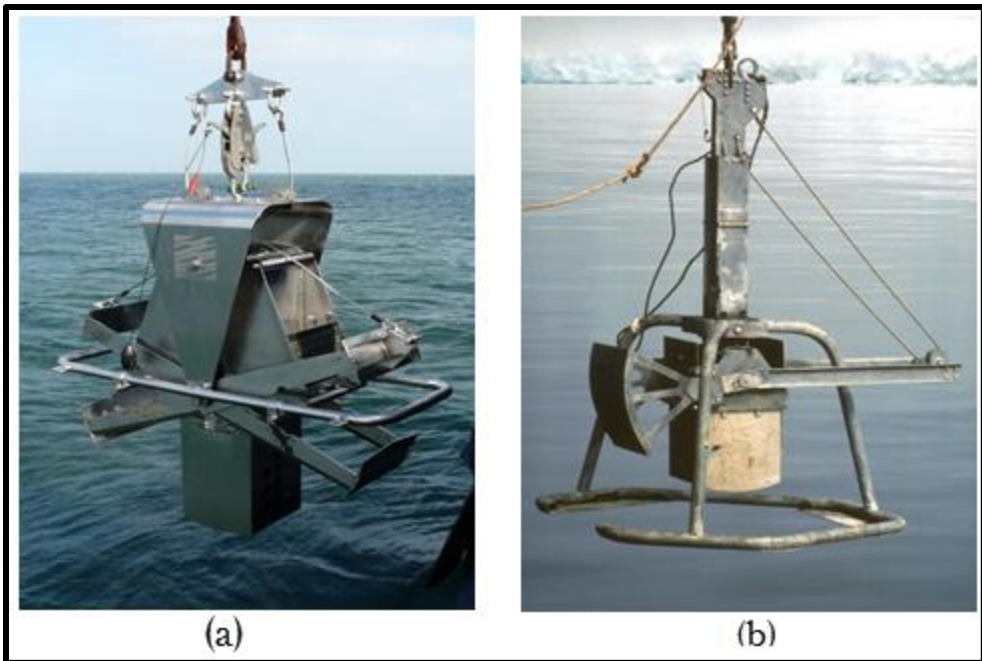


Figure 2.1: (a) IOS box corer (double spade), (b) Box corer with single-spade and tripod frame (www.wikipedia.org)

2.2.2.2 Open-Drive Gravity Corer

The open-drive gravity corer is one of the simplest and less expensive samplers that could be implemented to collect long soil samples from the seabed. It consists of a large head weight, which is attached to a core barrel at one end and a cable at the other end. A core cutter and a core catcher are attached at the lower end of the core barrel. The cross section of the core barrel can be either circular or square. A suction ball valve is occasionally fitted at the upper end of the core barrel to prevent the wash out of soil sample during recovery. The Open-drive Gravity corer as the name suggests is normally penetrated into seabed under its self-weight in presence of dynamic forces. One major disadvantage of this sampler is the recovery ratio of less than 70%, due to sediment plugging in the barrel during coring process (Parker, 1990). The recovery ratio is defined as the ratio of the length of the recovered sample to the core barrel penetration depth.

2.2.2.3 Kullenberg Type Gravity Piston Corer

The Kullenburge sampler was provided in order to resolve the low recovery ratio limitation which was the main drawback of previous samplers. The major difference of Kullenberg sampler is that the lower end of the core barrel is enclosed by a piston until penetration starts within the soil, after which the piston is supposed to remain at a fixed elevation while the corer embeds into seabed. The piston is connected directly to the main cable (Weaver, 1990). This sampler is capable of recovering soil up to the depth of 20 m. The major problems of Kullenberg corer is fluctuation of the piston cavity pressure within the corer (due to the possibility of improper placement of the piston at the initiation of sampling, incoherent movement of the piston during coring due to wire rebound, and upward movement of the piston during retrieval of the corer (Buckley, 1994).The experience of modified Kullenburge Samplers such as GPC and JPC for recovering soil samples from fields in water depth up to 5000m are well observed in studies done by Silva 1973 and 2000.

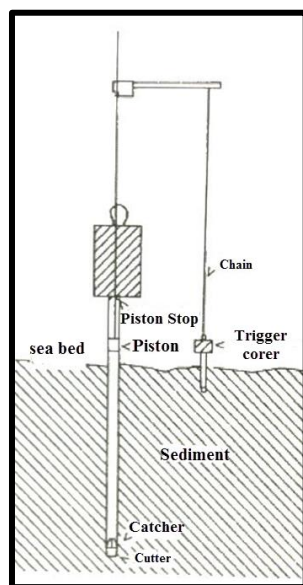


Figure 2.2: Kullenberg type gravity piston corer after triggering at the seabed (Weaver 1990)

2.2.2.4 Stationary Piston Corer (STACOR®)

Institute Francais de Petrole (IFP) developed STARCOR® to recover large and long samples of different soil types from the seabed (Lune, 2006). An effective stationary piston is the main difference of this sampler with Kullenberg corers. The piston immobility is achieved by attaching the piston to a seabed frame by a cable working on pulleys at both ends of the core barrel (Borel, 2002). The capability of STARCORER® in sampling the very soft soil is not completely proved owing to the induced displacement and disturbance of soils in front of the piston during impact.



Figure 2.3: STARCO® Stationary Piston Corer (Wong 2008)

2.2.2.5 Norwegian Geotechnical Institute Deepwater sampler (DWS)

This sampler was developed by Norwegian Geotechnical Institute in order to maintain recovery ratio of 95 % of about 20 m in length and up to water depth of 2000m. Although the DWS is still in the very early development, the quality of the soil samples recovered from limited trial tests was “excellent to very good” and “good to fair” (Lunne, 1997). A thorough description of the design of DWS was proposed by Lunne (2008).

2.2.2.6 Hydraulically Tethered Piston Core (HTPC)

HTPC is an advanced piston core sampler developed by Benthic Geotech Pty Ltd in the last decade. This sampler uses a fully independent unit called PROD (Portable Remotely Operated Drill) which is a fully independent seabed unit, connected to the support vessel via an electrical umbilical. PROD is capable of rotatory drilling and piston sampling down to maximum depth of 125 m below the seabed in water depths up to 2000 m. Overview of PROD is given by Carter (1999). Each HTPC can recover core of 2.75 m in length and 44mm in diameter. Full details of the design and deployment of the HTPC can be found in research done by Kelleher (2008).

2.3 Offshore In-Situ Testing

Existing offshore seabed corers have limitations in recovering high quality soil samples from deepwater sites and laboratory test results are reliable only if good practices are followed from the sampling operation to sample preparation in laboratory. Moreover, deepwater soil samples are vulnerable to exsolution (gas coming out of solution) because of the total stress relief. The gas exsolution will lead to fracturing of the sample on horizontal planes and possible formation of voids within the sample (Lunne, 2001).

All These limitation have forced engineer to come up with other options to improve the reliability of seabed soil characterization at deepwater sites. Undoubtedly, in-situ testing is one such option (Hossain, 2008).

In situ tools can be deployed in two modes, which are (Lunne, 200) :

- a) Downhole mode
- b) Seabed mode

In Downhole mode the in situ tool is lowered through the drill string from a surface vessel and latched into the base, after which the tool is pushed into the soil hydraulically at the bottom of the borehole. Downhole mode testing can be performed to a depth of 150 m or more below the seabed. However, the process is costly and time-consuming operation and the sample is vulnerable to disturbance beneath the base of borehole due to surface vessel movement.

In seabed mode, the in-situ tool is pushed into the soil using a seabed rig that is placed independently on the seabed. This method is comparatively less expensive and easier to be performed. The main drawback of the seabed mode testing is its limited testing depth. The majority of existing commercial seabed frames are only capable to perform tests down to 50 m below the seabed. Nonetheless, this testing depth capacity is enough for any geotechnical characterization. For design of subsea pipeline the depth of interest is typically limited to the upper 2 to 5 meter and for foundation this value is limited to the upper 30 to 40 m of the seabed.

The recent revolutionary developments in seabed testing technology have allowed high quality seabed mode testing to be carried out in a costly and time efficient manner at deepwater sites (Lunne, 2001). Typical offshore in-situ tests include:

- 1) Piezocone
- 2) Vane

- 3) T-bar penetrometer
- 4) Ball penetrometer

2.3.1 Piezocone

The first cone dates back to 1932, when Dutch developed a mechanical cone penetrometer to monitor the penetration resistance by a manometer (Lunne, 1997). The first electric cone penetrometer was developed during world war second which was a significant improvement over the mechanical cone penetrometer, because it stops measurement errors due to push rod friction and allows continuous penetration. The first cone that was able to measure penetration resistance and pore pressure was developed by Roy (1980). Nowadays, typical cones allow pore pressure measurements at the tip (U_t), face (U_1) and shoulder (U_2) of the cone or behind the friction sleeve (U_3). Piezocone penetrometer is now considered as an essential tool in most offshore soil investigations. It is estimated that more than 95% of all in-situ testing offshore consists of CPT/CPTU (Lunne, 2001).

Offshore cone penetrometer testing is carried out in general accordance with the International Reference Test Procedure (RITP) for the cone with a standard 35.7 mm diameter and projected area of 1000 mm² and cone of 35 apex angle. For the seabed mode, testing cones with the projected area of 1500 mm² are commonly reported. However, cones with the projected area of 100 mm² are also being deployed to improve the testing productivity in the upper few meters of the seabed (Lunne, 2001 and Hossain, 2008).

During the test, the cone penetrometer is pushed into the soil at a penetration rate of roughly 20 mm/s and measured pore pressure at least with U_2 position. The “unequal area effect” should be considered in cone resistance measurement using the following equation (Baligh 1981):

$$q_{\text{net}} = q_c + u_2(1 - \alpha) - Y\gamma_{\text{bulk}} . \quad (2.1)$$

In this equation, q_{net} is the corrected net cone resistance; U_2 is the measured pore pressure at the shoulder of the cone; q_c is the measured cone resistance; Y is soil depth; γ_{bulk} is total unit weight of soil and α is the unequal area ratio (ratio of inner area to the total area of the cone). The value can be measured from pressure calibration in a pressure vessel as described by Lunne (2001). Nowadays, there is a considerable demand for CPTU to be used to study soil parameter such as undrained shear strength and coefficient of consolidation in deepwaters. However, the CPTU is innately less accurate due to large corrections on the measured cone resistance and the contribution to the cone resistance from the overburden stress (see Equation 2.1). Moreover, due to high water pressure in deepwater, application of high capacity load cell is required. Therefore, measurement sensitivity in detecting small incremental resistance collected from the cone penetration significantly reduces. These CPTU limitations have led to the next generation of penetrometer which is called full-flow penetrometers (Hossain, 2008).

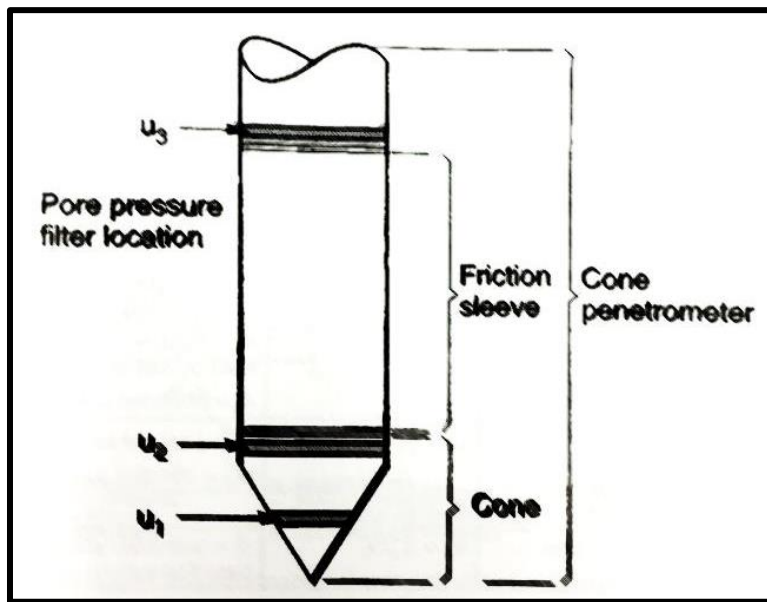


Figure 2.4: Cone penetrometer measurements including different pore pressure transducer location



Figure 2.5: Vane shear test facility

2.3.2 Vane

The first vane shear testing was performed in late 1940s in order to measure undrained shear strength in onshore soft to stiff clay with strength resistance less than 200kPa. The test started to be performed in offshore investigation since 1970s due to development of offshore activity worldwide and improvements in testing device deployment. High quality data obtained from offshore vane shear tests in the soft normally consolidated clays in the Gulf of Mexico have been outlined by Young (1988).

The main disadvantages of the vane shear test are

- 1) This procedure is time consuming when the peak and remoulded strength are required.
- 2) The shear resistance and pore pressure measurement are only available at discrete depth rather than a continuous profile.

Table 2.1 summarizes testing standards for the field vane shear test (Geise, 1988 and Hossain, 2008).

Table 2.1: Testing standards for the field vane shear test

| Parameters | ASTM-D2573-08 (2008) | BS 1377 (1990) | NGF (1982) |
|---|---------------------------|----------------------------|-------------------------------|
| Vane geometer | Rectangular/Tapered | Rectangular | Tapered |
| Height to diameter (mm) ratio | 2 | 2 | 2 |
| Vane blade diameter (mm) | 38.1/50.8/63.5/92.1 | 50/75 | 55/65 |
| Thickness of blade (mm) | 2 3.2 | | 2 |
| Diameter of vane rod (mm) | 12.7 | <13 | 12 |
| Accuracy of torque reading | $\pm 1.2 \text{ kPa}$ | 1 % of range (0 to 700 Nm) | $\pm 0.5 \%$ of maximum range |
| Drive of vane | Geared drive preferred | Geared drive | Geared drive preferred |
| Area ratio | <12 % | <12% | <12 % |
| Depth of insertion | 5 times borehole diameter | 3 times borehole diameter | 0.5 m |
| Rate of rotation ($^{\circ}/\text{min}$) | 6 | 6-12 | 12 |
| Time to failure(min) | 2-5 | 5 | 1 to 3 |
| Minimum rotation before remoulded shear strength measurement ($^{\circ}$) | 10 | 6 | 25 |
| Delay between insertion and testing (min) | None or <1 | 5 | <5 |
| Depth intervals between tests (m) | >0.76 | 0.5 | 0.5 to 1.0 |

2.3.3 Full-flow penetrometer

The first full-flow penetrometer was the T-bar penetrometer, which consists of a cylindrical bar mounted at right angles to the pushrods (Figure 2.6). The T-bar penetrometer was

originally developed at the University of Western Australia as a laboratory device to give improved definition of shear strength profiles in centrifuge testing and later prepared for field application (Steward, 1994). In order to rise above the T-bar penetrometer vulnerability to eccentric loading (which corrupting the measurement of penetration resistance due to induced bending moments), ball penetrometers have been introduced and was first used in 2003.

According to Randolph (2004), the main advantages of full-flow penetrometers relative to other in-situ samplers are:

- 1) Minimal correction for the overburden and pore pressure effects due to the flow around failure mechanism during the full-flow penetrometer penetration.
- 2) Remoulded shear strength may be assessed from cyclic penetration and extraction of full-flow penetrometer.

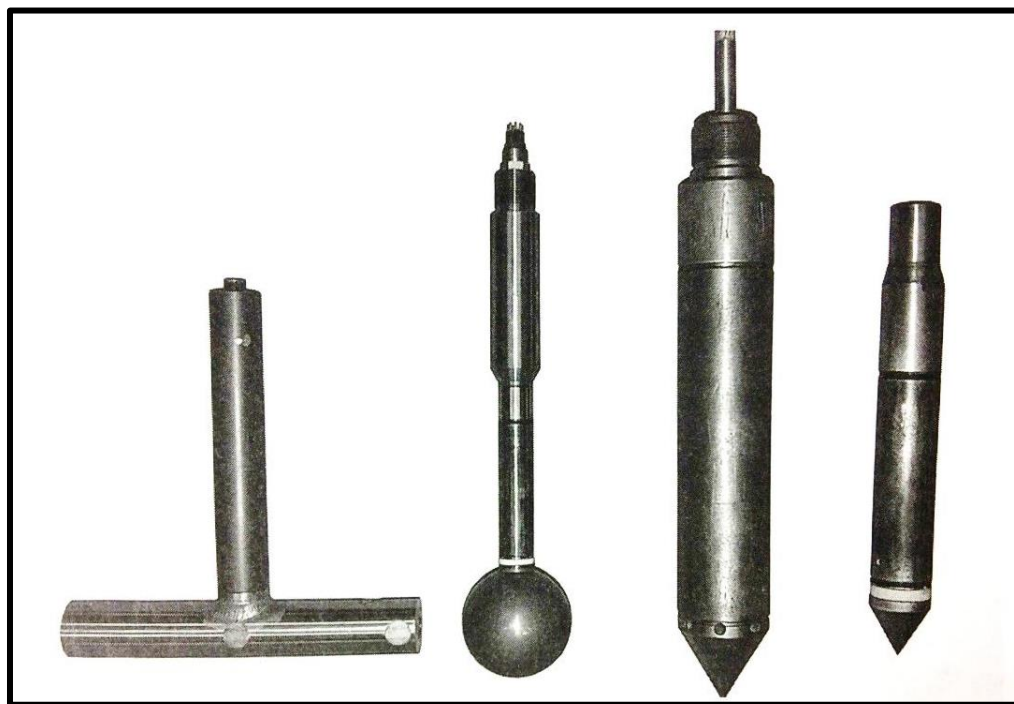


Figure 2.6: T-Bar, ball penetrometer, 33 cm^2 and 15 cm^2 piezocone penetrometer
(Mccorraon 2011)

2.3.4 FUGRO SMARTPIPE®

FUGRO Smartpipe® is an in-situ site investigation tool that is designed to measure pipe-soil interaction forces at the seabed (Figure 2.7). The equipment comprises a seabed frame with an instrumented model pipe that can be driven in the vertical, axial and lateral directions, whilst the corresponding loads and associated excess pore pressures are recorded. This unit is capable of performing in depth of up to 2500 m with axial displacement of 500 mm and lateral displacement of 1500 mm in a soft soil (i.e., 1 to 5 kPa). The merit of SMARTPIPE compared with other in-situ techniques, is that it measures the pipe-soil interaction in undisturbed soil conditions at the seabed surface, at close to full scale. This facility is capable of measuring vertical pipe penetration tests, dissipation of excess pore water pressure adjacent to the pipe that was generated during vertical penetration, and axial pipe-soil interaction (Ballard 2013).



Figure 2.7: FUGRO SMART PIPE in situ facility (Ballard 2013)

The summary of offshore in situ test is represented in the following table (modified from Lunne, 2001).

Table 2.2: Offshore in situ testing

| In situ test method | Category | Main purpose | Main reference on applicability |
|------------------------|--|---|---------------------------------|
| CPT/CPTU | Widely used | Soil profiling an soil parameter determination | (Lunne, 1997) |
| Vane | Used regularly for specific purpose | Determination of Undrained shear strength of clay | (Chandler, 1998) |
| Seismic CPT/CPTU | Used regularly for specific purpose | Soil profiling and soil parameter determination | (Campanella, 1994) |
| BAT/DGP | Used regularly for specific purpose | Pore water pressure and gas sampling an determination of gas content | (Mokkelbost, 1990) |
| Piezoprobe | New tool starting to be used more frequently | In situ pore pressure measurement and determination of coefficient of consolidation | (Dutt, 1997) |
| T-bar | New tool starting to be used more frequently | Soil profiling an determination of undrained shear strength of clay | (Randolph, 1998) |
| Ball Penetrometer | New tool starting to be used more frequently | Soil profiling an determination of undrained shear strength of clay | (Kelleher, 2005) |
| Electrical Resistivity | Used occasionally last 15-20 years | Determination of in situ density of sand and identification of soil contamination | (Campanella, 1993) |
| Nuclear density | Used occasionally last 15-20 years | Determination of in situ density of sand | (Tjelta , 1985) |
| Dilatometer | Used occasionally last 15-20 years | Soil profiling an soil parameter determination | (Marchetti,1997) |
| Heat flow | Used occasionally last 15-20 years | Thermal properties | (Zielinski, 1986) |

Table 2.2 (Continued)

| | | | |
|---------------------|--|---|------------------|
| Pressuremeter | Used occasionally last 15-20 years | Stress strain properties and in situ horizontal stress | (Clarke, 1995) |
| Hydraulic fracture | Used occasionally last 15-20 years | Conductor setting depth | (Aldridge, 1991) |
| FUGRO SMARTPIPE® | New tool starting to be used more frequently | Determination of Axial pipe soil interaction and undrained shear strength | (Ballard, 2013) |
| CIGMAT penetrometer | New tool starting to be used more frequently | Soil profiling and soil parameter determination | |

2.4 Subsea Pipeline

In deepwater, hydrodynamic loading is significantly reduced and pipelines are generally laid directly on the seabed without trenching or other form of secondary stabilization such as anchoring, axial resistors or sandbag depositing. Pipe laying is performed by laying barges incorporating two common methods namely S-lay or J-Lay method. The traditional method for installing offshore pipe-lines in relatively shallow water is commonly referred to as the S-Lay method because the profile of the pipe as it moves in a horizontal plane from the welding and inspection stations on the lay barge across the stern of the lay barge and onto the ocean floor forms an elongated “S”. To prevent pipeline buckling during S-lay process, proper tension is integral, which is maintained via tensioning rollers and a controlled forward thrust. S-lay can be performed in waters up to depth of 6500 ft (1981 m) and as many as 4 miles (6 kilometers) a day. Pipeline can be installed in this manner. On the other hand, The J-lay methodology is the main technique for laying pipelines in very deep waters. The pipe is laid through an almost vertical ramp positioned on board of a vessel. The deepwater pipeline is maintained in the optimal

angular position and pulled under a predetermined high tensile force while being lowered to the bottom. In J-lay installation, pipe stresses are maintained well within the linear elastic limit and lower lay tension required which results in reduced on-bottom tension and reduced freespan. However, J-lay installation is comparably slower method.

Assessment of the as-laid pipe embedment is one of the most critical steps in design of offshore pipeline, because other aspects of design such as lateral and axial resistance, and thermal transfer rate are tightly affected by embedment.

Applying conservative design value is not a safe approach since high and low embedment and then axial and lateral resistance, may work for or against a particular design project. Considerable amounts of expenditure could be saved by slight fine-tuning of pipe soil interaction values, through reduction of requirements for stabilization and anchoring measures and a reduced need to tolerate end expansions (Randolph, 2008).

In the case of deep-water pipelines, forces from hydrodynamic loading are generally small and the main forces are from high internal temperature and pressure, which cause expansion (Burton, 2008). Axial resistance between the pipe and the seabed works against this expansion. This axial resistance increase along the pipeline length up to hypothetical points, namely “Virtual Anchor”, that no axial displacement could be observed. Excessive compressive forces between these fixed points lead to buckling.. Buckling could significantly reduce the effective axial forces in the pipeline. On the contrary, Excessive uncontrolled buckling may lead to high bending strains in the pipe section. Hence the best solution is controlled buckling using buckle initiator or other mitigation methods at certain points along the pipeline and the thermal loads could be relieved. Accumulated axial movement is an undesirable phenomenon which may lead to global displacement of pipe. This phenomenon is termed “walking” (Carr, 2006). The

pipeline walking issues could be mitigated successfully by application of axial anchors, axial resistors, rock dumping, rock mattresses or Trenching and burying. The first step to control buckling and walking is predicting the available soil resistance on pipelines undergoing movement considering the associated changes in seabed geometry and strength. Majority of existing models are exclusively derived from stability analysis. This study is geared to extend existing models to account for geometry changes, rate of displacement of pipe, initial embedment and other factors.

During pipe-lay, deepwater pipelines embed by about 10% to 50% of pipe diameter, due to their own weight and the dynamic motions during laying (Westgaye, 2010). After the pipe was laid, it undergoes cycles of large displacement and finally lateral buckling occurs. Key design parameters are the initial peak lateral resistance during the first breakout cycles, and then the steady state resistance during each cycle (Chatterjee, 2012).

Load-Displacement responses during lateral breakout have been reported from laboratory model test by Vipulanandan (2013) and from centrifuge model study by Dingle (2008). In lateral movement, during peak break out resistance slip surface is built in front of pipe but no slip surface could be observed in the soil behind the pipe. Hence, soil strength was not mobilized in this area before separation of the pipe from the soil. After breakout, distinct slip planes are formed in front of pipe and tensile resistance at the rear is lost. During large amplitude lateral movement, soil is pushed ahead of pipe and the berms are formed in both side of pipe. Numerical solutions by Chatterjee (2012) and Aubeny (2005); plasticity solutions by Cheuk (2008) and Randolph (2008); laboratory models by Vipulanandan (2013) and Cheuk (2007) have been used to assess breakout resistance.

The literature available on pipe-soil interaction can be divided into three main categories.

First are solutions based on classical plasticity theory, second are finite element analysis and finally there are empirical approaches based on model tests (Chatterjee, 2012).

2.4.1 Plasticity solutions:

First plasticity solution was proposed by Randolph (1984) for the limiting pressure on a circular pile moving laterally through undrained soil. In a broader sense, the solution applies to any cylindrical object such as pipeline moving laterally through soil. Plasticity theory was utilized to establish lower and upper bound solutions for a long cylinder moving laterally in an infinite perfectly plastic cohesive soil. In a lower-bound solution, the calculated load are less than or equal to the real collapse load. This approach is based on stress distribution in static equilibrium and the stress field is not in conflict with failure criterion. In the upper bound approach, the calculated load is greater than or equal to the real collapse load. In this approach the final collapse load is calculated from energy method whereby, the rate of plastic work of the soil is equated with the work done by external load. The difference between upper bound and lower bound solutions determine the error involved in calculations. Randolph solution was considered exact (showing equal upper and lower bound solutions) up to when Murff (1989) proved an error in the upper-bound solution by applying a modified form of the solution for ultimate collapse load. Murff (1989) illustrated that this error resulted from the presence of region of localized conflict between the strain rate field and the stress field for any value of $\alpha < 1$, where α is the ratio of the limiting pipe-soil friction (the interface friction just before moving) to the shear strength of the soil . Murff corrected the solution by changing the shear strength to the absolute value of the maximum shear strain rate and integrating the particular component of plastic work numerically. This modified solution yet was not acceptable for the smooth pipe (α

approaching zero) with a maximum error (having difference between upper and lower bound solutions) of 9.1 %. No attempt was done to minimize this error until Martin (2006) proposed two upper bound solutions for ultimate load capacity of a circular pile undergoing lateral movement in undrained clay. In the first solution, Martin introduced a mechanism that successfully applies for smooth pipes (small α). According to Martin, a crescent shape body of soil undergoing rigid body rotation about a point located in the axis of the pile perpendicular to the lateral movement direction. In the second solution, Martin combined Randolph (1984) solution for rough pipe and his first solution for smooth pipes and was able to reduce the maximum discrepancy between upper and lower bound solutions to 0.65 % for all value of α . All these studies were focused on one directional (lateral) movement.

In 2008, Randolph and White developed an upper bound yield envelopes for shallowly embedded pipes in undrained clay under combined vertical and horizontal loading (Randolph, 2008). Their study was generalization of Martin mechanism by assuming that the center of rotation of the main block of failing soil (either homogenous or with depth dependent shear strength) in lateral movement does not necessarily lie on a plain normal to the direction of the pipe.

The first studies to consider strain-rate dependence of shear strength and soil remoulding (gradual loss of strength) were done by Einav (2005). He proposed Upper-Bound-Based Strain Path Method (UBSPM) which merges conventional strain path method and classical upper-bound solutions. In this strain path method, the analysis was based on the flow pattern stemmed from an upper bound solution instead of irrotational non-viscosity mechanism. The upper-bound solution was optimized for ideal rigid plastic soil and integrated with the strain path method. This study introduced a modified version of the Tresca constitutive model to assess the penetration

resistance of T-bar and ball penetrometer and later was adopted by Chatterjee (2012) for numerical analysis of pipe soil interaction.

2.4.2 Numerical analysis

In the literature there are extensive numerical studies concerning penetration and lateral movement of steel pipe on a soft soil in undrained condition. These studies are classified into two main groups. First group is focused on conventional small-strain finite element analysis. Aubeny (2005) performed a plane-strain analysis for different embedment depth of vertically loaded “wished-in place” pipe in a clayey trench. In this study embedment of ranging from 0.1 to 5 times diameter of the pipe was carried out and the solutions for soil with either constant shear strength or linearly varying shear strength were reported and finally the results were compared with lower bound and upper bound plasticity solutions. In 2008, Merifield published results of finite element analysis of shallowly penetrated pipe under combinations of horizontal and vertical load. The results were compared with the yield envelopes drawn from the upper-bound analysis of Randolph (2008). According to Merifield (2008), the limiting loads resulted from the small strain finite element analysis were in very good agreement with the upper-bound curves of Randolph. Krost in 2011, performed numerical simulation for consolidation of partially embedded pipelines with the help of small strain finite element analysis and presumed the soil responses to be elastic. The generation and dissipation of pore water pressure at different levels of embedment were also examined.

The second group of numerical analysis is more indulged in non-linear analysis of geomechanics problems involving large deformation finite element analysis. Non-linear finite element analysis can be classified into three main categories: material non-linearity, geometric nonlinearity, and boundary non-linearity (Bath 1996). In material non-linear analysis, strains and

displacements are infinitesimal, but stress-strain relationships are non-linear. Geometric non-linear analysis is divided into two types-(i) large displacement, large rotations, but strains are small and (ii) large displacements, large rotations and strains are large. In boundary non-linearity problems, the boundary conditions change during the motions of the body. Up to now, material nonlinearity, which is an inherent characteristic of soil behavior, has been the most studied aspect. There are four widely used finite element technique to solve large deformation problem: Lagrangian approach, Eulerian approach, Couple Eulerian Lagrangian (CEL) and Arbitrary Lagrangian Eulerian (ALE) approach.

2.4.2.1 Lagrangian Formulation

In the Lagrangian approach, the nodes of the finite element mesh move with the associated material point during analysis. The principal advantage of a purely Lagrangian formulation is that, first it has to satisfy relatively simple governing equations and the interface between the pipe an soil is precisely defined and tracked. However, large deformations within the soil region will result in mesh tangling and distortion in purely Lagrangian reference frame. Various approaches have been used to resolve the mesh tangling problem including rezoning and slideline algorithms in conjunction with element failure models to delete elements (Anderson, 1987). The disadvantage of this method was the need to develop a physically realistic element failure model which was computationally expensive. Continued research into target rezoning is certainly warranted and is being conducted at Sandia (Jung 2001).

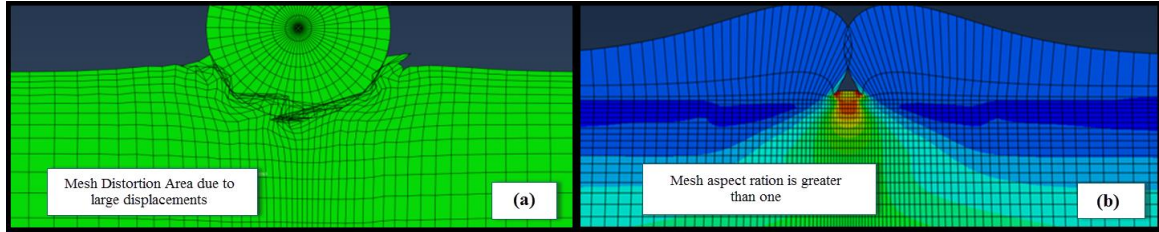


Figure 2.8: Severe mesh distortion by applying pure Lagrangian approach: (a) vertical penetration of pipe in soft soil (b) vertical penetration of rigid footing in a very soft soil (Sarraf, 2013).

2.4.2.2 Eulerian Formulation

In this approach, the mesh remains fixed and the material moves through mesh as time progresses. Eulerian approach avoids the difficulty of mesh tangling in soil area but loses the precise interface description provided by the Lagrangian formulation. This may result in excessive erosion of the penetrator materials (pipe) in a soft target (soil) (Silling, 1993). Eulerian approach has been widely used in fluid flow problems but van den Berg (1991) has successfully applied this formulation for deep penetration problem in geomechanics.

2.4.2.3 Coupled Eulerian Lagrangian (CEL) formulation

This method attempts to capture the strengths of the Lagrangian and Eulerian methods discussed above. In general, a Lagrangian reference frame is used to discretize the penetrator (pipe) while an Eulerian frame is used to discretize the target (soil). The boundary of the Lagrangian domain is typically taken to represent the actual interface between the penetrator and the target (Brown, 2002). Interface models use the velocity of the Lagrangian boundary as a kinematic constraint in the Eulerian calculation and the stress within the Eulerian cell to calculate the resulting surface force on the Lagrangian domain (Benson, 1992). Different algorithm such as SHISM or Ghost fluid method is characterized by defining different interface condition.

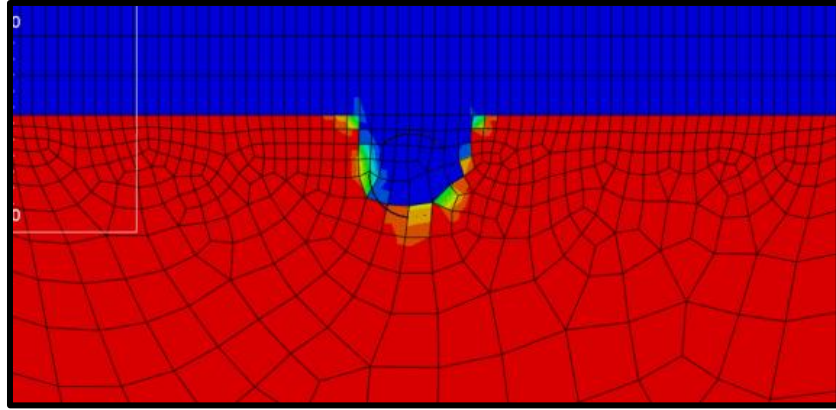


Figure 2.9: Application of CEL approach in penetration of subsea pipe in very soft soil (Sarraf, 2013)

Dutta in 2012, performed a numerical simulation of steel pipe under vertical loading employing Coupled Eulerian Lagrangian (CEL) analysis. In this study, the soil modeled as elastic perfectly plastic. ABAQUS software was utilized and void space in Eulerian domain using Eulerian Volume Fraction (EVF) tool. In order to overcome the limitation of ABAQUS CEL (which is the Eulerian material might penetrate through Lagrangian material), finer mesh were defined for Lagrangian material. In order to define linear variation of undrained shear strength with depth, FORTRAN subroutines was written and then merged in python syntax of ABAQUS. Finally, the results for both case of rough and smooth pipes compared with centrifuge results (Dingle, 2008). Abdalla (2009) developed a three dimensional finite element analysis of ice soil pipe interaction using CEL approach in ABAQUS. Simulation results from the developed model were validated by comparing the free field subgouge soil displacement to measured centrifuge test data and other FE models.

2.4.3 Arbitrary Lagrangian Eulerian (ALE) Formulation

This approach was developed to combine the advantages of both Lagrangian and Eulerian methods. This approach was proposed in a finite difference context by Noh (1964) and Frank (1964). Ghosh (1988) for the first time introduced the ALE technique to non-linear solid

mechanics problems. ALE methods provide for the arbitrary motion of the computational mesh and provide a means of developing a continuous mesh between a fixed and the deforming parts. As a result, the pipe-soil interface is internal to the discretization and many of the heuristics employed by CEL methods can be removed or simplified (Brown, 2002). In other words, In ALE mesh and material displacements are uncoupled to avoid mesh distortion and entanglement and the motion of both grid and material are determined, but tightly ALE involves a finite element grid of constant topology.

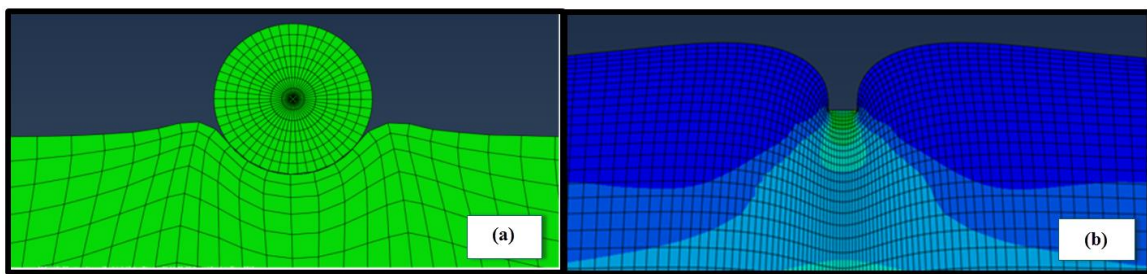


Figure 2.10: Applying ALE formulation (a) pipe soil interaction (b) exaggerated foundation soil interaction (M. V. Sarraf 2013).

In 2004, Hesar for the first time tried to capture the large movements of pipelines in soft clay using finite element software ABAQUS. Adaptive meshing properties were defined in step modulus of ABAQUS explicit to prevent mesh distortion. The effects of initial pipe embedment and submerged pipe weight on lateral pipe soil interaction forces were discussed. However no attempt was made to provide general solutions. In 2007, Konuk carried out large displacement pipe-soil interaction problem using an Arbitrary Lagrangian Eulerian (ALE) formulation in FE software LS-DYNA. Two dimensional and three dimensional models were prepared and a cap plasticity constitutive model was used for soil. Konuk mentioned the inadequacy of traditional design methods (such as Winkler and Coulomb) against lateral buckling. In 2009, Merifield performed numerical analysis on vertical penetration of pipes and subsequent horizontal resistance for pushed-in-place (PIP) pipes. In order to limit mesh distortion ALE formulation was

adopted in ABAQUS by Merifield. The effects of local heave generated during pipe penetration were explored and mathematical solutions of vertical and horizontal bearing capacity were presented.

2.4.3.1 Meshfree Method

Meshfree method sometimes is considered as particular type of Lagrangian methods but it worth to be discussed separately due to their unique characteristics. Meshfree methods such as smooth particle hydrodynamics (Wingate, 1993) avoid the problem of mesh tangling in the target (soil) since they do not employ explicit nodal connectivity. Hence, nodes are allowed to move about the domain in a Lagrangian fashion, are determined as a part of the computation. However, this determination of nodal interactions without an explicit mesh tends to make Meshfree methods computationally expensive (Brown, 2002).

2.4.3.2 Remeshing and Interpolation Technique with Small Strain (RITSS)

The RITSS method was developed by University of Western Australia (Hu, 1998). In this approach total displacement is divided into a series of small incremental step and for each step, small strain analyses were performed. After a given number of steps, the deformed geometry is remeshed prior to the next series of small strain analysis. Field variable such as stress and material properties, are updated from the old mesh to the new mesh (Chatterjee, 2012). This method can be combined with commercial finite element packages such as ABAQUS (Hossain, 2008). Hossain modified a simple elastic perfectly plastic Tresca constitutive model to incorporate the effects of strain softening and strain-rate. In any stage of his analysis, the shear was revised to constitute reduction due to strain softening and augmentation due to high strain rate. In 2010 for the first time RITSS approach was adopted by finite element software

ABAQUS and vertical and horizontal resistance during lateral motion for different weight of the pipe was examined (Wang, 2010).

It was presented that the effect of soil softening and berm build-up in front of the pipe could be summarized by defining an “effective embedment” of the pipe. The results were in good match with plasticity solutions and centrifuge test data.

Chatterjee (2012) performed a numerical simulation using RITSS approach concerning effects of strain rate and strain softening. As a result of each incremental displacement in ABAQUS software, two new variables (shear strain rate and cumulative plastic strain) were recorded at each Gauss point. Then these two variables interpolated to the new mesh, in addition to stresses and other parameters. The original shear strength at each new Gauss point was then modified and updated as a function of these two variables.

Tian (2014) proposed a practical method to implement RITSS for geotechnical applications by utilizing the ABAQUS in-built procedure for interpolation and remeshing. A series of four example problems benchmarking RITSS were also solved. These examples include Deep penetration of a T-bar penetrometer, penetration of surface footing, keying of a plate anchor and penetration of shallow embedded pipeline.

2.4.4 Experimental Model Tests

In 2007, Cheuk performed a series of full-scale model tests on Kaolin clay and West African soft soil to investigate pipe soil lateral interaction due to cyclic loading. Four stages of the force-displacement response were identified: breakout, suction release, steady berm growth and dormant berm collection. Increase in resistance due to activating the dormant berm was also discussed in this study and finally an upper bound model curve-fitted the experimental results.

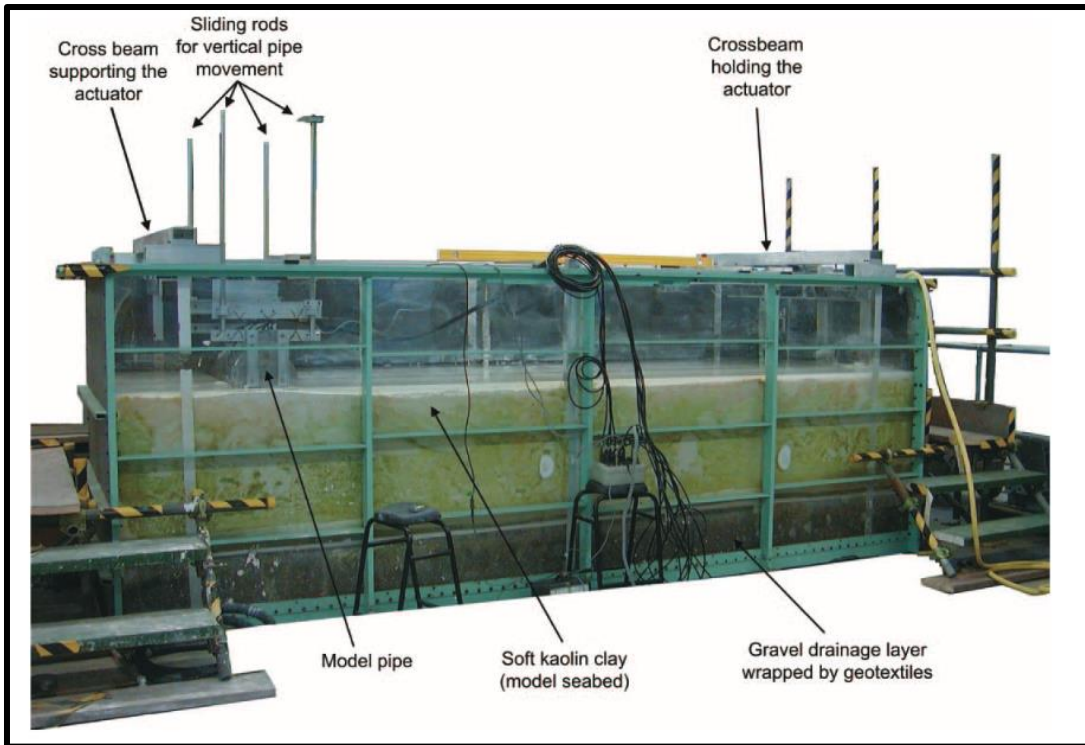


Figure 2.11: Full scale testing facility at University of Hong Kong

In 2008 Dingle performed centrifuge model tests in order to calculate vertical penetration and lateral break-out resistance of pipeline laid on very soft soil. In this study, digital image analysis and Particle Image Velocity (VIV) was utilized for tracking soil deformation. The results showed minor differences to plasticity solutions due to difference in shear strength calculation of near mud-line.

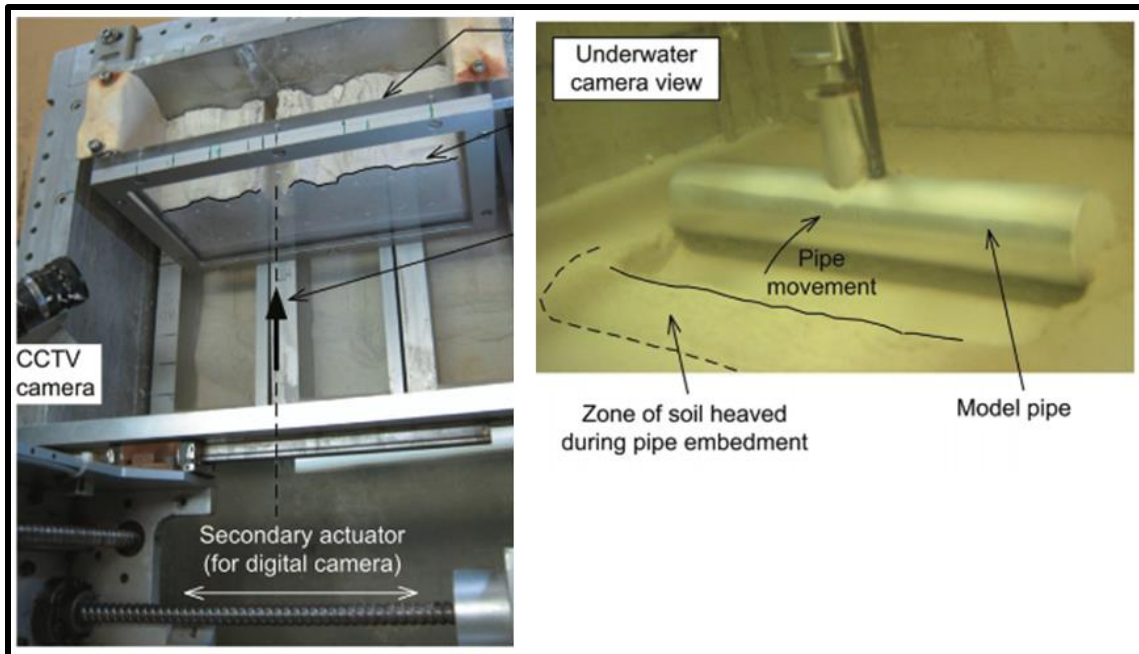


Figure 2.12: Centrifuge model test facilities



Figure 2.13: General view of soil tank assembled at IPT facilities

In 2010, Cardoso published results of full scale model tests to study large deformation lateral resistance of pipe in soft clay. In this study results were normalized and empirical equations reasonably provided to predict experimental results (Figure 2.12)

In 2011, Cheuk studied the relationship between dynamic lay effects and pipeline embedment by performing cyclic tests on centrifuge model (Figure 2.14). It was concluded that only a few cycles of small amplitude oscillation could double or triple static embedment due to combined effect of lateral ploughing and softening (Chatterjee 2012).

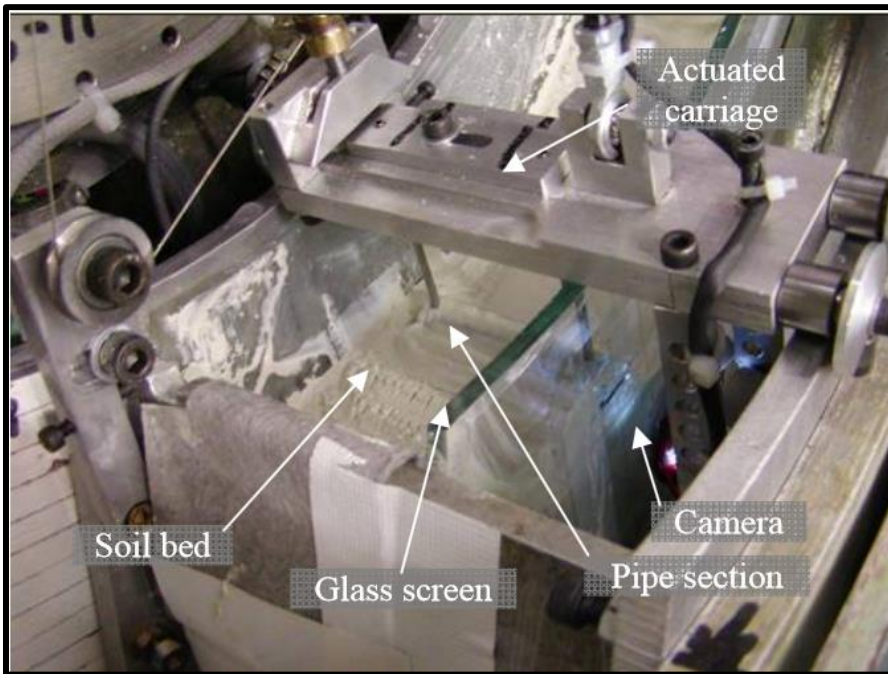


Figure 2.14: Details of Testbed within the (Small-Scale) mini-drum centrifuge

In 2013, several physical models have been designed and constructed at the Center for Innovative Grouting Material and Technologies (CIGMAT) Laboratory to investigate the behavior of pipes on very soft soil (Vipulanandan). Vipulanandan and Sarraf performed a series of full-scale and small-scale model test to investigate axial and lateral pipe soil interaction responses on Bentonite clay.

The effect of excess pore pressure, boundary condition, rate of loading for steel and plastic pipe was also discussed.



Figure 2.15: Medium size soil tank at CiGMAT laboratory



Figure 2.16: Full-scale soil tank at CIGMAT facilities

2.4.5 Design Practice

Design of subsea pipeline include many different stages and checks such as Hoop stress analysis, Longitudinal analysis, span analysis, vortex shedding analysis, stability analysis, expansion analysis, buckling analysis and etc. In the following our attention is only focused on pipes soil interaction design.

2.4.5.1 DNV-RP-F110

In DNV-RP-F110 (2007), which is the most common practice code for global buckling of submarine pipelines, it is mentioned that soil data for pipeline engineering is related to the upper layer of the seabed, often the upper 0.5 m and seldom below 2 m. In this practice, the components of the pipe-soil interaction involved in the potential buckling modes of a pipeline are introduced as:

- Downward

The downward stiffness is important for smoothening of survey data and for upheaval buckling design

- Lateral

For an exposed pipeline free to buckle laterally, the lateral pipe-soil interaction is the key parameter for the lateral buckling as it influences both mobilization load (break-out resistance) and pipeline post buckling configuration (residual soil resistance after break-out).

- Axial

The axial pipe-soil interaction is relevant when any buckling mode is triggered as it affects the post-buckling configuration. The axial feed-in of the straight sections into the buckled region is determined by the mobilized axial reaction (of the natural soil and/or of the gravel/rock

cover). The axial pipe-soil interaction is also important for the axial load build-up; either at the pipeline ends or after a buckle has occurred.

- Upward

The vertical pipe-soil interaction during up-lift is relevant when upheaval buckling is of major concern, as it affects the mobilization load. A multi-linear interaction model is normally required.

This code also mentions that the formulae for calculating the total resistance reported in literature vary due to three initial hypotheses/models. Generally speaking this is due to:

- 1) Differences inherent to the assumptions on which the proposed analytical models are based (for example, regarding soil failure mechanisms)
- 2) Extrapolation of experimental data with reference to limited case records
- 3) Simplifications which are the basis of numerical models.

The code makes it clear that the design of exposed pipelines will aim for; either to document that the pipeline will not buckle laterally, or, that the pipeline will buckle laterally and the post-buckling condition is acceptable.

2.4.5.2 DNV-RP-F109

DNV-RP-F109 (2010) remarks that If the specific weight of the pipe is less than that of the soil (including water contents), no further analysis is required to document the safety against sinking. If the soil is, or is likely to be liquefied, the depth of sinking should be limited to a satisfactory value, by consideration of the depth of liquefaction or the build-up of resistance during sinking.

Considering dynamic lateral stability analysis, this code brings in a thorough discussion regarding different factors accounting for lateral stability of subsea pipelines. The key part of on

bottom stability analysis is correct measurement of soil resistance. It is stated that a typical model for passive soil lateral resistance consists of four distinct regions:

- 1) An elastic region where the lateral displacement is less than typically 2% of the pipe diameter.
- 2) A region where significant displacement may be experienced, up to half the pipe diameter for sand and clay soils in which the pipe soil interaction causes an increase in the penetration and thus in the passive soil resistance.
- 3) After break-out where the resistance and penetration decrease.
- 4) When the displacement exceeds typically one pipe diameter, the passive resistance and penetration may be assumed constant.

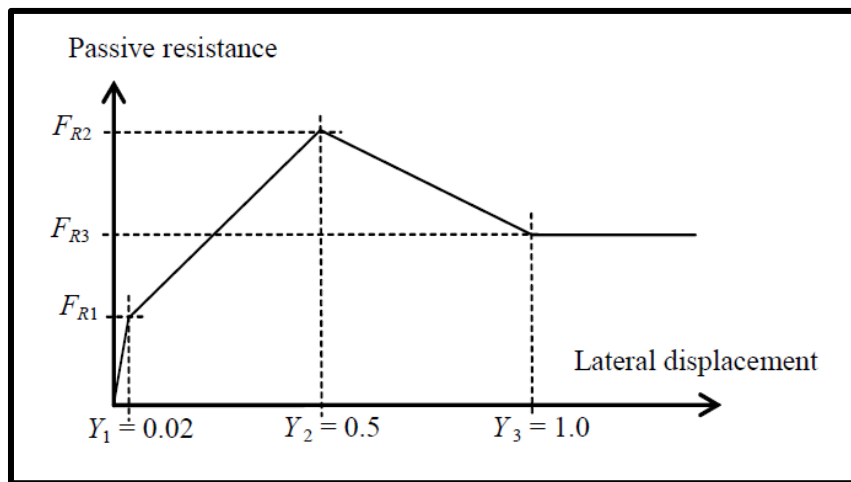


Figure 2.17: Simplified mechanism for lateral pipe soil interaction (DNV-RP-F109)

As Figure 2.17 shows, in the elastic region, $Y \leq Y_1$, the stiffness k can be taken as 50-100 N/m for sand and 20-40 N/m for clay. The stiffness increases with sand density and clay shear strength. No work is done and penetration is constant and equal to the initial penetration.

In the region $Y_1 < Y \leq Y_2$, the pipe soil interaction creates work which again increases the penetration and thus the passive resistance. If the displacement exceeds Y_2 , the pipe is

assumed to break out. The accumulated work is set to zero and no work is done in this region. Penetration is reduced linearly from the break out value at Y_2 to half this value at $Y = Y_3$ and passive resistance is reduced accordingly.

For a displacement larger than Y_3 , penetration and passive resistance can be assumed constant and no work is done. Empirical solutions were suggested by this code as:

$$\frac{F_R}{F_C} = \frac{4.1 * k_c}{G_C^{0.39}} * \left(\frac{Z_P}{D}\right)^{1.31}, \quad (2.2)$$

$$G_C = \frac{S_u}{D * \gamma_s} \text{ and } k_c = \frac{S_u * D}{W_s - F_Z} = \frac{S_u * D}{F_C}, \quad (2.3)$$

$$Z_P = Z_{pi} + Z_{pm}, \text{ and} \quad (2.4)$$

$$\frac{Z_{pi}}{D} = 0.0071 * \left(\frac{G_C^{0.3}}{K_c}\right)^{3.2} + 0.062 * \left(\frac{G_C^{0.3}}{K_c}\right)^{0.7}, \quad (2.5)$$

where F_R is passive lateral soil resistance, F_C is vertical contact force between pipe and soil, F_Z is vertical hydrodynamic (lift) load, G_C is soil strength parameter, Z_p is penetration depth, Z_{pi} is Initial penetration, Z_{pm} is penetration due to pipe movement and D is pipe diameter.

2.4.6 DNV-RP-F105

DNV-RP-F105, (2006) is focused on free spanning pipelines. This practice code remarks on different elements causes free spanning including: Seabed unevenness, change of seabed topology (scouring); artificial supports and strudel scours. This practice also brings in a discussion about soil vertical stiffness and models.

2.4.7 SAFEBUCK

In 2002, SAFEBUCK JIP was started at University of Cambridge, with focus on large displacement cyclic lateral loading of pipelines on very soft deep-water marine clays. Using

small and large-scale model tests, Burton (2006) provided recommendations on key parameters that affect the lateral pipe-soil interaction response in soft clay. Different state of pipe soil response, including embedment of pipe during installation, break-out during buckling, large amplitude displacement and repeated cyclic behavior, were discussed and suitable empirical equation were developed for each of these steps.

Other researches such as Dendani (2008) presented practical methods for calculating pipe-soil interactions based on site-specific data. Several steps of lateral resistance and non-stopping increase in resistance due to continuous build-up of soil berms also debated.

2.5 Mitigation Methods

The majority of deepwater pipelines operating in Gulf of Mexico carry hydrocarbons at a high pressure and high temperature and are susceptible to cyclic thermal expansion due to shutting down and restarting of high temperature flowline system. If these thermal expansions are not properly mitigated, the pipeline will be prone to axial displacement and lateral buckling and consequently failure. Axial displacement is also known as pipe walking where the constant displacement of pipeline over production cycles can result in global axial movement of the pipeline. From a general perspective, there are two alternative approaches which can be taken with respect to thermal expansion mitigation. The first approach is restraining the pipeline to limit the resulting displacements. The second approach is a compliant approach where the locations for the displacements are chosen to prevent excessive stress variations in the pipe. The first approach (anchoring approach) is more desirable in mitigating pipe walking and the second approach (compliant) is more desirable to mitigate lateral buckling (Prinet, 2006).

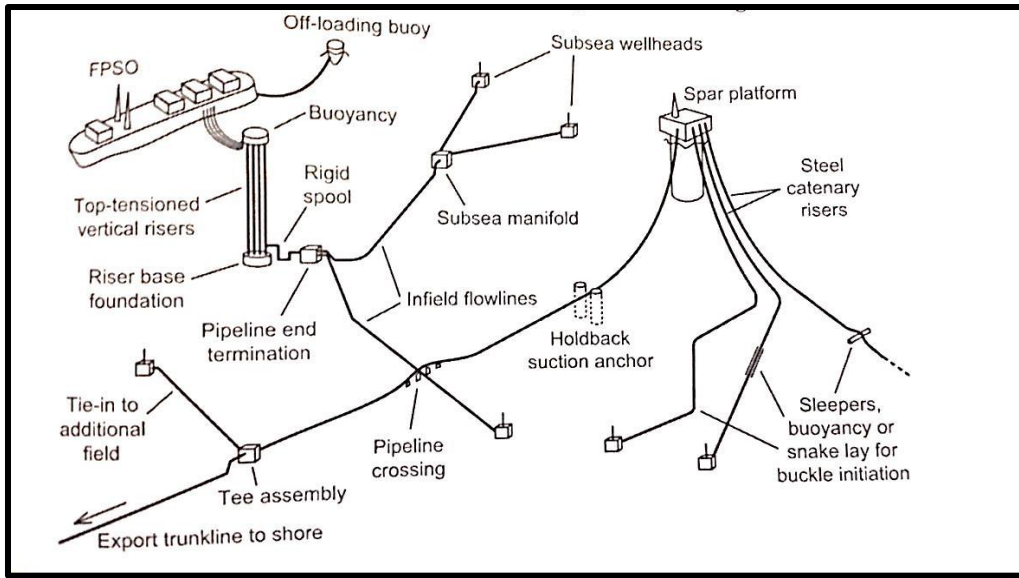


Figure 2.18: Pipeline networks and associated infrastructure (Randolph, 2011)

2.5.1 Axial walking mitigation

In order to stop pipeline walking, pipeline engineer should anchor down the pipe in some way. Anchoring the first end of pipeline could be simply achieved by using suction anchors or using stab and hinge over system. However, anchoring the second end of the pipeline requires a more complicated solution. One of this solution is using preinstalled set of anchors that are connected to pipeline via a set of chains and a clamp (Figure 2.19 and Figure 2.20). Spot rock dumping, rock mattresses, trench and burry techniques are also other common way to increase axial friction in deepwater HPHT pipelines. However large quantities of these methods will substantially increase the installation time and cost.

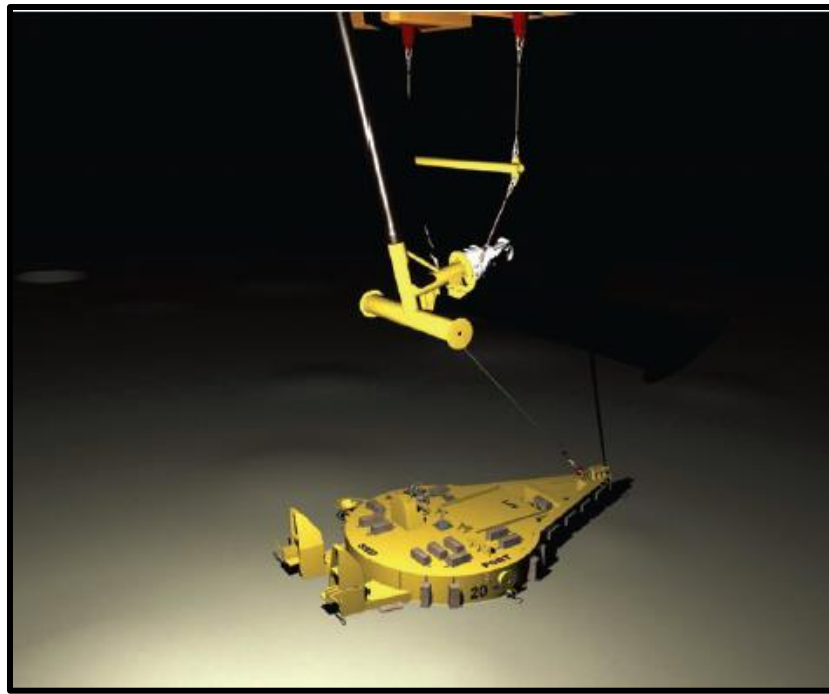


Figure 2.19: Pipeline anchor with stab and hinge over system

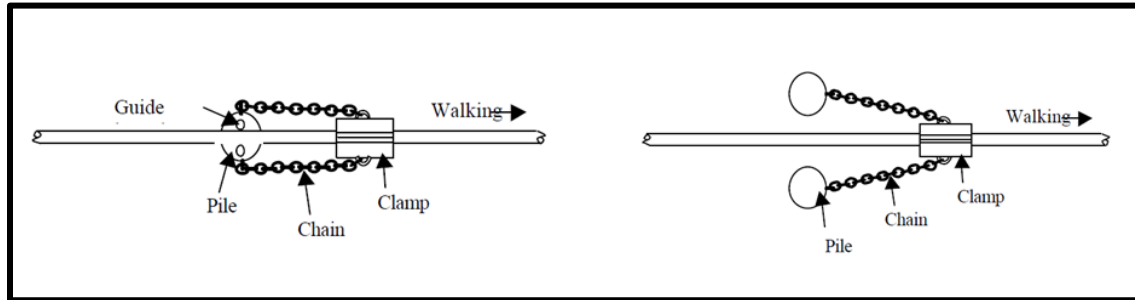


Figure 2.20: Anchor and chain restraint for pipeline (Prinet 2006).

It should be mentioned that if the axial walking is not properly addressed, the pipeline will experience a net displacement towards the Steel Catenary Riser at every production shut down cycle. At the touch down zone of the SCR, the riser will induce a tensile force into the pipeline which is in contact with soil. In the presence of temperature loading and absence of axial mitigation the pipeline expand at both ends of the pipeline (towards the SCR and towards the other end). Accordingly the pipeline will experience an expansion and movement at both sides of a fixed point. when the pipeline goes through a production shut down the pipeline will

cool down and on the both sides of the fixed point. But the pipeline is still under the effect of the tensile load of the riser and as a result these fixed points are at different locations depending on whether the pipe is expanding or contracting. The point is that when the pipeline is cooling down and retracting, the fixed point will be much closer to the SCR than during the start up situation. So that, the pipeline undergoes a net displacement towards the SCR at every production shut down cycle (Prinet, 2006). Cumulative fatigue damage, failure and rupture of pipeline are other possible repercussions of axial walking.

2.5.2 Lateral Buckling Mitigation

Due to soil restraint, the pressure and thermal expansion can generate a significant level of compression that causes flowline to buckling globally like a steel bar. It is common by the industry to initiate such global flowline buckling in a controlled manner in order to release the compressive load and to avoid the excessive expansion and pipe bending at arbitrary locations. At the controlled buckle locations, pipeline sections are welded in a lower flaw size and higher fatigue acceptance criterion, so to have prudent safety against the bending load and fatigue damage from the global buckling. The commonly used design strategy against lateral buckling for the deepwater HPHT pipelines is to control the pipeline thermal expansion and lateral buckling, in location and scale. The mechanisms are to trigger the lateral buckling in multiple locations by placing the vertical upset, namely sleeper and by reducing the pipeline section submerged weight, namely distributed buoyancy section(module) (sun, 2012).



Figure 2.21: Buoyancy Modules used in Canapu Field (sun, 2012)

In 2009, Canapu field development used the distributed buoyancy sections to control the lateral buckling (Solano, 2009). Three trigger locations were designed. Each trigger was 130 m long and achieved 85% reduction in pipeline submerged weight. The design was based on the methodologies defined in the SAFEBUCK (Burton, 2008).

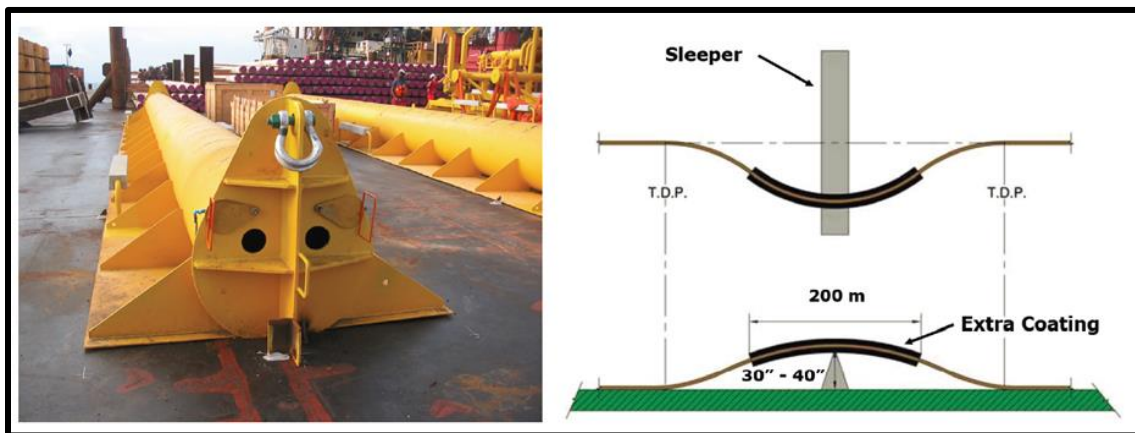


Figure 2.22: Sleeper system

BP King Flowlines, located in the Mississippi Canyon of the Gulf of Mexico, are one of the earliest deepwater pipelines using sleepers for the lateral buckling mitigation. Design and

implementation of sleepers in this project is thoroughly discussed in a paper written by Harrison (2003).

Another Common mitigation solution for the lateral buckling is the application of snake laying or pre-snaking. The idea of snake lay is to provide an over length of the pipeline within the deliberate curves developed during pipe laying, which will absorb the expansion of the pipeline. However, some researchers such as Prinet (2006) believe that snake lay method is not a suitable mitigation technique for deepwater pipelines.

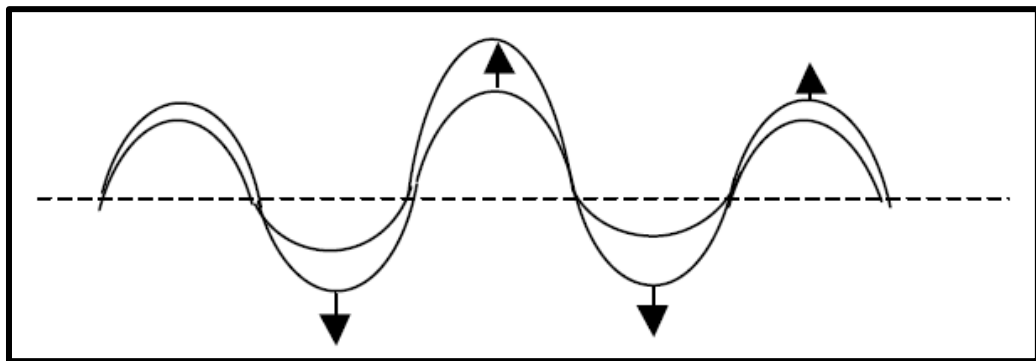


Figure 2.23: snake lay mitigation solution

Chapter 3. MATERIALS AND METHODS

3.1 Preparation of Soil

The pipe soil tests were performed on clayey specimens of commercially available bentonite. Homogeneous slurry was prepared by mixing reconstituted bentonite clay powder with deionized water at different range of water content to get shear strength as low as 0.02 kPa to 0.2 kPa. For primary correlation of water content to undrained shear strength in the mix design, Raheem (2013) equations were employed as:

$$S_u = -6.0 * \ln(W/C \%) + 15; \quad \text{when } W/C < 300\% \quad \text{and} \quad LL < 500\%, \quad (3.1)$$

and

$$S_u = 14.4 * e^{(-0.004 * \frac{w}{c}\%)} + \frac{1}{e^{(\frac{w}{c}\% - LL\%)}}; \quad \text{when } W/C > 300 \% \quad \text{and} \quad LL > 500\%, \quad (3.2)$$

Where S_u is undrained shear strength, w/c represents soil moisture content, w is natural water content and LL is liquid limit. At the end of soil preparation, vane shear test was performed to assure that desired undrained shear strength was captured. Raheem shear strength solutions were in very good match with the shear strength of produced soil with discrepancy of less than 8% for all batches.

Similar to Husain (2008) a thorough mixing procedure was adopted comprising the following steps:

- 1) Mixing about three hours
- 2) Leave about two hours for completion of soaking
- 3) Monitor and manual break down the clogs
- 4) Mixed about two hours

The CIGMAT mixer was armed with a vacuum pump via a jubilee connection. A vacuum close to 30 kPa was implemented at the commencement of the last stage and upheld all over in order to complete de-airing slurry. The slurry was then transferred to soil tanks for the proper consolidation via six drainage (open-up) pipes that had been implemented during big tank fabrication. Although all the tests were performed under undrained situation, before each test, the produced soil was rested for 48 hours inside the soil tanks (box) in order to make sure that the natural particle alignment of the soil has completely occurred. In order to resemble the field situation, a free water layer was placed on the soil surface right before the test. Water content and vane shear tests were performed regularly before, during and after each test, and in different points of soil tank to guarantee undrained shear strength consistency. The minimum thickness of the soft soil profile used in both model studies was 0.305 m (12 inch).

3.2 Equipment

3.2.1 Medium-scale soil box with viewing sides

It was critical to develop representative seabed with proper soil strength for the model study. A purpose-designed soil box with plexiglass sides was built to allow observation of the soil deformation through the transparent sides. The box has an internal size of 0.91 m(3ft) length, 0.61 m (2ft) width and 0.61 m (2 ft) height and was designed with proper drainage at bottom and buckling stiffener (to prevent sides bucking and consequent leakage) at CIGMAT (Center for Innovative Grouting Materials and Technology) to model real sea bed condition (see Figure 3.1). This model test was used in early studies but the main part of laboratory tests were conducted on full scale facilities which will be discussed later. The main limitation of medium-scale facility is that, the boundary effect induced from the size of facility could increase uncertainties of pipe-soil interaction responses. As a result, the length of pipeline could not exceed 22 in in axial

testing and 15 in lateral testing. However, this facility enabled us to accurately track deformed soil during each experiments and enabled us to conveniently change soil properties for several times. Before running full scale tests, some of the specific tests were first performed on this facility to get quick responses. The schematic of the experimental setup is shown in Figure 3.2. The machine used to test the sliding pipe was displacement controlled and the pipe was attached to the loading machine using a strong string. The plastic pipe represents the insulation surface of the actual subsea pipe (Kulkarni, 2006). It was important to develop a loading system that will allow the pipes to move without external influence. In total, 27 axial and lateral pipe-soil interaction tests were performed on this facility to measure horizontal load displacement responses and variation of pore water pressure during each test.

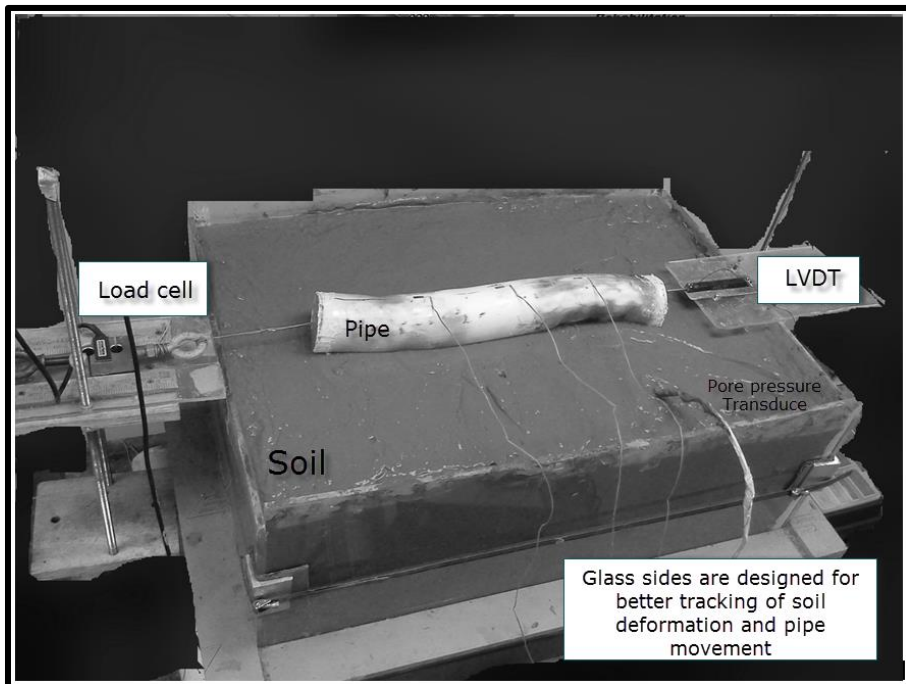


Figure 3.1 Medium-size soil box at CIGMAT laboratory

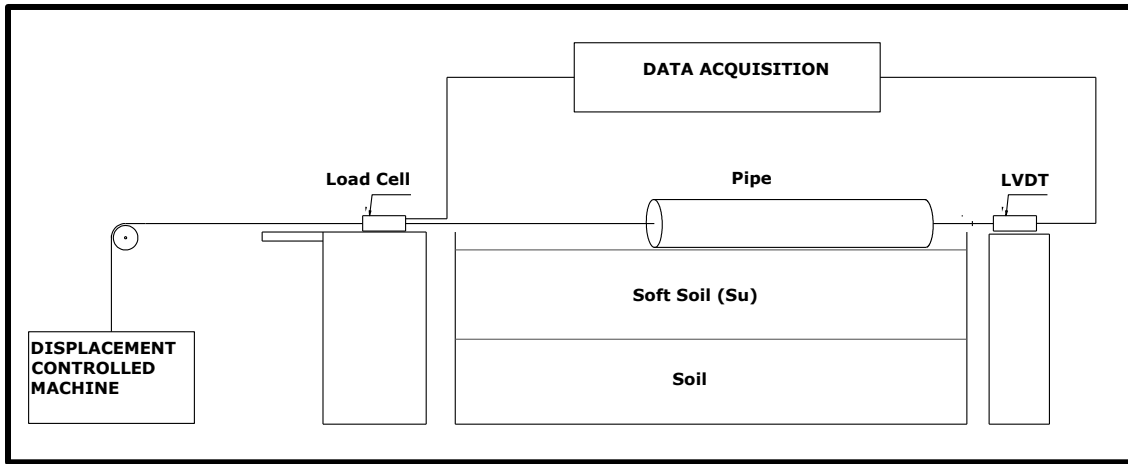


Figure 3.2 Schematic of the medium-size test setup for axial and lateral displacement study (Vipulanandan, 2013)

3.2.2 Full-scale soil box

Large scale model test was used to simulate the pipe interaction with the soft clay soil representing the seabed. The large scale test facility was 2.44m (8ft) in length, 2.44 m (8ft) width and 1.83 m (6 ft) height and was designed with proper drainage and loading frame at CIGMAT (Center for Innovative Grouting Materials and Technology). The machine used to test the sliding pipe for both axial and lateral was displacement controlled and the pipe was attached to the loading machine using a pulley system with string. During the axial test, the machine pulled the pipe at varying rates. The experimental setup is shown in Figure 3.3 for axial loading and in Figure 3.4 for lateral loading. The sliding resistance of pipe on the soft soil was measured using a load cell. The load cell was calibrated and was accurate to 0.01 lb. The pipe displacement in vertical and horizontal directions was monitored using two sets of linear variable differential transducers (LVDT). Excess pore water pressure during axial and lateral cyclic test was monitored by pore pressure transducer installed beneath the pipe invert. The schematic of the experimental setup for axial and lateral loading is shown in Figure 3.5 and Figure 3.6.

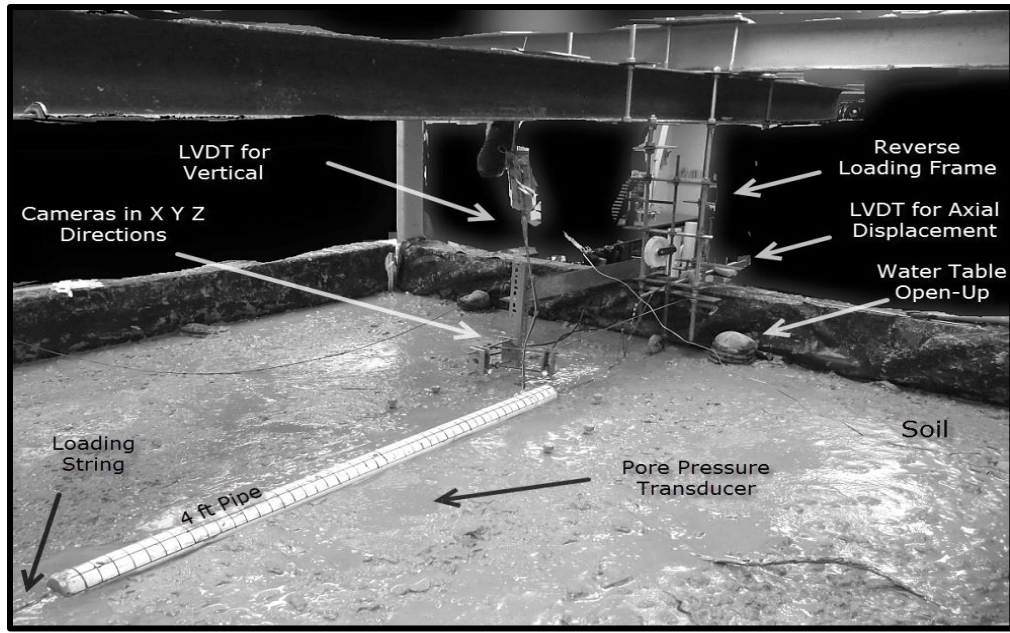


Figure 3.3 Axial pipe soil interaction testing facility at CIGMAT (Center for Innovative Grouting Materials and Technology)

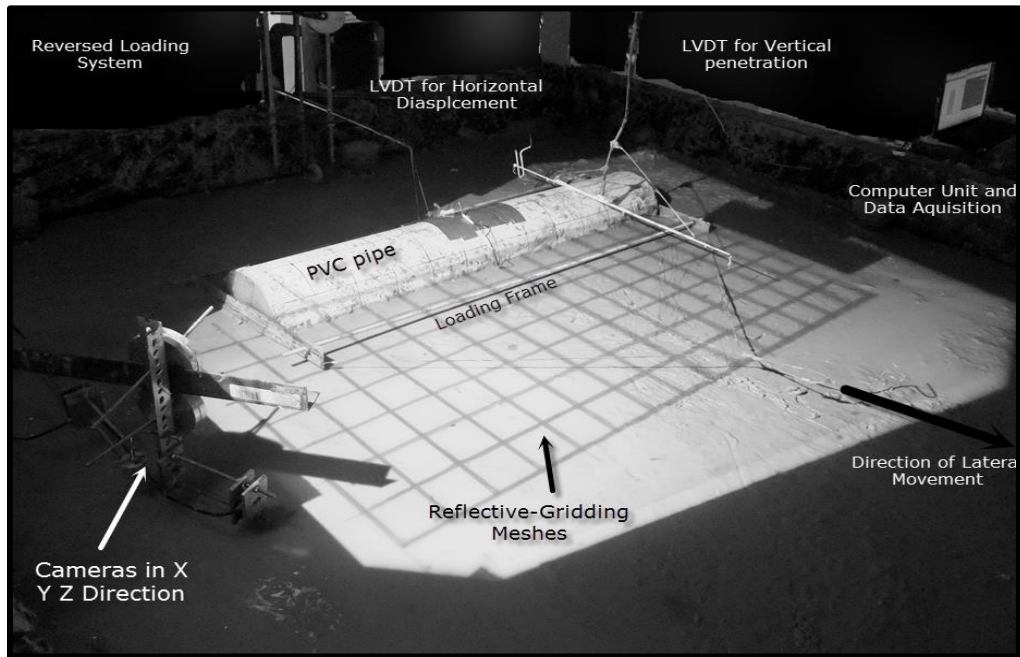


Figure 3.4 Lateral pipe soil interaction testing facility at CIGMAT (Center for Innovative Grouting Materials and Technology)

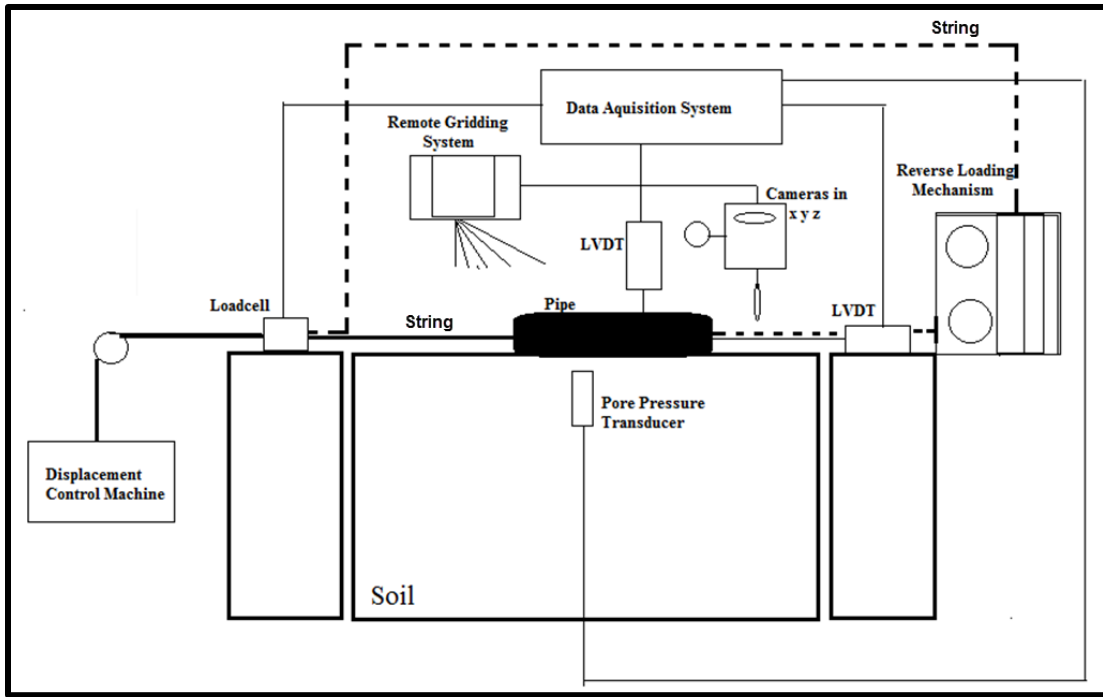


Figure 3.5 Schematic of the axial sliding testing setup

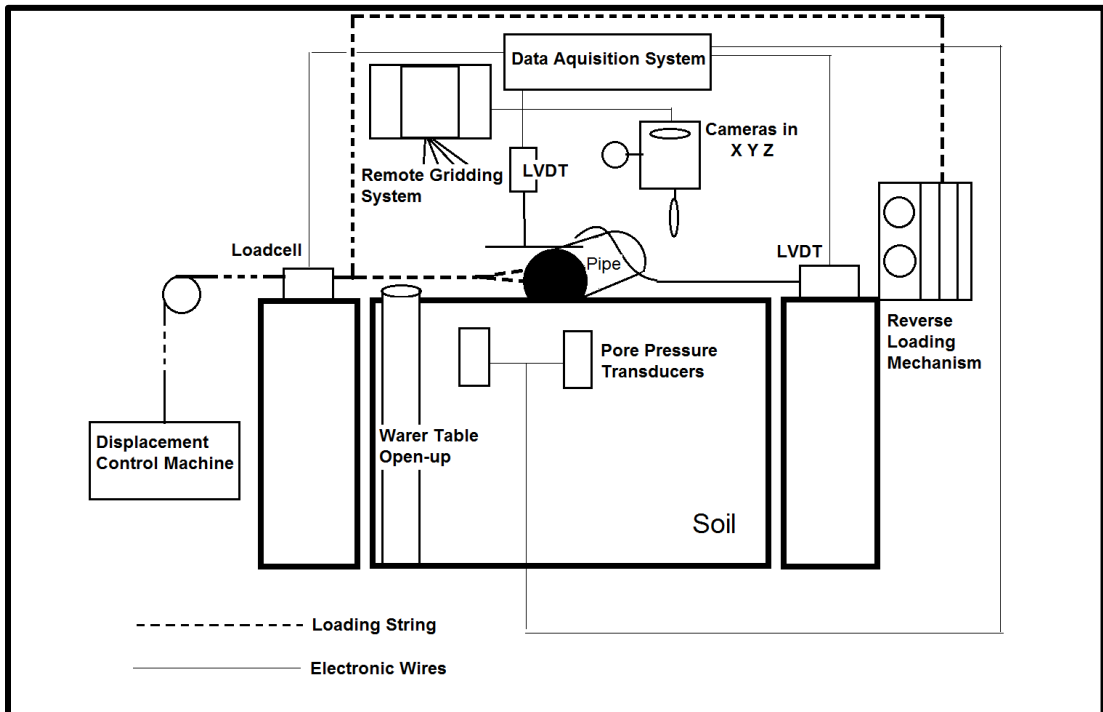


Figure 3.6 Schematic of the lateral loading testing setup

3.2.2.1 Lateral Loading frame

Specific loading mechanism was first design during this study to investigate lateral pipe soil responses for different model pipes. The key advantage of this mechanism includes:

- 1) Minimum external influence

The external influences and manipulations from loading actuators are minimized in this design. In other words, the pipe is allowed to follow its very natural behavior during expansion, since the pipe is loaded in one adjustable direction and during movement it is not constrained by any loading apparatus or sensing instruments. The horizontal and lateral LVDTs are connected to pipeline by using very light-weighted, frictionless, arc-shaped rod and slippery edge, So that negligible friction forces or extra vertical loaded was observed.

- 2) changeable pipe end boundaries from free-end to fixed-end via authentic loading frame

In this design the lateral loads were transferred to the pipeline via solid loading frame (The frame dimension was adjustable according to pipe size and length). The pipe was rested inside an aluminum rectangular frame which induced two different modes for frame-pipe boundary (see Figure 3.7 and Figure 3.8).

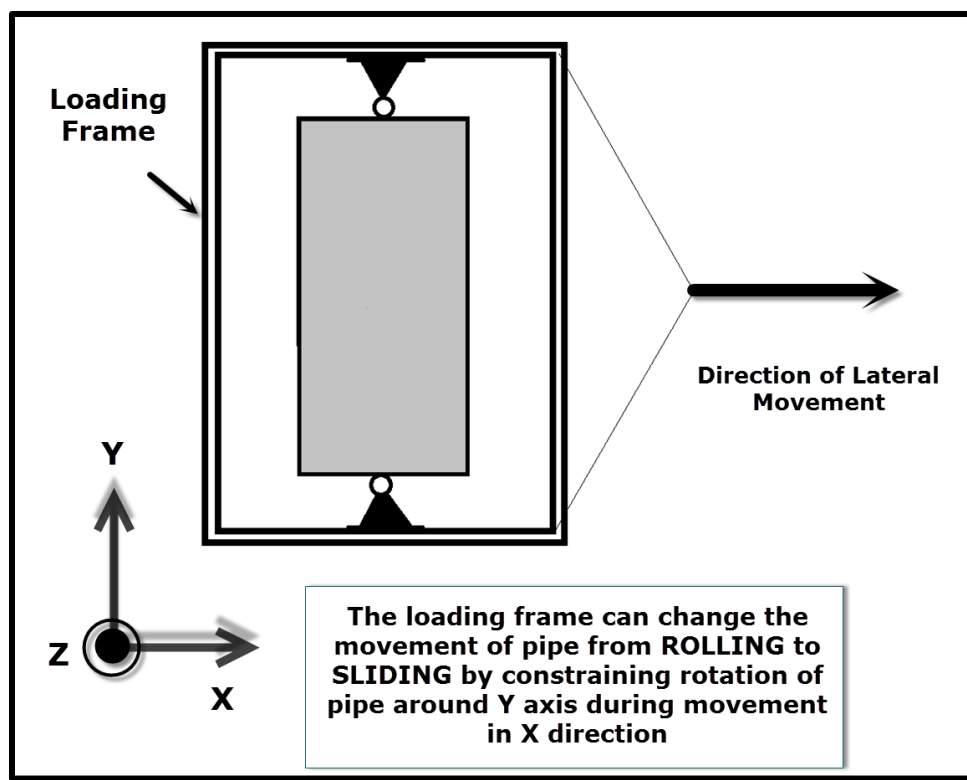


Figure 3.7 Schematic of loading frame in lateral movement

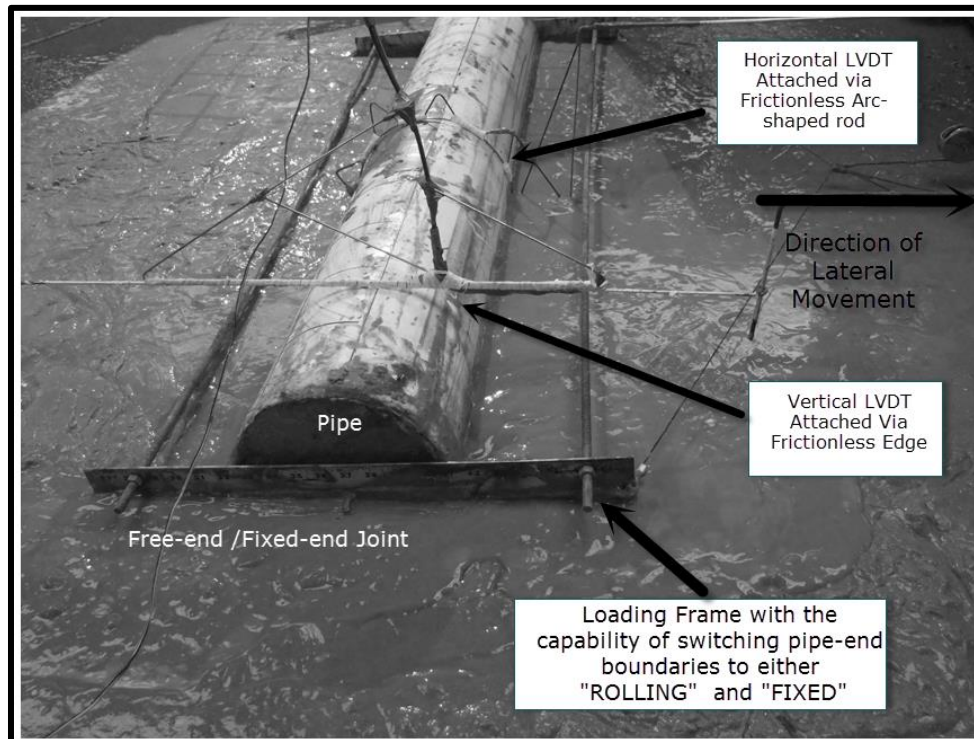


Figure 3.8 Loading mechanism in lateral setup

3.2.3 Soil strength Assessment Tool: Vane shear

The soil in the deepwater seabed will have varying strength properties. Modified vane shear machine was used to measure the shear strength of the soil. The range of soft clay used in this study had undrained shear strength of 0.01 kPa (0.0015 psi) to 0.2 kPa (0.029 psi) which represents a realistic and challenging subsea soil.

Maintaining soil homogeneity before and during the tests requires consistent measurements of soil sample. As for large scale model test, with the surface area of 5.95 m^2 (64 ft^2), five different points on the soil surface selected (see Figure 3.9), which undrained shear strength was measured before, after and during each test. The average of undrained shear strength was calculated for load normalization such as $\frac{F_v}{S_u * D}$, where F_v is vertical force, S_u is undrained shear strength and D is the pipe diameter.

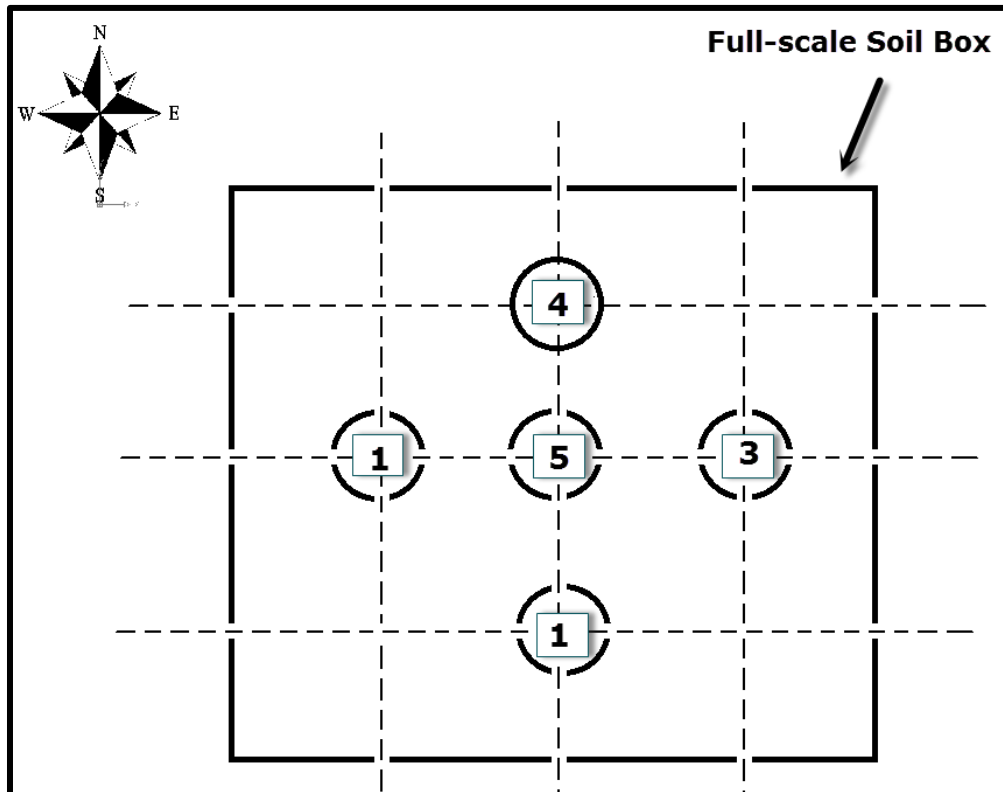


Figure 3.9: Place of vane shear test measurements in the full-scale soil box

3.2.4 CIGMAT Reflective Gridding and Remote Gridding Systems

Reflective Gridding System (RGS®) is comprised of a projector and series of transparent grids that are reflected on the surface of model test. Set of three cameras are placed along axis of x, y and z to capture soil displacement at desired area at any time. In order to make the soil displacement traceable for camera, specific color chips were placed on top layer of soil. RGS help cameras better synchronize pipe movement and soil deformation at any time increment (Figure 3.10).

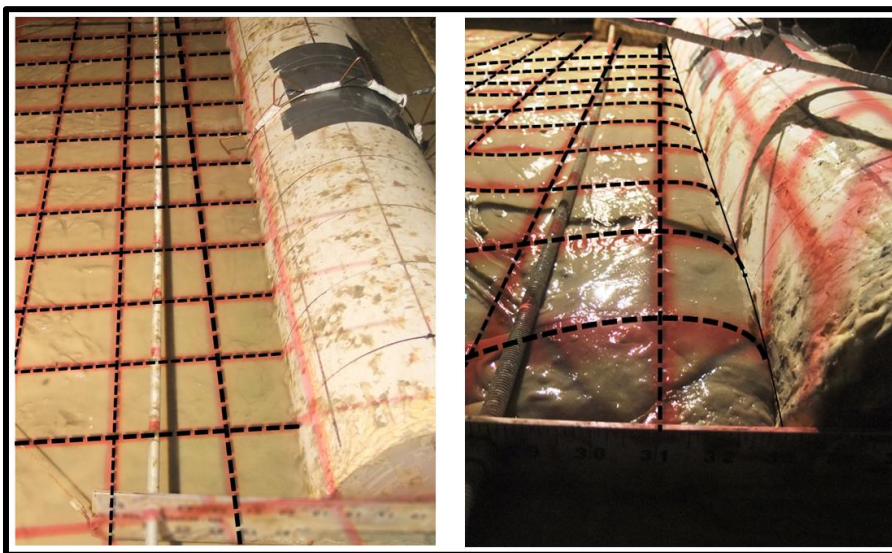


Figure 3.10: Change in gridlines configuration before and after lateral displacement

Steps of RGS implementation are as following:

- 1) Designing and assembling RGS pattern sheets by copying the gridlines from a parent model outside the soil tank to transparent sheets. These transparent sheets are then fixed on the projector and reflected on the soil model. The angle and distance of projector should be considered in a way that gridlines are straight and perpendicular on the whole surface of soil model.

2) Calibrating and correlating the change in shape and angles of reflected grids to the new topography of soil in every square. Imagine “pattern 1” is reflected on the soil model and due to pipe movement one or some of the gridline squares turn into “shape A” as shown in Figure 3.11. By a quick guess, it is obvious that this new gridline represent a decrease in the elevation of soil in that area or a puddle but the main challenge here is to quantitatively associate any change in the angle or configuration of gridline to the new topology of model. To address this challenge different topography of soil with different slopes were built up in CIGMAT laboratory and new gridline patterns meticulously photographed and recorded to make a data base.

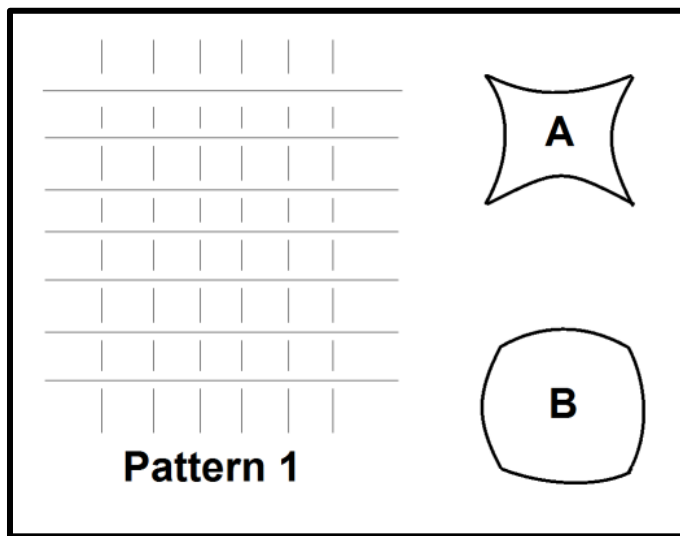
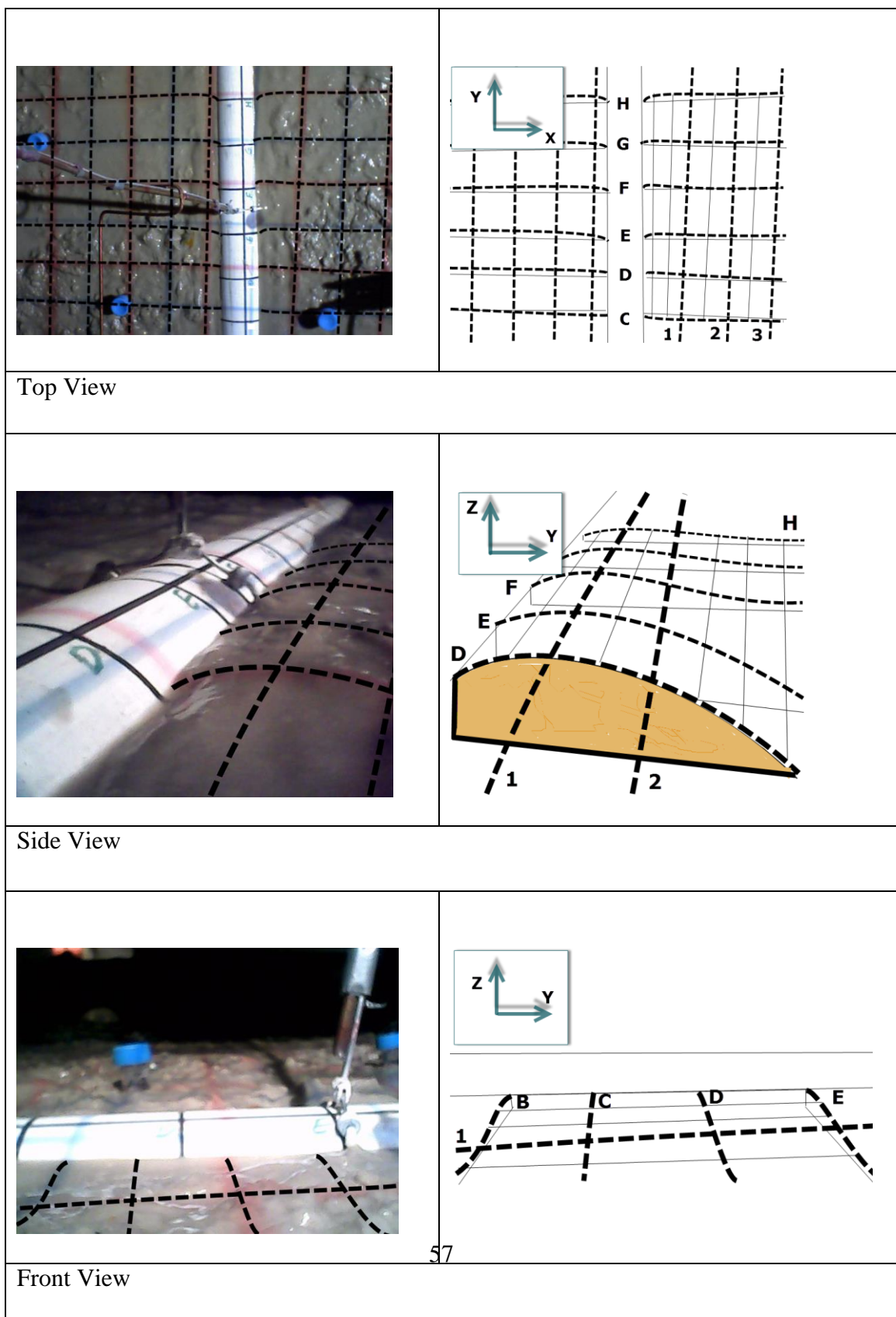


Figure 3.11: Interpretation of deformed gridline from plan view

3) Placing light-weighted color chips on the surface of soil model before start of the test. During the test this very small chips will move with particles of soil (soft soil with undrained shear strength of 0.01 to 0.11 kPa) and due to their distinct color they are easier to be tracked. This step is highly recommended if displacement fields in the soil surface are wanted. For berm formation studies during the pipe movement this step could be escaped.

Table 3.1: RGS was utilized to investigate berm formation during axial movement of pipe and the grids were transferred to mathematical coordinates. The gridlines are differentiated from the rest of photo by broken lines



- 4) Running the test and recording pipe and soil movements from three cameras in x, y and z axes simultaneously.
- 5) For any time increment, the photos should be analyzed and nodes (grids intersection) in each photo should be assigned to mathematical coordinates using computer programs. Some commercial photographic software are capable to automatically delineate points of different exposure (in here bright gridlines from the rest of photo). Berms and heaves geometry is exactly determined by merging nodes' coordinates from X, Y, Z cameras.

3.3 Model pipes

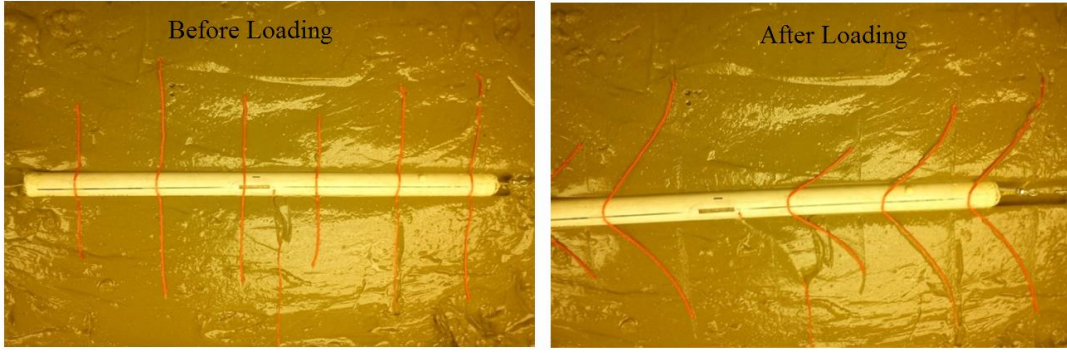
Twenty-one model tests are designed and fabricated at CIGMAT laboratory for two medium size and full-scale soil boxes. The pipes are classified into two groups: A (Non-mitigation pipe models), and M (Mitigation pipe models). Non-mitigation pipe models are classified into Axial, Lateral and Axial/Lateral categories and Mitigation pipe models are also sorted into Axial, Lateral and Axial/Lateral categories. Table 3.2 to Table 3.21 describe details of different model pipe used in this study.

Table 3.2 Summary of Pipe Models

| Class | Category | Type | Discretion | Table |
|-------|------------------------|--|---|------------|
| A | Axial (A) | A101 | Slim Axial Pipe | Table 3-3 |
| | | A102 | Short Axial Pipe | Table 3-4 |
| | Lateral(L) | ----- ----- | ----- ----- | |
| | Axial/Lateral(AL) | AL101 A, AL101 B, AL101 C | Frequent PVC pipe | Table 3-5 |
| | | AL102 METAL | Frequent Large PVC Pipe | Table 3-6 |
| | | AL103 | Frequent Metal Pipe | Table 3-7 |
| M | Axial Mitigation (MA) | MA 101 A, MA 101 B | Perforated Axial Resistors | Table 3-8 |
| | | MA 102 | Single Axial Resistors | Table 3-9 |
| | | MA 103 A, MA 103 B | Double Axial Resistors | Table 3-10 |
| | | MA 104 | Short Axial Resistors | Table 3-11 |
| | | MA105 | Double Axial Resistors with Compressive Springs | Table 3-12 |
| | | MA106 | Double Axial Resistors with Tensile Springs | Table 3-13 |
| | | MA401 | Anchored Pipe to Utility pipeline | Table 3-14 |
| | Lateral Mitigation(ML) | ML 201 A, ML 201 B | Separated Buoyancy Section | Table 3-15 |
| | | ML202 A,ML 202 B | Global Buoyancy Section | Table 3-16 |
| | | ML 203 A, ML 203 B, ML 203 C, ML 203 D | Short Buoyancy Section | Table 3-17 |

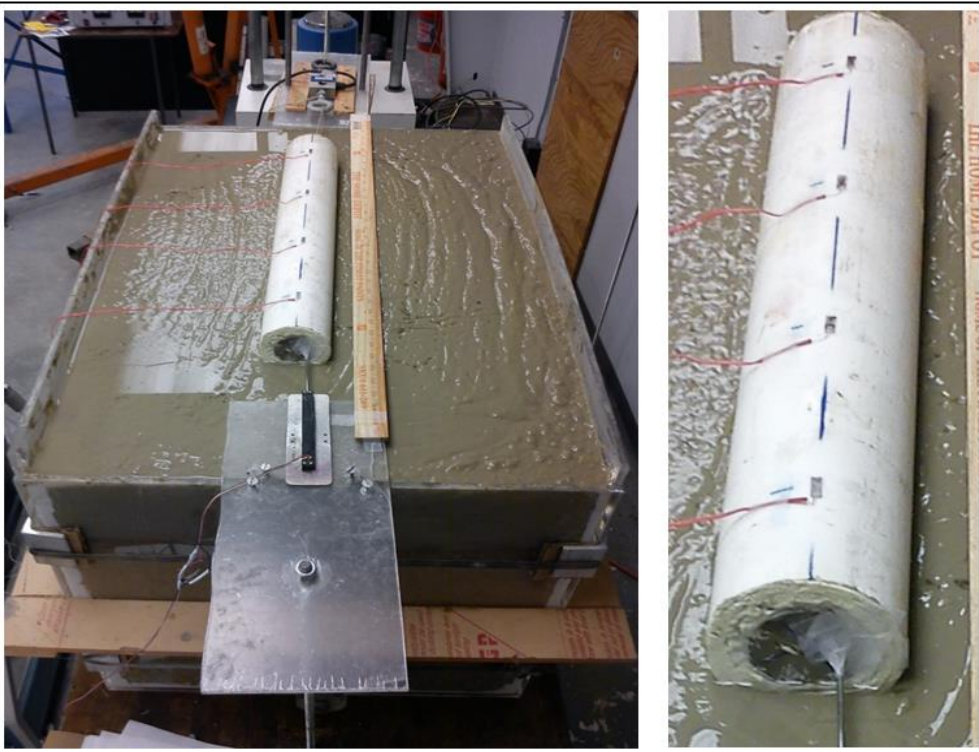
Table 3.2 (Continued)

| | | ML 204 A, ML 204 B | Single Buoyancy Section | Table 3-18 |
|---|--------------------------------------|-----------------------|-------------------------|------------|
| M | Axial/Lateral Mitigation(MAL) | MAL 301 | Medium Snake Lay | Table 3-19 |
| | | MAL 302 | Slight Snake Lay | Table 3-20 |
| | | MAL 303 | Severe Snake Lay | Table 3-21 |

Table 3.3 Details of Slim Axial Pipe


| Slim Axial Pipe | | | |
|-------------------------|------------|--------------|---------------------|
| Category: Axial Loading | | — | |
| Type: A 101 | | | |
| Total Weight (lb) | Length(in) | Diameter(in) | Wall Thickness (in) |
| 1.54 | 22.7 | 1.3 | 0.13 |

Table 3.4 Details of Short Axial Pipe



| Short Axial Pipe | | | |
|-------------------------|------------|--------------|---------------------|
| Category: Axial Loading | | | |
| Type: A 102 | | | |
| Total Weight (lb) | Length(in) | Diameter(in) | Wall Thickness (in) |
| 2.8 | 22 | 3.5 | 0.22 |

Table 3.5: Details of Frequent PVC Pipe



| <p>Frequent PVC Pipe</p> <p>Category: Axial Loading, Lateral Loading</p> <p>Type: AL 101 A, AL 101 B, AL 101 C</p> <p>101 A= 3 ft. Length</p> <p>101 B= 4 ft. Length</p> <p>101 C= 5 ft. Length</p> | | | | | | | | | |
|---|-------------------|--------------|---------------------|---------------------|------------------|-------|-----|------|--|
| <table border="1" data-bbox="208 1072 768 1220"> <thead> <tr> <th>Total Weight (lb)</th><th>Length(ft)</th><th>Diameter(in)</th><th>Wall Thickness (in)</th></tr> </thead> <tbody> <tr> <td>2.8 for AL 101 B</td><td>3,4,5</td><td>3.5</td><td>0.22</td></tr> </tbody> </table> | Total Weight (lb) | Length(ft) | Diameter(in) | Wall Thickness (in) | 2.8 for AL 101 B | 3,4,5 | 3.5 | 0.22 | |
| Total Weight (lb) | Length(ft) | Diameter(in) | Wall Thickness (in) | | | | | | |
| 2.8 for AL 101 B | 3,4,5 | 3.5 | 0.22 | | | | | | |

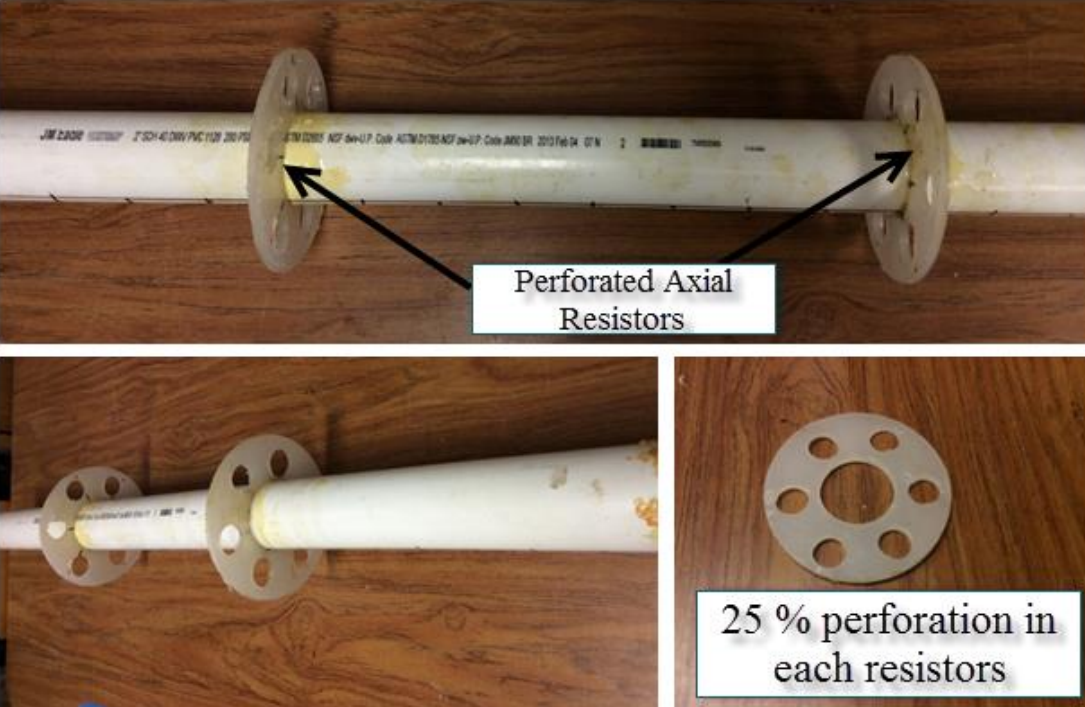
Table 3.6 Details of Frequent Large PVC Pipe

|  |  | | |
|---|--|--------------|---------------------|
| Frequent Large PVC Pipe | | | |
| Category: Axial Loading, Lateral Loading | | | |
| Type: AL 102 | | | |
| Total Weight (lb) | Length(ft) | Diameter(in) | Wall Thickness (in) |
| 33 | 4 | 8.5 | 0.34 |

Table 3.7 Details of Frequent Metal Pipe

|  | | | |
|---|------------|--------------|---------------------|
| Frequent Metal Pipe | | | M E T A L |
| Category: Axial Loading, Lateral Loading | | | |
| Type: AL 103 METAL | | | |
| Total Weight (Ib) | Length(ft) | Diameter(in) | Wall Thickness (in) |
| 30.28 | 4 | 3 | 0.22 |

Table 3.8 Details of Perforated Axial Resistors



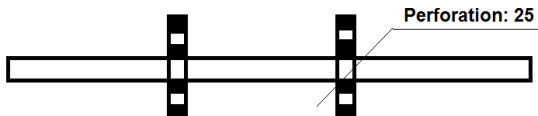
| | | | | | | | | |
|--|-------------|--------------------|---------------------|-----------------------|--------------------------|--------------------|-------------------------------|--|
| <p>Perforated Axial Resistors</p> <p>Category: Axial Mitigation</p> <p>Type: MA 101 A and MA 101 B</p> <p>A= 25 % perforation</p> <p>B=15 % perforation</p> | | | | | | | |  |
| Weight (lb) | Length (ft) | Pipe Diameter (in) | Number of Resistors | Resistor Spacing (in) | Resistors thickness (in) | Resistors Diameter | Weight of Each Resistors (lb) | |
| 2.68 | 4 | 2.4 | 2 | 16 | 0.25 | 6 | 0.2 | |

Table 3.9 Details of Single Axial Resistors

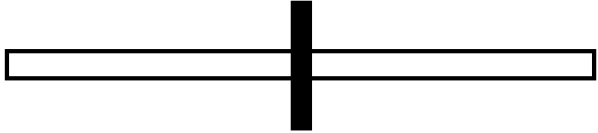
|  | | | | | | |
|--|-------------|--|---------------------|--------------------------|--------------------|-------------------------------|
| Single Axial Resistors | | | | | | |
| Category: Axial Mitigation | |  | | | | |
| Type: MA 102 | | | | | | |
| Total Weight(lb) | Length (ft) | Pipe Diameter (in) | Number of resistors | Resistors thickness (in) | Resistors Diameter | Weight of Each Resistors (lb) |
| 3.4 | 4 | 2.4 | 2 | 1/4 | 6 | 0.2 |

Table 3.10 Details of Double Axial Resistors

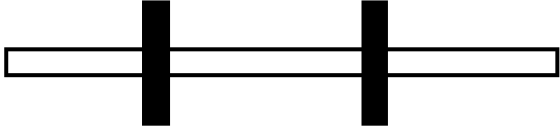
|  | | | | | | |
|--|-------------|--------------------|---|--------------------------|--------------------|-------------------------------|
| <p>Double Axial Resistors</p> <p>Category: Axial Mitigation</p> <p>Type: MA 103 A, MA 103 B</p> <p>A= 3 ft Pipe Length</p> <p>B= 4 ft Pipe Length</p> | | |  | | | |
| Total Weight (lb) | Length (ft) | Pipe Diameter (in) | Number of resistors | Resistors thickness (in) | Resistors Diameter | Weight of Each Resistors (lb) |
| A= 2.9 B= 3.75 | 3 and 4 | 2.4 | 2 | 1/4 | 6 | 0.2 |

Table 3.11 Details of Short Axial Resistors

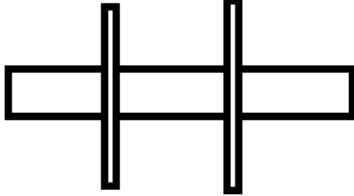
|  | | | | | | | |
|--|-------------|--------------------|---------------------|---|--------------------|-------------------------------|--|
| Short Axial Resistors Category: Axial Mitigation Type: M 104 | | | |  | | | |
| Total Weight (lb) | Length (ft) | Pipe Diameter (in) | Number of resistors | Resistors thickness (in) | Resistors Diameter | Weight of Each Resistors (lb) | |
| 2.25 | 15 | 3.5 | 2 | 1/8 | 6 | 0.14 | |

Table 3.12 Details of Double Axial Resistors with Compressive Springs

| | | | | | | | | | | |
|---|-------------|--------------------|-------------------------|---------------------------------------|-------------------|-------------------------------|--------------------|-------------------------|------------------------------|--|
| | | | | | | | | | | |
| Double Axial Resistors with Compressive Springs Category: Axial Mitigation Type: MA 105 | | | | | | | | | | |
| Weight (lb) | Length (in) | Pipe Diameter (in) | Resistor Thickness (in) | Resistors Spacing (in) Before Loading | Number of springs | Each Spring Stiffness (lb/in) | Number of Resistor | Resistors Diameter (in) | Weight of Each Resistor (lb) | |
| 2.24 | 15 | 3.5 | 1/8 | 1.5 | 6 | 6.7 | 2 | 6 | 0.15 | |

Table 3.13 Details of Double Axial Resistors with Tensile Springs

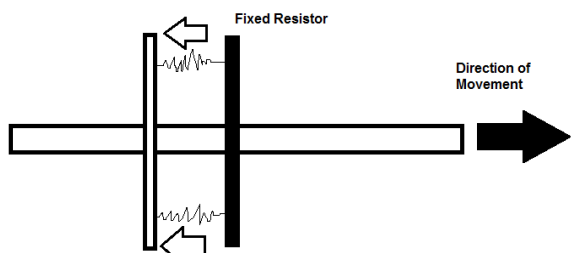
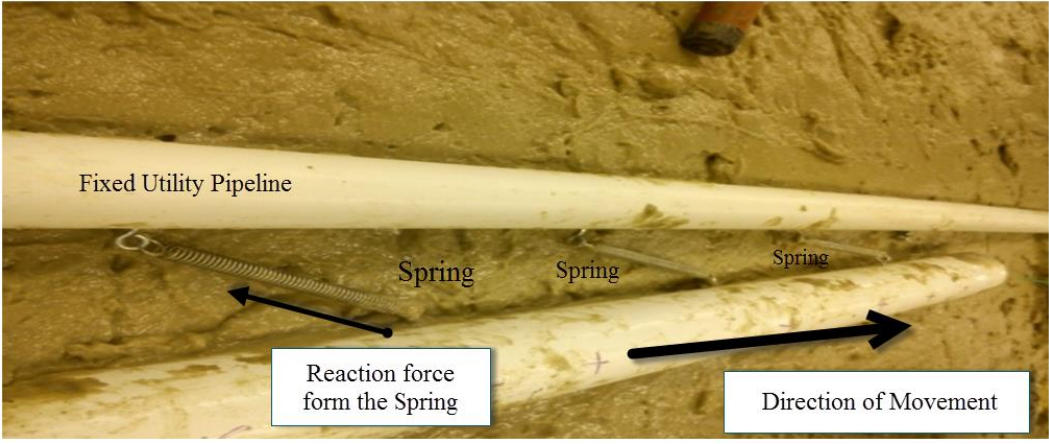
|  | | | | | | | | | | | |
|---|-------------|--------------------|-------------------------|---|-------------------|-------------------------------|---------------------|-------------------------|-------------------------------|--|--|
| <p>Double Axial Resistors with Tensile Springs</p> <p>Category: Axial Mitigation</p> <p>Type: MA 106</p> | | | |  | | | | | | | |
| Weight (Ib) | Length (in) | Pipe Diameter (in) | Resistor Thickness (in) | Resistors Spacing Before Loading (in) | Number of Springs | Each Spring Stiffness (Ib/in) | Number of Resistors | Resistors Diameter (in) | Weight of Each Resistors (Ib) | | |
| 2.24 | 15 | 3.5 | 1/8 | 4 | 6 | 0.5 | 2 | 6 | 0.15 | | |

Table 3.14 Details of pipe anchored to other pipe



The photograph shows a horizontal "Fixed Utility Pipeline" in a trench. Three coiled springs are attached to the pipe at different points. A black arrow labeled "Reaction force from the Spring" points towards the pipe from the left, and another black arrow labeled "Direction of Movement" points away from the pipe to the right.

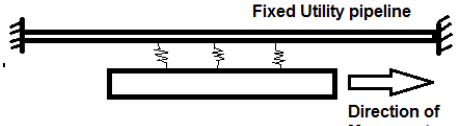
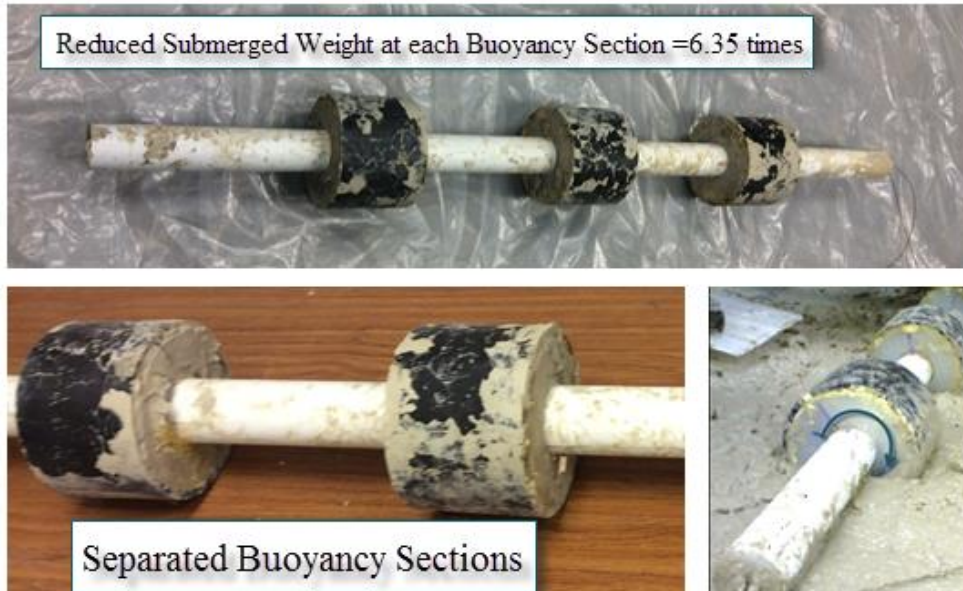
| Anchored Pipe to Utility pipeline Category: Axial Mitigation Type: MA 401 | | | | | | | | |  <p>The schematic shows a horizontal "Fixed Utility pipeline" with two vertical supports. A second horizontal pipe, representing the "Moving Pipe", is shown to the right, with an arrow pointing to the right labeled "Direction of Movement".</p> |
|--|-------------------------|---------------------------|------------------------|--------------------------|-------------------|-------------------------|-------------------------------|--|---|
| Moving Pipe Weight (lb) | Moving Pipe Length (ft) | Moving Pipe Diameter (in) | Fixed Pipe Length (ft) | Fixed Pipe Diameter (in) | Number of Springs | Spacing Between Springs | Each Spring Stiffness (lb/in) | Spacing Between Two Pipes Before Loading | |
| 2.15 | 3 | 2.4 | 8 | 1.3 | 3 | 7.5 | 0.39 | 3.2 | |

Table 3.15 Details of Separated Buoyancy Sections



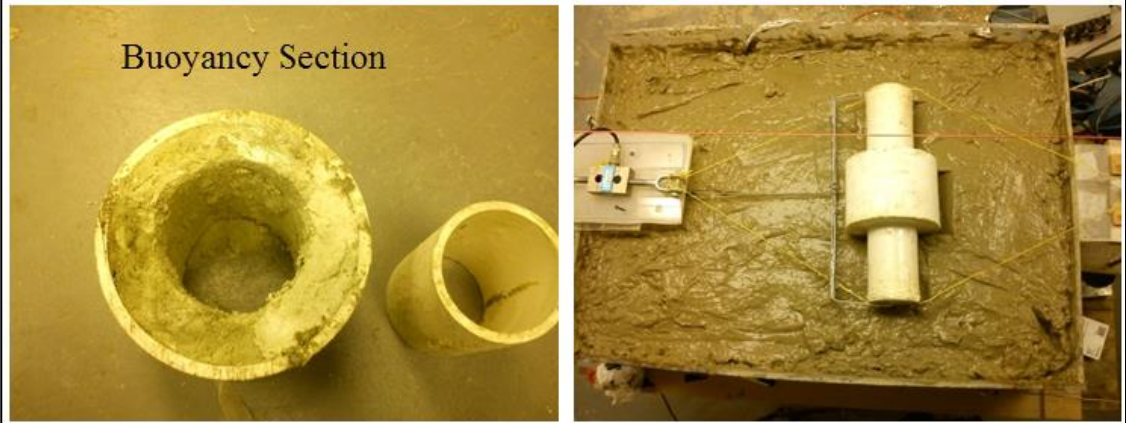
| | | | | | | | | | |
|--|-------------|--------------------|----------------------|-----------------------|--|------------------------|-------------------------|---|--|
| <p>Reduced Submerged Weight at each Buoyancy Section =6.35 times</p> <p>Separated Buoyancy Sections</p> | | | | | | | | | |
| <p>Separated Buoyancy Sections</p> <p>Category : Lateral Mitigation</p> <p>Type: ML 201A, ML 201 B</p> <p>A=Fixed Buoyancy</p> <p>B= Rolling /Free Buoyancy</p> | | | | |  | | | | |
| Total Weight (lb) | Length (ft) | Pipe Diameter (in) | Number of Buoyancies | Buoyancy Spacing (in) | Buoyancy Length (in) | Buoyancy Diameter (in) | Weight of Each Buoyancy | Reduced Submerged Weight at Buoyancy Sections | |
| 11.75 | 5 | 2.4 | 2 | 10 | 5 | 6.5 | 2.1 | 6.5 times | |

Table 3.16 Details of Global Buoyancy Sections



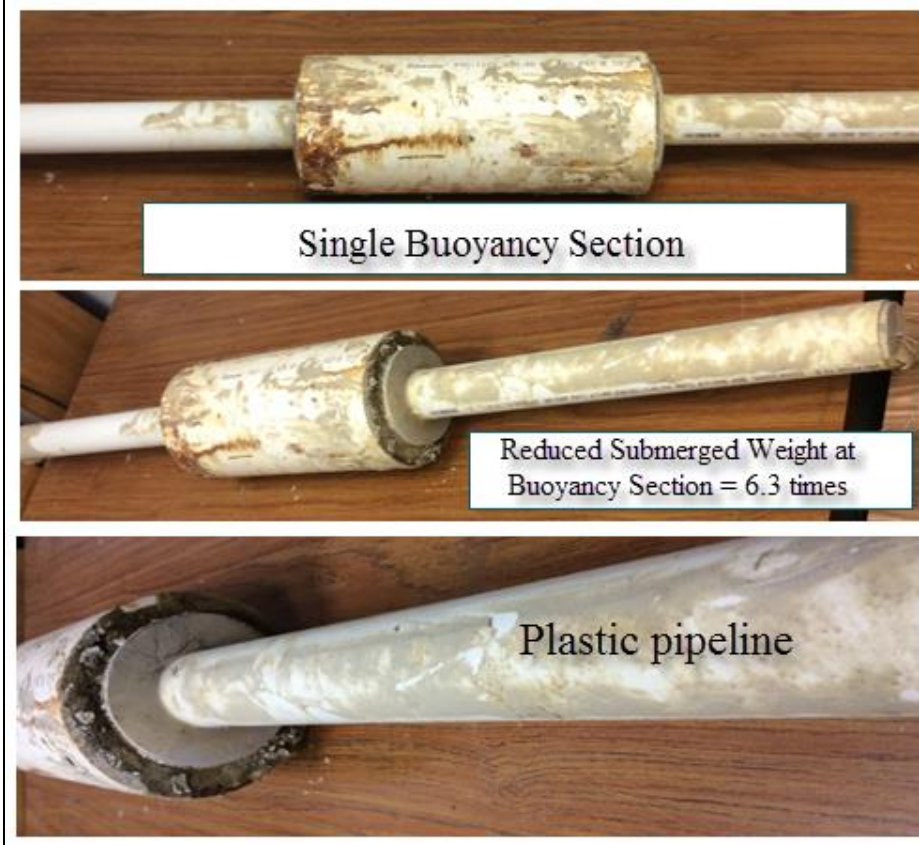
| <p>Global Buoyancy Sections</p> <p>Category: Lateral Mitigation</p> <p>Type: ML 202 A , ML 202 B</p> <p>A= Fixed Buoyancy</p> <p>B=Rotating / Free Buoyancy</p> |  | | | | | | | | | | | | | | | | | | |
|---|--|--------------------|----------------------|----------------------|--------------------------------------|--------------------------------------|-------------------------------------|---|---|------|-----|-----|----|---|----|-----|------|------------|--|
| <table border="1"> <thead> <tr> <th>Total Weight (Ib)</th> <th>Length (in)</th> <th>Pipe Diameter (in)</th> <th>Buoyancy Length (in)</th> <th>Number of Buoyancy</th> <th>Buoyancy Spacing (face to face) (in)</th> <th>Buoyancy Section Diameter (in)</th> <th>Weight of Each Buoyancy Section(Ib)</th> <th>Reduced Submerged Weight at each Buoyancy Section</th> </tr> </thead> <tbody> <tr> <td>12.3</td> <td>6.5</td> <td>2.4</td> <td>10</td> <td>2</td> <td>25</td> <td>4.5</td> <td>2.55</td> <td>2.11 times</td> </tr> </tbody> </table> | Total Weight (Ib) | Length (in) | Pipe Diameter (in) | Buoyancy Length (in) | Number of Buoyancy | Buoyancy Spacing (face to face) (in) | Buoyancy Section Diameter (in) | Weight of Each Buoyancy Section(Ib) | Reduced Submerged Weight at each Buoyancy Section | 12.3 | 6.5 | 2.4 | 10 | 2 | 25 | 4.5 | 2.55 | 2.11 times | |
| Total Weight (Ib) | Length (in) | Pipe Diameter (in) | Buoyancy Length (in) | Number of Buoyancy | Buoyancy Spacing (face to face) (in) | Buoyancy Section Diameter (in) | Weight of Each Buoyancy Section(Ib) | Reduced Submerged Weight at each Buoyancy Section | | | | | | | | | | | |
| 12.3 | 6.5 | 2.4 | 10 | 2 | 25 | 4.5 | 2.55 | 2.11 times | | | | | | | | | | | |

Table 3.17 Details of Short Buoyancy Sections



| <p>short Buoyancy Sections</p> <p>Category: Lateral Mitigation</p> <p>Type: ML 203 A , M 203 B, M 203 C, ML 203 D</p> <p>A= Fixed Lighter Buoyancy</p> <p>B=Rotating / Free Lighter Buoyancy</p> <p>C=Fixed Heavier Buoyancy</p> <p>D=Rotatory/ Free Lighter Buoyancy</p> |  | | | | | | | | | | | | | | | | | | |
|---|---|--------------------|----------------------|----------------------|--------------------------------------|--------------------------------------|-------------------------------------|---|---|------|------|-----|---|---|---|-----|-------------------|--|--|
| <table border="1"> <thead> <tr> <th>Total Weight (lb)</th><th>Length (in)</th><th>Pipe Diameter (in)</th><th>Buoyancy Length (in)</th><th>Number of Buoyancy</th><th>Buoyancy spacing (face to face) (in)</th><th>Buoyancy Section Diameter (in)</th><th>Weight of Each Buoyancy Section(lb)</th><th>Reduced Submerged Weight at Each Buoyancy Section</th></tr> </thead> <tbody> <tr> <td>3.95</td><td>15.5</td><td>3.5</td><td>5</td><td>1</td><td>-</td><td>6.5</td><td>A=1.65, C=2.21</td><td>A=2.94 times and C=2.43 times</td></tr> </tbody> </table> | Total Weight (lb) | Length (in) | Pipe Diameter (in) | Buoyancy Length (in) | Number of Buoyancy | Buoyancy spacing (face to face) (in) | Buoyancy Section Diameter (in) | Weight of Each Buoyancy Section(lb) | Reduced Submerged Weight at Each Buoyancy Section | 3.95 | 15.5 | 3.5 | 5 | 1 | - | 6.5 | A=1.65, C=2.21 | A=2.94 times and C=2.43 times | |
| Total Weight (lb) | Length (in) | Pipe Diameter (in) | Buoyancy Length (in) | Number of Buoyancy | Buoyancy spacing (face to face) (in) | Buoyancy Section Diameter (in) | Weight of Each Buoyancy Section(lb) | Reduced Submerged Weight at Each Buoyancy Section | | | | | | | | | | | |
| 3.95 | 15.5 | 3.5 | 5 | 1 | - | 6.5 | A=1.65, C=2.21 | A=2.94 times and C=2.43 times | | | | | | | | | | | |

Table 3.18 Details of Single Buoyancy Sections



| <p>Single Buoyancy Sections</p> <p>Category: Lateral Mitigation</p> <p>Type: ML 204 A , ML 204 B</p> <p>A= Fixed Buoyancy</p> <p>B=Rotating / Free Buoyancy</p> | | | | | | | |
|--|-------------|----------------------|--------------------|--------------------|-----------------------|--------------------------------------|---|
| Total Weight (Ib) | Length (ft) | Buoyancy Length (in) | Number of Buoyancy | Pipe Diameter (in) | Buoyancy Diameter(in) | Weight of Each Buoyancy Section (Ib) | Reduced Submerged Weight at Each Buoyancy Section |
| 15 | 5 | 17 | 1 | 2.4 | 6.5 | 11.08 | 4.35 times |

Table 3.19 Details of Medium Snake Lay Pipe

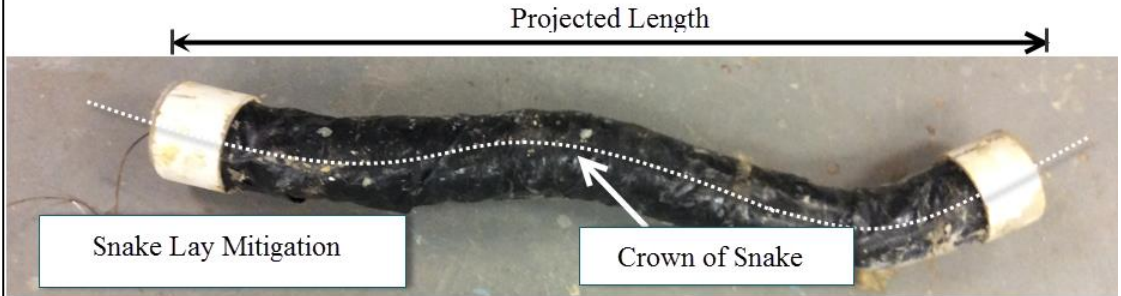
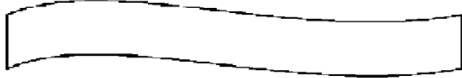
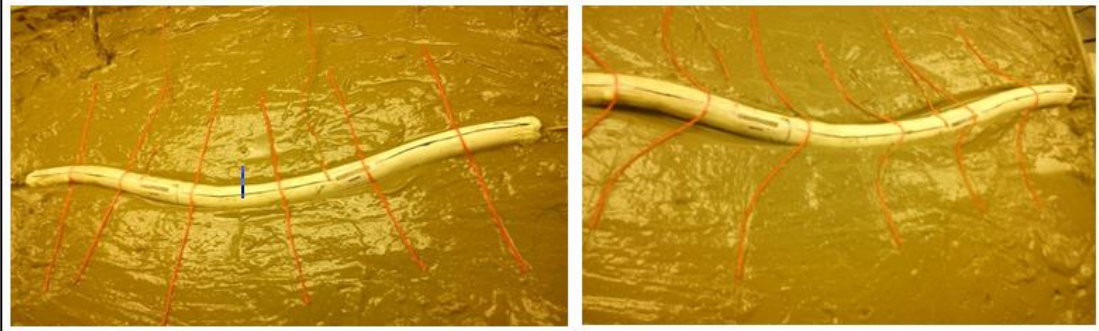
|  <p>Projected Length</p> <p>Snake Lay Mitigation</p> <p>Crown of Snake</p> | | | | |
|--|-------------|-----------------------|--------------------------|---|
| Medium Snake Lay | | | | |
| Category: Axial and Lateral Mitigation | | | |  |
| Type: MAL 301 | Weight (lb) | Projected Length (in) | Out of Straightness (in) | Increased Axial Length Due to Snaking (%) |
| | 2.9 | 40 | 5.1 | 3.5 |

Table 3.20 Details of Slight Snake Lay

|  | | | | |
|--|----------------------|--|---|---------------|
| Slight Snake Lay | |  | | |
| Category: Axial and Lateral Mitigation | | | | |
| Type: MAL 302 | | | | |
| Weight (lb) | Projected Length(in) | Out of Straightness (in) | Increased Axial Length Due to Snaking (%) | Diameter (in) |
| 2.9 | 23.5 | 1.1 | 4 | 3.5 |

Table 3.21 Details of Severe Snake Lay



| <table border="1"> <tr> <td colspan="2">Severe Snake Lay</td><td colspan="3"></td></tr> <tr> <td colspan="2">Category: Axial and Lateral Mitigation</td><td colspan="3">  </td></tr> <tr> <td colspan="2">Type: MAL 303</td><td colspan="3"></td></tr> <tr> <th>Weight (lb)</th><th>Projected Length(in)</th><th>Out of Straightness (in)</th><th>Increased Axial Length Due to Snaking (%)</th><th>Diameter (in)</th></tr> <tr> <td>1.54</td><td>23.5</td><td>3.5</td><td>16</td><td>1.3</td></tr> </table> | | Severe Snake Lay | | | | | Category: Axial and Lateral Mitigation | |  | | | Type: MAL 303 | | | | | Weight (lb) | Projected Length(in) | Out of Straightness (in) | Increased Axial Length Due to Snaking (%) | Diameter (in) | 1.54 | 23.5 | 3.5 | 16 | 1.3 | | | |
|---|----------------------|--|---|---------------|--|--|--|--|--|--|--|----------------------|--|--|--|--|-------------|----------------------|--------------------------|---|---------------|------|------|-----|----|-----|--|--|--|
| Severe Snake Lay | | | | | | | | | | | | | | | | | | | | | | | | | | | | | |
| Category: Axial and Lateral Mitigation | |  | | | | | | | | | | | | | | | | | | | | | | | | | | | |
| Type: MAL 303 | | | | | | | | | | | | | | | | | | | | | | | | | | | | | |
| Weight (lb) | Projected Length(in) | Out of Straightness (in) | Increased Axial Length Due to Snaking (%) | Diameter (in) | | | | | | | | | | | | | | | | | | | | | | | | | |
| 1.54 | 23.5 | 3.5 | 16 | 1.3 | | | | | | | | | | | | | | | | | | | | | | | | | |

3.4 Summary

Full scale soil box with area of 64 ft^2 , medium-size soil box with glass sides and Twenty-one model pipes were designed, built and instrumented exclusively for the purpose of this study at CIGMAT laboratory. In order to realistically simulate subsea pipe soil interaction, soil with undrained shear strength of 0.02 kPa to 0.2 kPa was prepared and maintained during 143 axial and lateral loading tests. The main contribution of this chapter was Introducing:

(1) Lateral Loading Frame: The key advantages of these loading frame was minimum external influence during loading and the capability of changing pipe boundary from free to fixed.

(2) Reflective Gridding System: RGS help cameras better synchronize pipe movement and soil deformation at any time increment. By using RGS, surface displacement field of soil particles and induced berms and heaves during axial and lateral loading are quantitatively measurable.

Chapter 4. AXIAL PIPE SOIL INTERACTION

4.1 Experimental

At the CIGMAT Laboratory several physical models have been designed and constructed to investigate the behavior of various types of pipes on the simulated sea bed. Series of large scale model tests were performed by loading the pipes from the ends and using instrumented pipes of various types (steel, plastic) and sizes (up to 200 mm in diameter) placed on the soft clay soil (undrained shear strength ranged from 0.01 kPa to 0.11 kPa) to better quantify the axial soil-pipe interactions. The variations of the frictional parameter with the type and size of pipe, axial rate of loading and weight of the pipe and other parameters have been quantified.



Figure 4.1: Axial pipe sliding in CIGMAT full scale soil tank

4.1.1 Parametric study

The main focus of this chapter was to investigate the various factors influencing the axial sliding frictional resistance (ϕ) (also named “frictional factor” or “frictional factor”). This

frictional resistance is defined as $\frac{F}{W} = \tan(\phi)$, where F is the axial force and W is the vertical load.

4.1.1.1 Effect of Pipeline Material

A plastic pipe with a length of 1.22 m (4 ft) and diameter of 61 mm (2.4 in) with a dead load of 0.003kN/m (2.4 lb/ft) (Type: AL 101 as discussed in chapter 3) and a steel pipe of same diameter and length with the dead load of 0.01kN/m (7.57 lb/ft) (Type: AL 103 METAL) were used for this study. The undrained shear strength of soil was 0.03 kPa (0.0043 psi) which measured before during and after each test to ensure soil consistency. For both plastic and steel pipes, the initial penetration of 10 mm (0.4 in), 16 % of the pipe diameter (0.16D), was observed after 24 hours laying of pipe on the soil. With the constant rate of horizontal displacement of 0.05 in/min, the plastic pipe had a partial penetration into the soil of 25mm (1 in), 42% of the pipe diameter (0.42D) after horizontal displacement of 190 mm (7.5 in). As shown in Figure 4.3, the plastic pipe reached a steady state of frictional resistance ($\tan(\phi)$) of 0.17 at a displacement of 3.36 inch or 140% of diameter. In addition, step frictional development was observed for plastic pipe, that is, axial break out resistance of 0.21 was developed in two steps. First, at a relative displacement of 0.1 D, the pipe reached a frictional resistance of 0.175 and then at a relative displacement of 0.4 D, the pipe reached frictional resistance of 0.2 (Figure 4.3).

For the metal pipe, the partial penetration of 0.8 in, 33% of the pipe diameter (0.33D) was detected (0.33D) after horizontal displacement of 213 mm (8.4 in). The pipe penetration was higher than what has been predicted from the relationships in the literature. The sliding pipe smoothly reached to the maximum steady state of frictional resistance ($\tan(\phi)$) of 0.145 at a displacement of 165 mm (6.48 in) or 270% of diameter (2.7D) without any break out resistance.

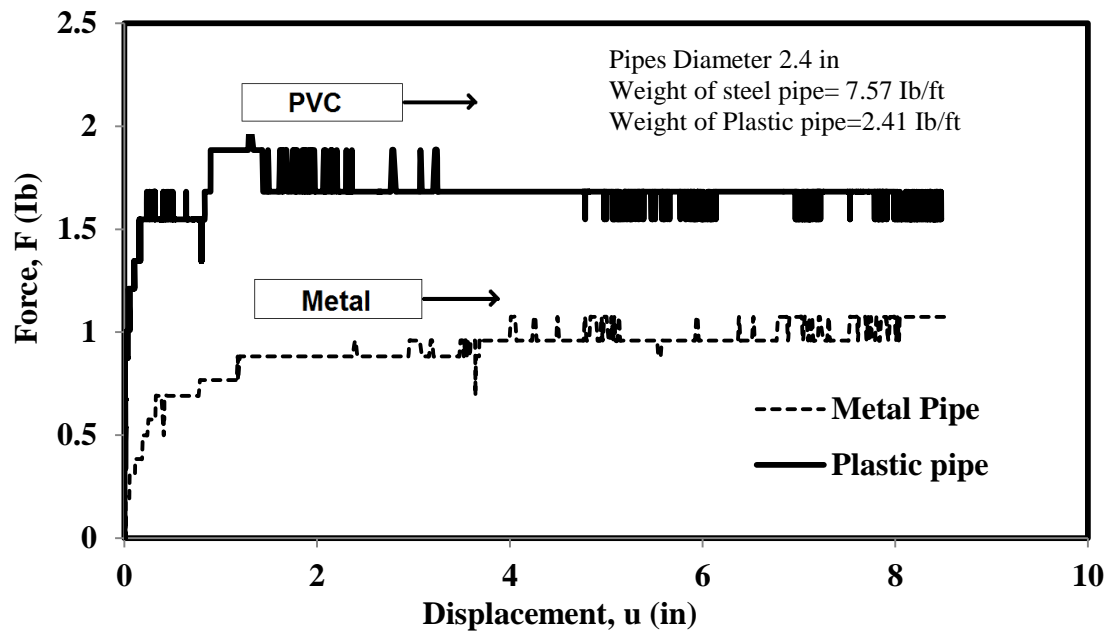


Figure 4.2: Force-displacement responses for steel and plastic pipes

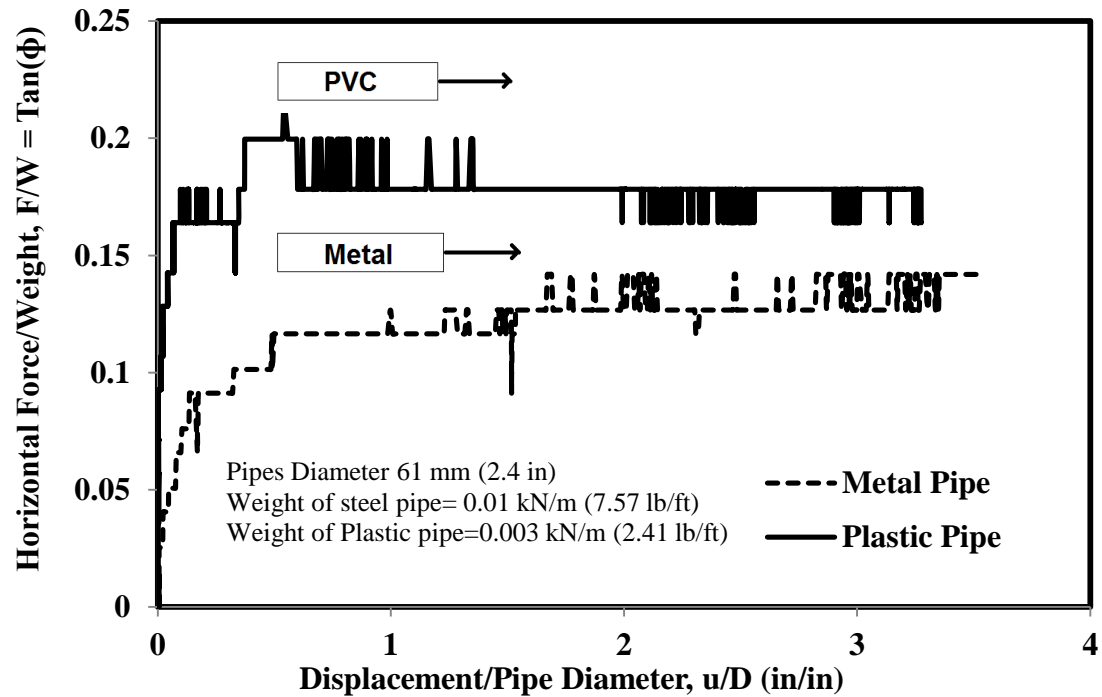


Figure 4.3: Pipe-soil interaction responses for steel and plastic pipes

The steady state (residual) of frictional resistance for plastic pipe was 17% more than steel pipe. One reason could be the difference in penetration of pipeline during the test. However, the major difference stems from the pattern of soil deformation in the interface of pipe and soil. As shown in Figure 4.4, the soil in the plastic interface tends to adhere to pipe and form outward heaves in the vicinity of pipe, yet, this behavior was rarely observed in the steel interface during axial loading.

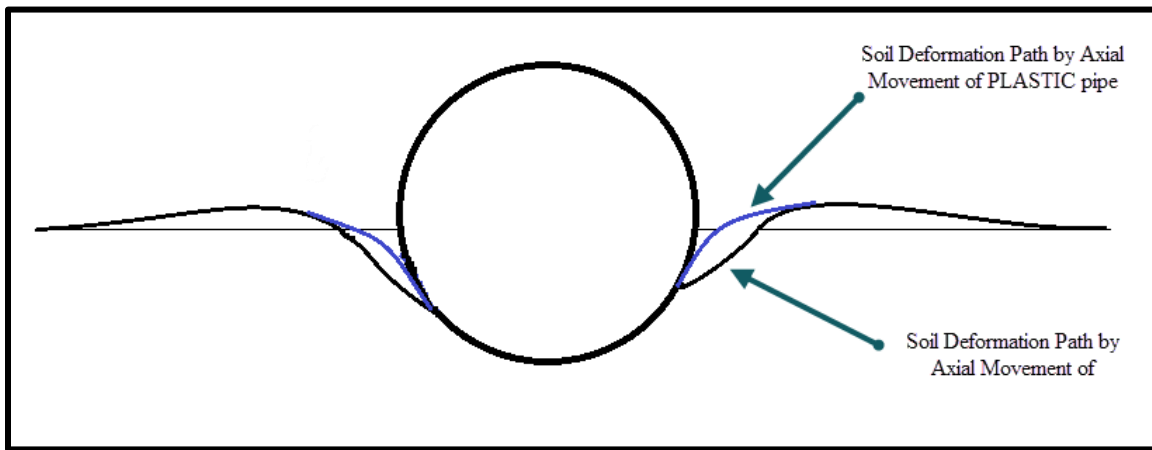


Figure 4.4: Schematic of soil contact with steel and plastic pipes during axial sliding

4.1.1.2 Effect of Soil Shear Strength

To study the effect of undrained shear strength on axial responses, a plastic pipe with a length of 1.22 m (4 ft) and diameter of 61 mm (2.4 in) with a dead load of 0.003kN/m (2.4 lb/ft) (Type: L 101 B) was laid first on 0.01 kPa (0.0015psi) soil for 24 hours to study initial penetration. Then, the axial test was performed with the constant rate of 1.3 mm/min (0.05 in/min). Later, the same test was repeated with soil shear strength of 0.11 kPa (0.016 psi). Continuous measurement of undrained shear strength before, after and during the test with reasonable time interval performed in five area of soil box to ensure soil homogeneity. For the first soil sample ($S_u=0.01$ kPa) the initial penetration was 15 mm (0.6 in), 25 % of the pipe

diameter, 1 day after laying pipe. The pipe demonstrated a partial penetration of 33 mm (1.3 in), 54% of the pipe diameter after horizontal displacement of 3.6D. As shown in Figure 4.5, the sliding pipe reached a steady state resistance of 0.148 at a displacement of 55 mm (2.16 in) or 90% of diameter (0.9D).

The second test ($S_u=0.11$) with the initial penetration of 9 mm (0.35 in) and partial penetration of 20 mm (0.8 in) at the horizontal displacement of 3.2D, reached a steady state of frictional resistance ($\tan(\phi)$) of 0.22 at a displacement of 130 mm (5.1 in) or 150% of diameter. In this test, the axial break out frictional factor (resistance) of 0.25 was detected after displacement 48 mm (1.9 in) or 81% of diameter. With about 10 times increase in undrained shear strength of the soil, the steady state of (residual)axial sliding resistance increased by 80% (see Figure 4.5).

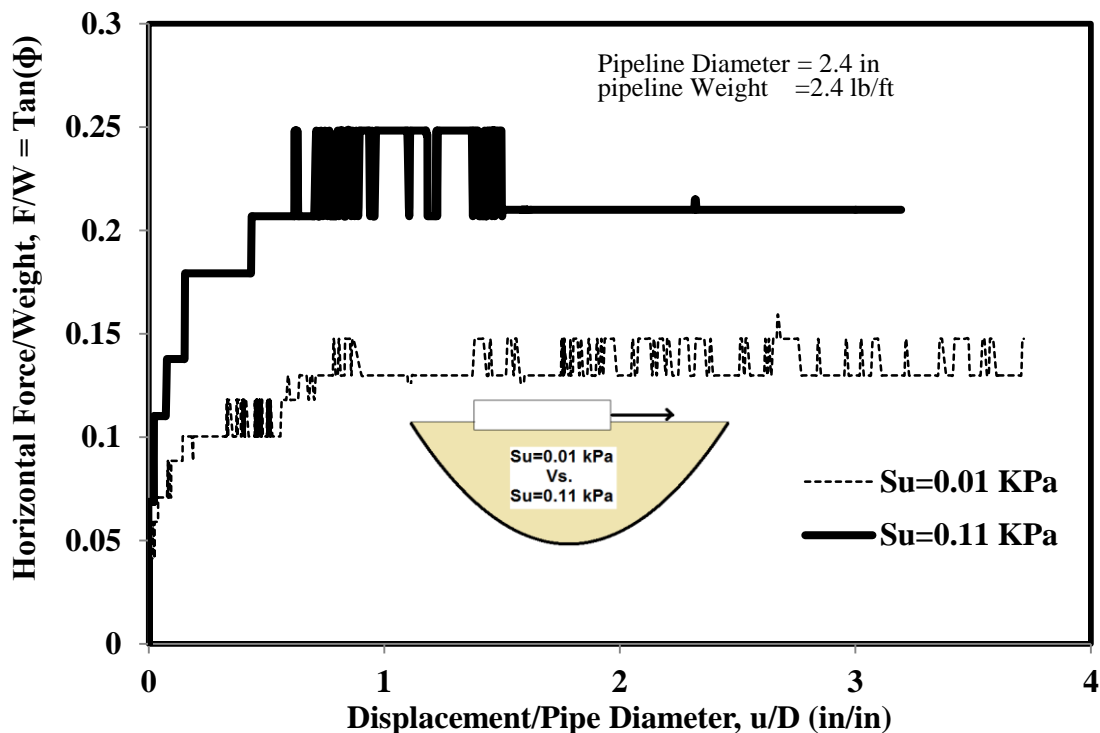


Figure 4.5: Effect of undrained shear strength on pipe soil interaction

4.1.1.3 Effect of Weight of Pipeline

A plastic pipe with a length of 1.22 m (4 ft) and diameter of 61 mm (2.4 in) was used for this study (Type: AL 101 B). The dead load increased from 0.001 kN/m (0.73 lb/ft) to 0.003 kN/m (2.4 lb/ft) over 320% increases in vertical load. At the end of the test, the light pipe penetrated into the soil approximately 13 mm (0.5 in), 21% of the pipe diameter. Due to the increase in the dead load of the pipe, the pipe penetration increased by about 10 mm (0.4 in) which is 80% increase over the pipe with dead load of 0.001 kN/m (0.73 lb/ft). The maximum axial frictional resistance (horizontal force/ weight) for both heavy and light pipe was 0.185 (Figure 4.7). The results show that the weight of the pipe had minimal effect on the frictional coefficient within the studied range under the monotonic loading.

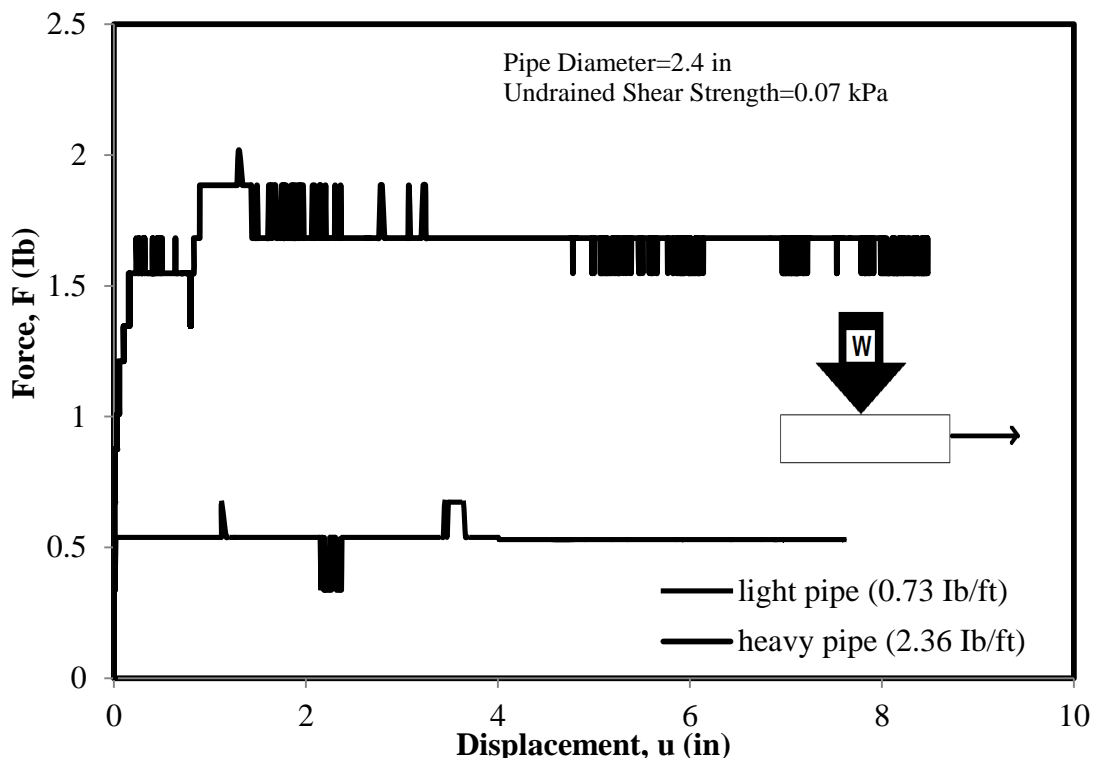


Figure 4.6: Axial force-displacement responses for two pipes with different vertical load laid on the same soil

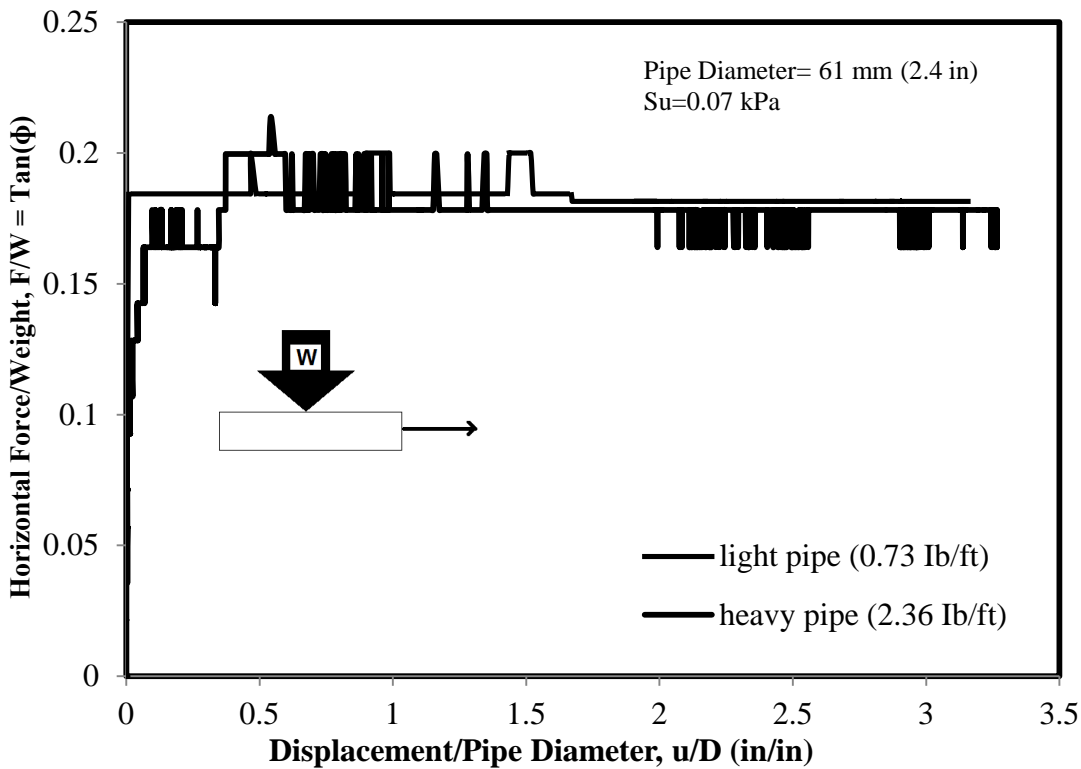


Figure 4.7: Effect of vertical force (weight of pipe) on the axial pipe soil interaction

4.1.1.4 Effect of Pipe Size

Two plastic pipes with length of 1.22 m (4 ft) and diameter of 61 mm (2.4 in) as “small pipe” (Type: AL 101 B) and 216 mm (8.5 in) as “big pipe” (Type: AL 102) was used for this part of study. The axial test was performed with the constant rate of 1.3 mm/min (0.05 in/min) for both small and big pipe. The undrained shear strength was 0.07 kPa and continuous measurement of undrained shear strength before, after and during the test with reasonable time interval performed to ensure soil homogeneity. The small pipe reached a steady state resistance of 0.185 at a very small displacement of 3 mm (0.16 in) or 5% of diameter (0.05D) instantly and no break out resistance was observed (Figure 4.8). However, big pipe reached a steady state resistance of 0.18 with a very gradual attitude at displacement of 496 mm (19.55 in) or 230 % of diameter (2.3 D) and the break out resistance of 0.204 observed after axial displacement of 18 in

which is close to onset of residual (steady state) resistance. The results suggested that the size of the pipe had minimal effect on the frictional coefficient within the studied range under the monotonic loading.

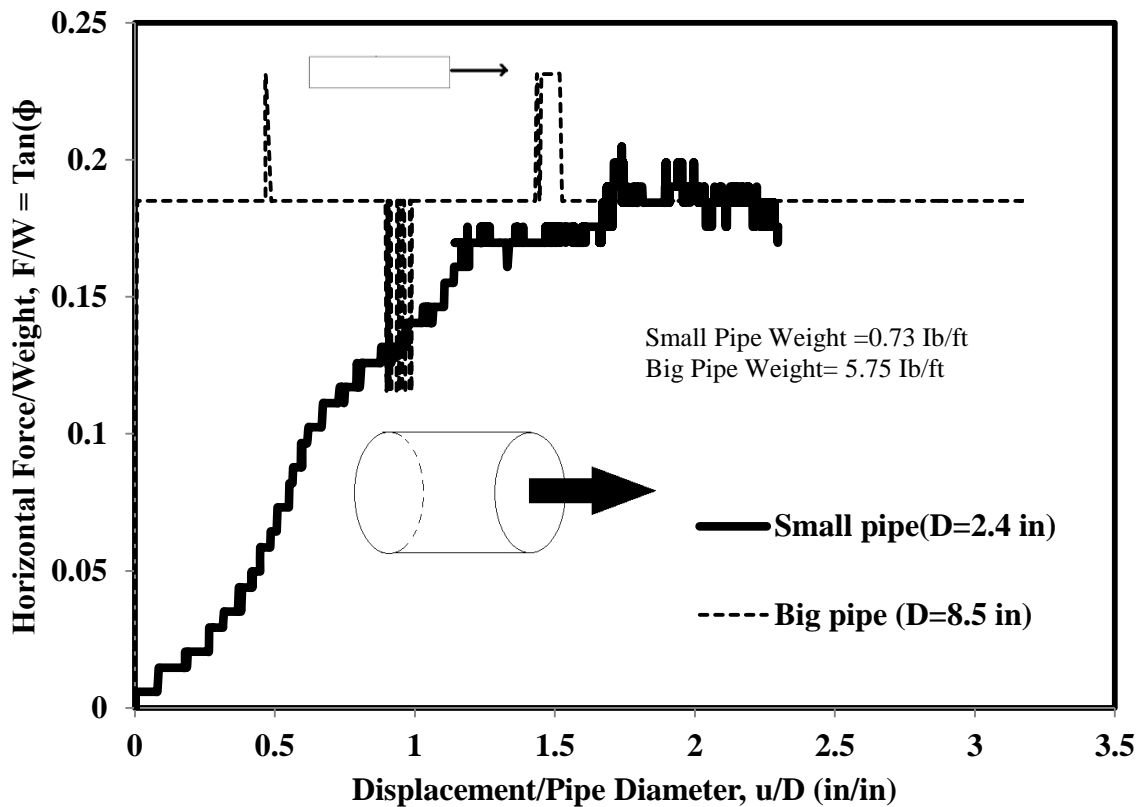


Figure 4.8 Effect of pipe size (diameter) on the axial pipe soil interaction

Effects of cyclic loading on penetration and force-displacement responses of small pipe (Type: AL 102 B) is discussed later in this chapter. Nevertheless, a brief history of soil deformation and the consequent berms for both small and big pipes are represented in Figure 4.9. The major dissimilarity in penetration of small and big pipe is that, for big pipes the soil berms are smoother in the vicinity of pipe but for the small pipe the soil berms are heightened and after the third cycle the berms are accumulated notably. The results are collected from RGS which discussed in the previous chapter.

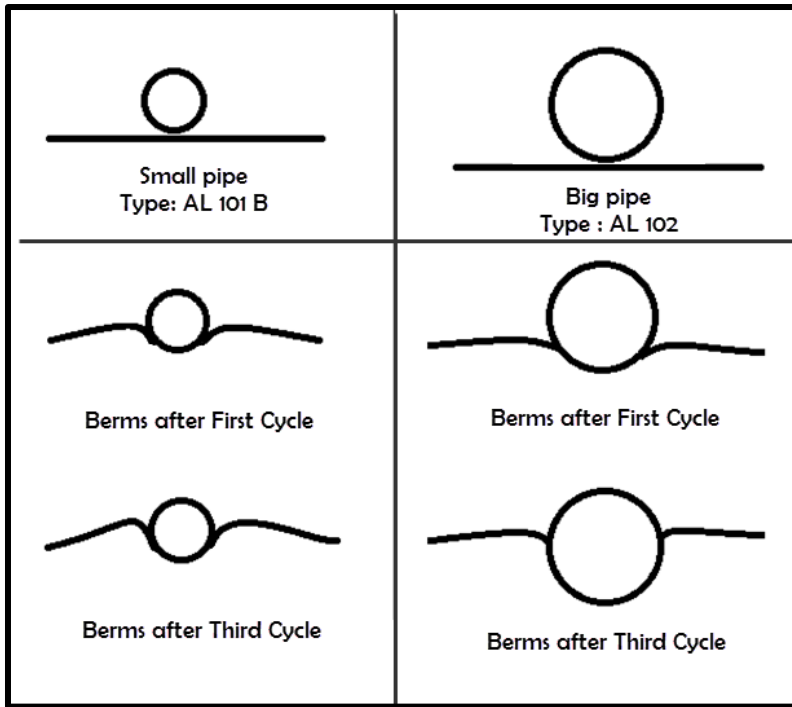


Figure 4.9: Schematic of soil deformation path during axial cyclic loading for small ($D=2.4\text{in}$) and large ($D=8.5\text{in}$) pipe

4.1.1.5 Effect of Rate of Loading

A plastic pipe with a length of 1.22 m (4 ft) and diameter of 61 mm (2.4 in) with a dead load of 0.003kN/m (2.4 lb/ft) and displacement rates of 2.54mm/min (0.1 in/min), 26mm/min (1.02 in/min) and 127 mm/min (5 in/min) was used in this part of study. With increase in the rate of displacement the steady state of frictional resistance ($\tan(\phi)$) reduced respectively by 13% and 35%, but the peak value was attained almost at the same displacement of 30.5 mm (1.2 in), equivalent to about 50% of the pipe diameter. The maximum axial frictional factor (horizontal force/ weight) was 0.31 which was observed for slow rate of loading (Figure 4.10 and Figure 4.11).

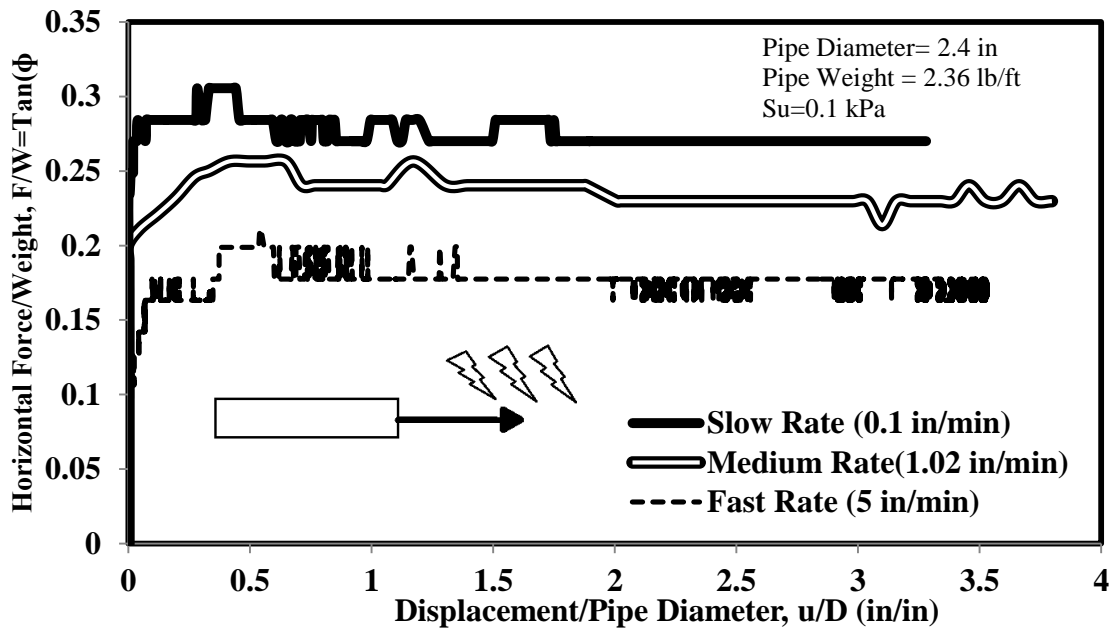


Figure 4.10: Axial force-displacement responses for different rate of loading

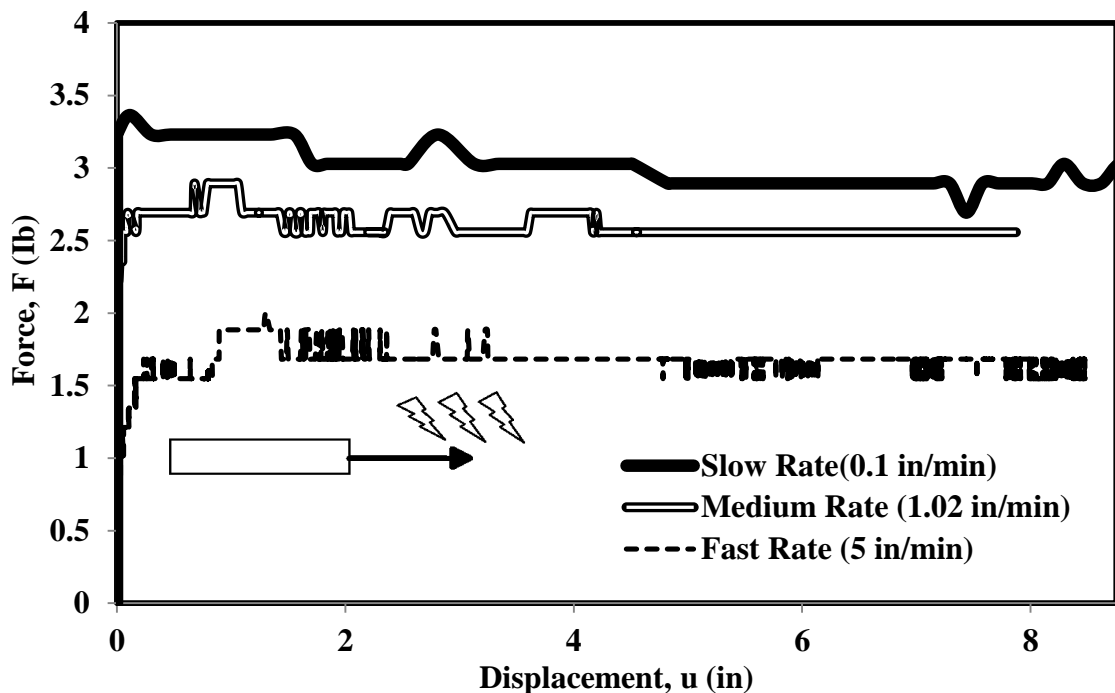


Figure 4.11: Effect of rate of loading on axial pipe soil interaction responses

4.1.1.6 Effect of Cyclic Loading

A plastic pipe with a length of 1.22 m (4 ft) and diameter of 61 mm (2.4 in) (Type: AL 102 B) with a dead load of 0.003kN/m (2.36 lb/ft) and displacement rates of 1.27 mm/min (0.05 in/min) was laid on soil with undrained shear stress of 0.07 kPa. The test was performed in three full cycles (each full cycle included one forward and one backward movement). The pipe penetration was plotted within time for each cycle of loading. After the laying, the initial penetration of 10 mm (0.4 in) was observed. By the end of first, second and third cycles, pipe penetration respectively increased to 33mm (1.3 in) or 54% of pipe diameter, 28 mm (1.9 in) or 79 % of pipe diameter and 56 mm (2.2 in) 92% of pipe diameter (Figure 4.13). With the increase in the penetration of pipe after each cycle, the steady state of axial sliding resistance significantly increased by 42% at the end of second cycle and by 8 % at the end of third cycle. With increase in penetration for each cycle, the peak value (break out resistance) shifted slightly to the left. For example, the peak value for the first cycle detected at the displacement of 30.5 mm (1.2 in) or 50 % of pipe diameter, whereas the pick value for the second cycle observed at the displacement of 23 mm (0.9 in) which is equivalent to approximately 37 % of the pipe diameter (Table 4.1).

Table 4.1

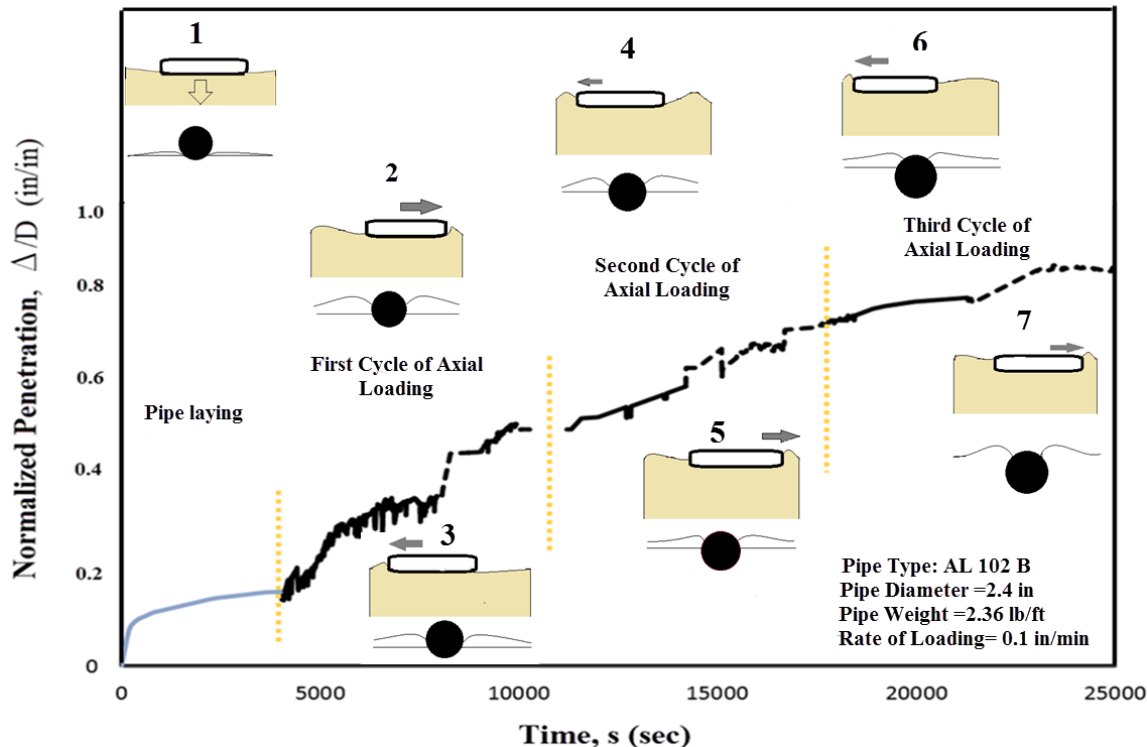


Figure 4.12: Pipeline embedment for the first three axial cycles

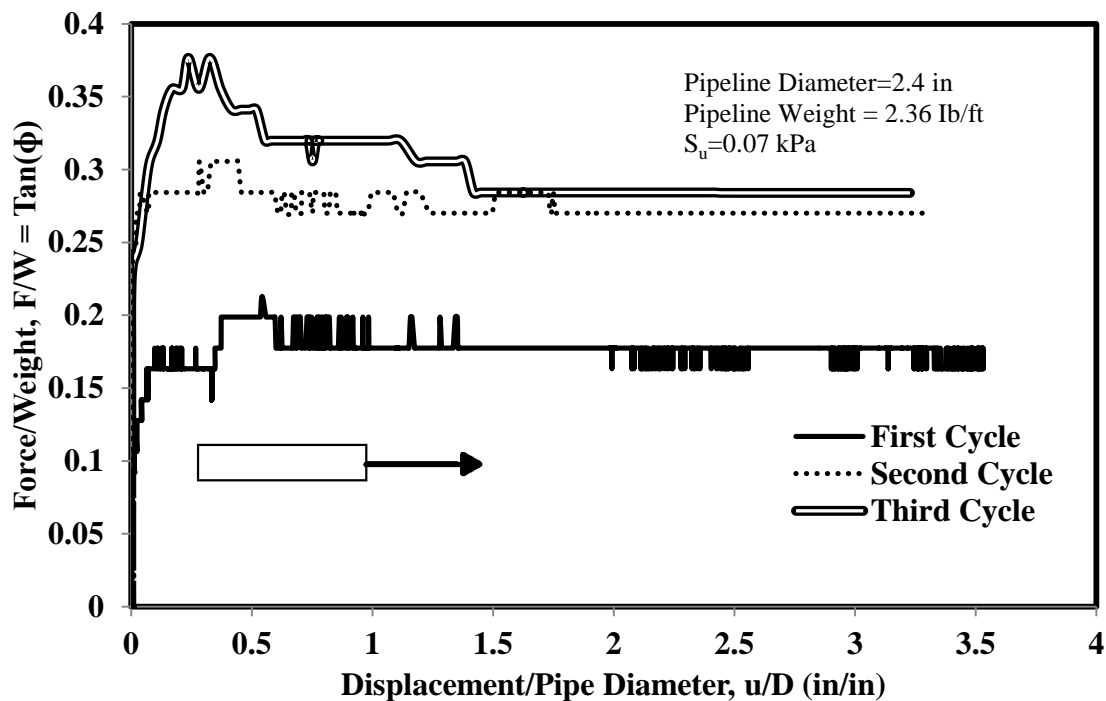
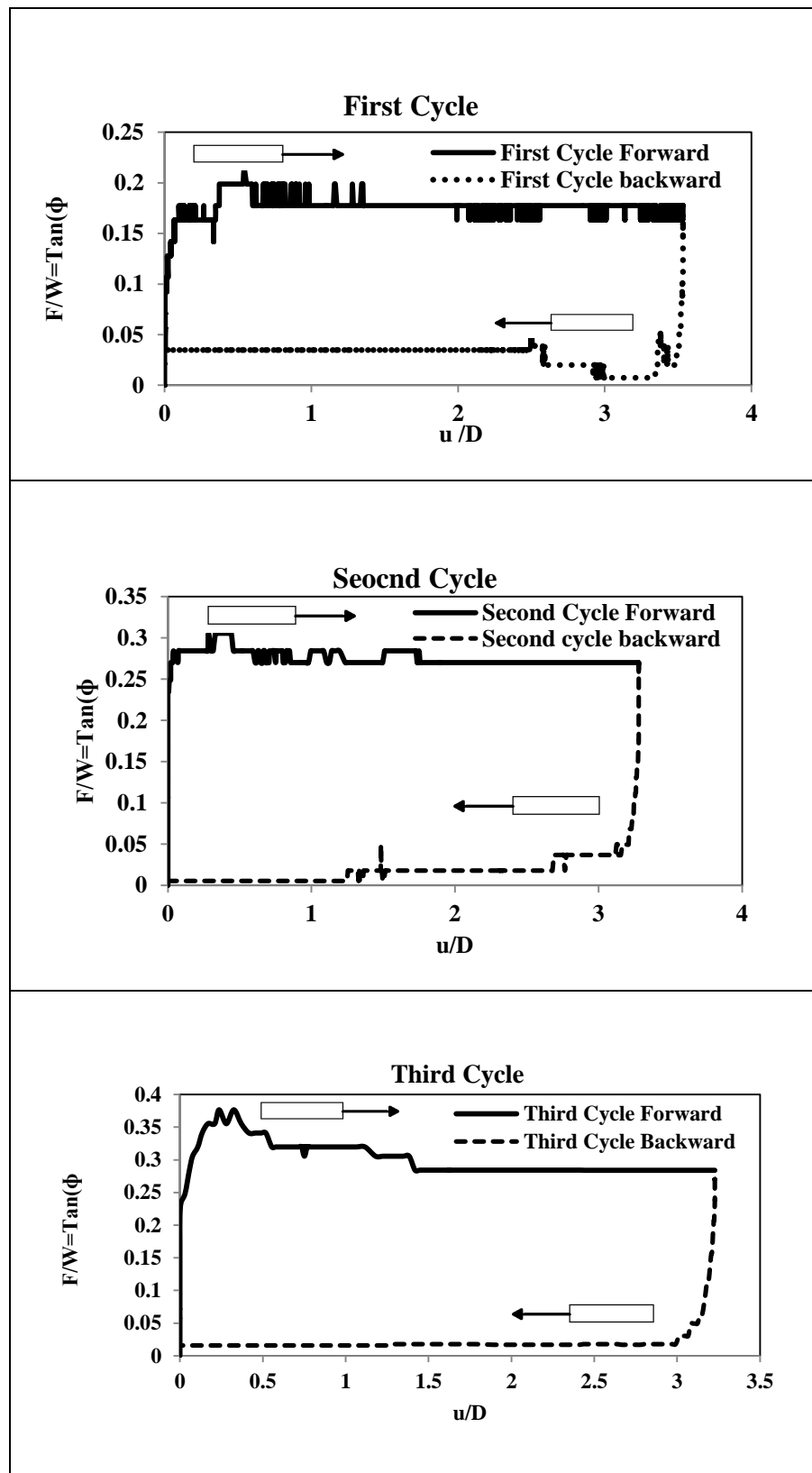


Figure 4.13: Axial pipe soil interaction for cyclic loading

Table 4.1: Axial force-displacement responses for the first three cycles



4.1.1.7 Effects of Boundary Condition (Length)

A plastic pipe with a length of 1.22 m (4 ft) and diameter of 61 mm (2.4 in) (Type: AL 102 B) with a dead load of 0.001 kN/m (0.73 lb/ft) and displacement rates of 25.4 mm/min (1 in/min) was instrumented for this part of study. The test was performed in one full cycle for three different boundary conditions. Deep epoxy glass sheets completely embedded in the soil model at two different distances in order to define two new boundary conditions (length). As a result, the full-scale soil box changed to two smaller soil models (Figure 4.14). With the decrease in distances of boundaries for each axial test, the steady state of (residual) axial resistance notably decreased by 34% for 2 ft boundary (4 times decrease in boundary length) and 65 % for 10 in boundary (9.6 times decrease in boundary length). The peak value (break out resistance) occurred at approximately the same displacement for all three tests. The peak value for the wider boundary (8ft) was 0.46, whereas the pick values for the second test (with boundary length of 2 ft) and third test (with boundary length of 10 in) were respectively 0.36 and 0.35 as illustrated in Figure 4.15.

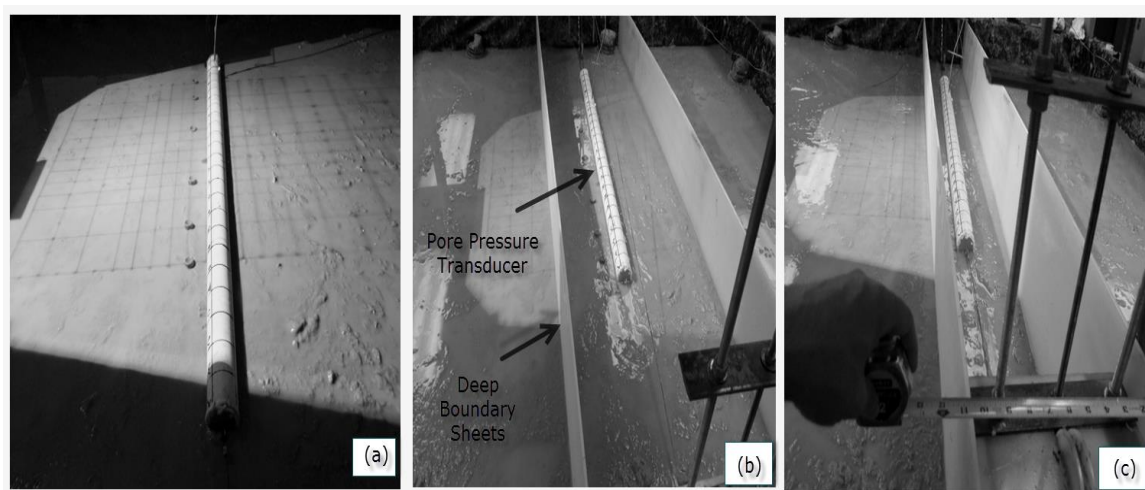


Figure 4.14: Effects of different boundary length was investigated on axial pipe soil interaction responses

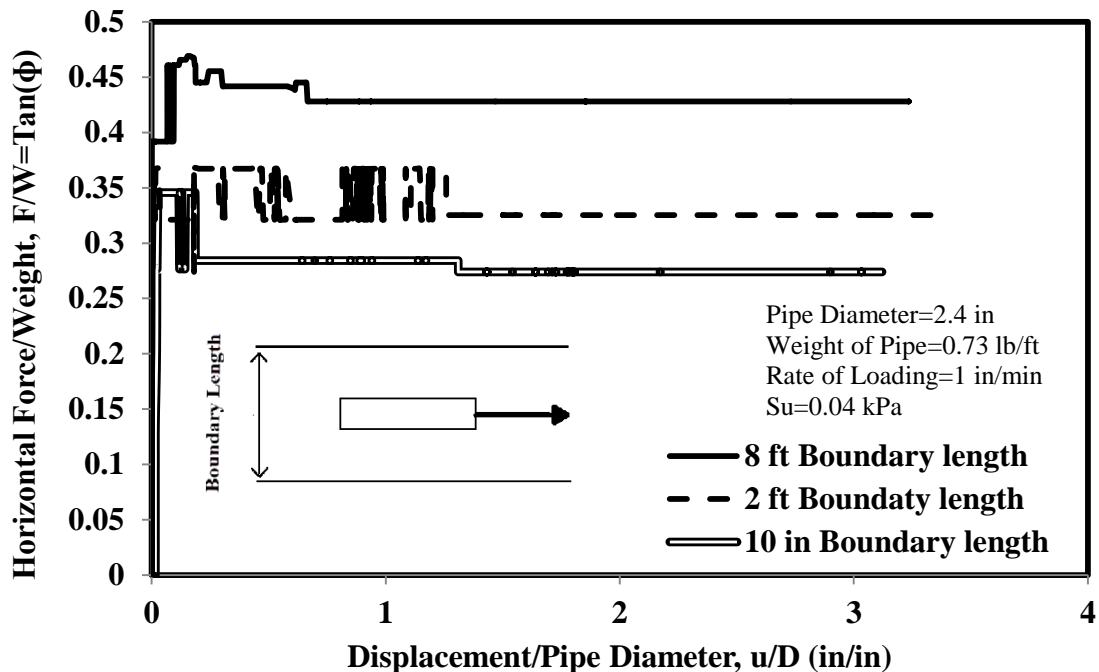


Figure 4.15: Effect of boundary length on axial pipe soil interaction

The main reason for significant drop in axial break out and axial residual resistance after decreasing the boundary length could be rationalized only by analyzing the history of excess pore water pressure just below the pipe (in here 1 D beneath the pipe invert) at the start of movement. Figure 4.16 demonstrates that by movement of the pipe, the excess pore water pressure will sharply increase and reaches plateau. At this point, since the soil is highly plastic soft clay, there is reluctance from the soil to dissipate pore water pressure. Therefore, the total pore water pressure of the soil at the vicinity of movement increases. The resistance stresses at the interface of pipe are influenced by pore pressure. In a very similar scenario, as the effective stress decreases by the growth of pore water pressure, the pipe-soil resistance will also decrease by increase in pore water pressure. Figure 4.16 correspondingly shows that the more constrained the soil model is, the more pore water pressure increase in the soil will be observed during pipe

movement. As a conclusion, decrease in boundary length will also decrease the residual and break out frictional resistance.

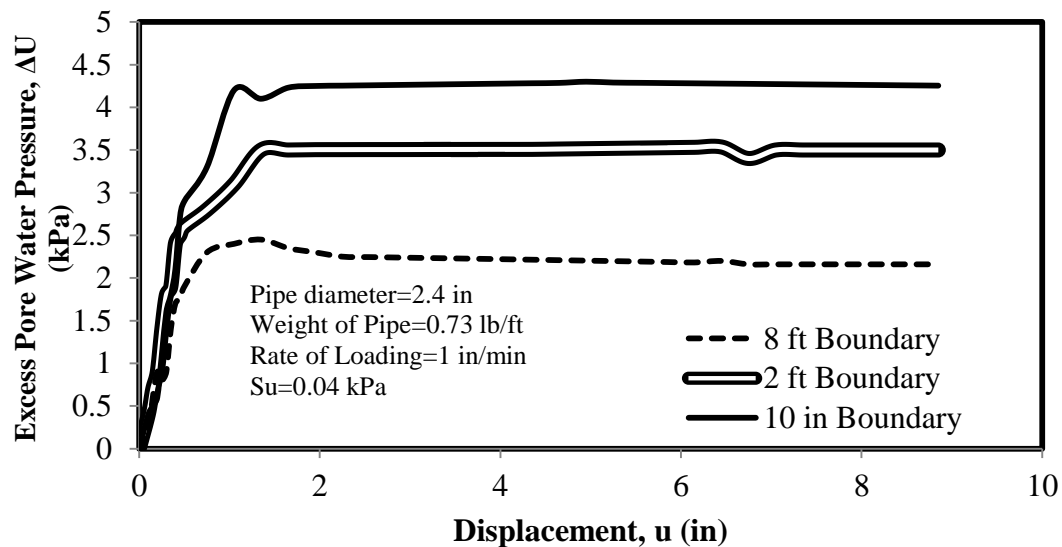


Figure 4.16: Excess pore water pressure development during axial loading with different boundary lengths

4.1.1.8 Effect of Initial Embedment

A plastic pipe with a length of 1.22 m (4 ft) and diameter of 61 mm (2.4 in) (Type: AL 102 B) with a dead load of 0.001 kN/m (0.73 lb/ft) and displacement rates of 25.4 mm/min (1 in/min) was instrumented for axial loading. The first pipe laid on the soil for 24 hours and after the natural penetration of laid pipe which was 0.14 D , the axial test was performed (this test is named as no-over-penetration case). For three other cases, initially the pipe was pushed vertically to different loads, unloaded to a specified vertical load, and then moved axially to 4.5 times its diameter. Different initial embedments of 0.25 D, 0.35D and 0.45 D were considered. With the increase in initial penetration for each axial test, the steady state of (residual) axial resistance force increased by 42% for 0.25 D, 96 % for 0.35D and 230 % for 0.45 D. The peak value (break out resistance) for these three cases occurred instantly at the beginning of

movement (Figure 4.17). The vertical movement of pipe during axial motion is shown in Figure 4.18. For all cases ,except no over-penetration case, the pipe moves upward back to the original surface.

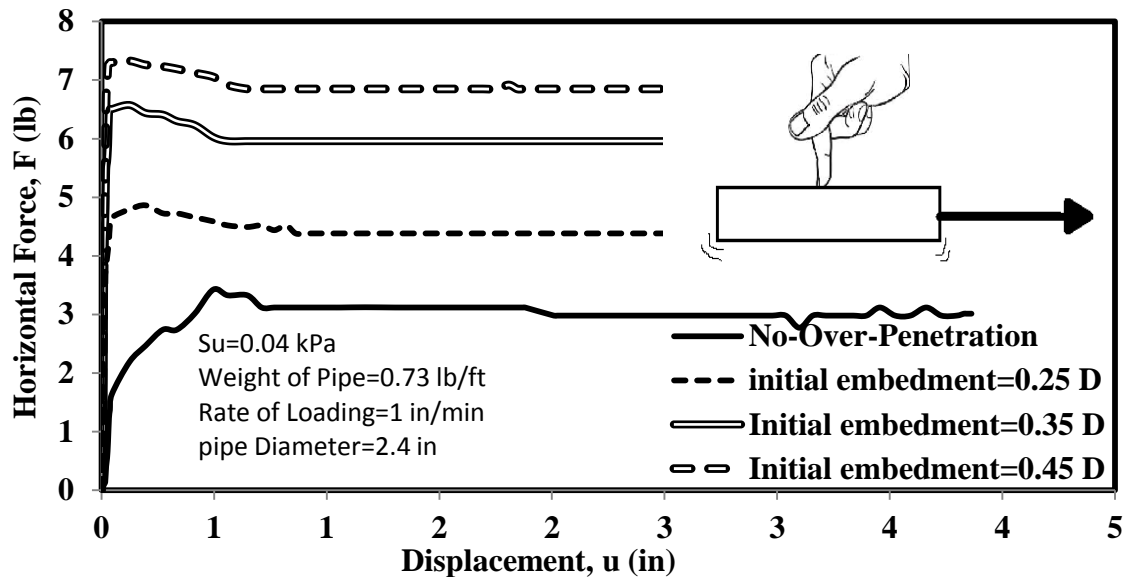


Figure 4.17: Effect of initial embedment on axial force-displacement responses

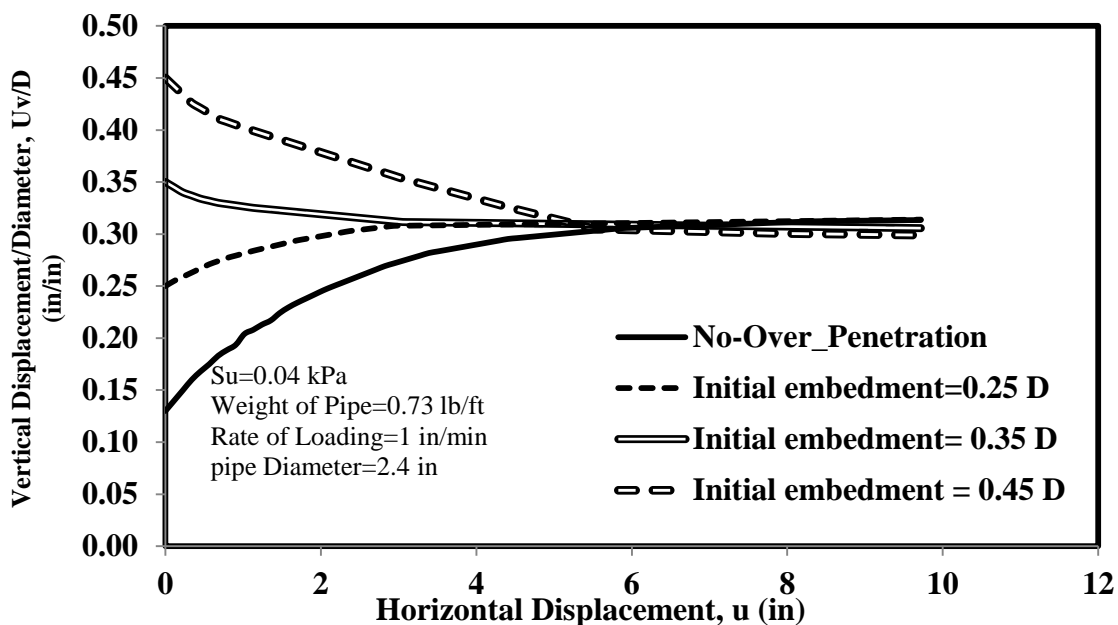


Figure 4.18: Horizontal-vertical displacement for pipes with different initial embedment

4.1.2 Modeling

The classical undrained method to define the axial resistance capacity of pile shaft in cohesive soils known as total stress “alpha method” are widely where axial force is computed as product of the shear strength S_u , the contact area between the pipe-soil A_i and a factor named α dependent on the pipe surface roughness. It is assumed that after the breakout, the shear strength reduces to the remoulded shear strength. In every undrained pipe soil interaction model, the main attempt has been made to characterize “break-out resistance”, “residual resistance” and the distance at which break-out and residual resistance occurred. In this part of study, these parameters are modeled based on the parametric study performed in section 4.3.1 on the axial force-displacement responses.

4.1.2.1 Axial Break-Out

In our study, the horizontal resistance at break-out, $F_{\text{break-out}}$, is expressed in dimensionless fashion as $f_{\text{break-out}} = \frac{F_{\text{break-out}}}{S_u * D}$. Analysis of more than 75 studies in medium-size and large scale soil tanks showed that $f_{\text{break-out}}$ depends on the current vertical load W (here weight of pipe for the whole loading), the normalized initial embedment δ_{in} , boundary length λ and the rate of axial loading V_p . It is considered that $F_{\text{break-out}}$ is comprised of a frictional component of resistance below the pipe, installation properties and inherent properties of the pipeline system. The average undrained shear strength calculated at point 1 through point 5 of soil sample (explained in chapter 3) was used for normalization. The axial resistance formulae are proposed as:

$$\frac{f_{\text{break-out}}}{S_u * D} = 120 * \frac{W}{S_u * D}^{0.1} * \frac{\delta_{in}}{D}^{1.3} * \frac{\lambda}{D}^{3.2} * \frac{V_p}{V_{ref}}, \quad \text{with } R^2 = 0.81 \text{ and} \quad (4.1)$$

$$\frac{F_{\text{BRO}}}{S_u * D} = 11.3 + 0.01 \frac{W}{S_u * D} + 0.31 \frac{W}{S_u * D}^{0.21} \frac{\delta_{in}}{D} + 215 \frac{W}{S_u * D}^{0.02} \frac{\delta_{in}}{D}^{5.64} \frac{\lambda}{D} - 0.77 \frac{V_p}{V_{ref}}^{0.55}, \quad (4.2)$$

With $R^2=0.87$. In Equation (4.1) and Equation (4.2) the units are lb-force, inch, min and psi (pound per square inch), respectively, for force, length, time and stress. With V_{ref} is defined as the 1 in/min and the max value of $\frac{\lambda}{D}$ should not exceed 40 for any case. If one or more determining factors such as boundary length or rate of loading were missing, is recommended with substituting zero for the unknown values. Figure 4.19 and Figure 4.20 vindicates that Equation (4.2) gives a very good prediction for $f_{break-out}$ resistance of soil with undrained shear strength between 0.01 kPa to 0.11 kPa.

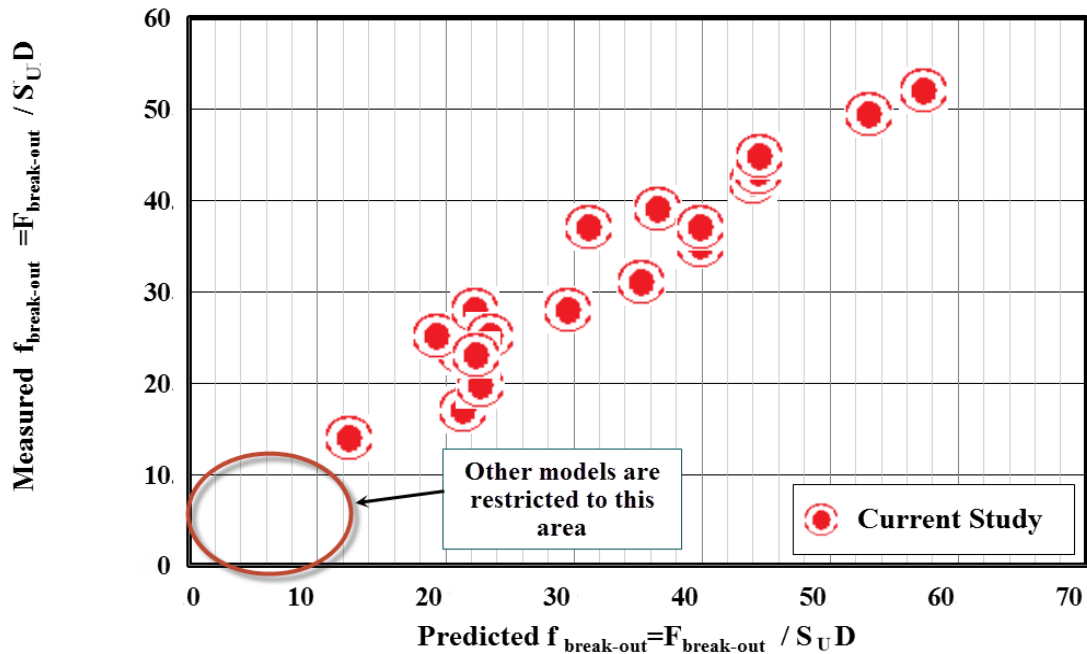


Figure 4.19: Comparison of the measured and predicted breakout resistance calculated from Equation 4.2

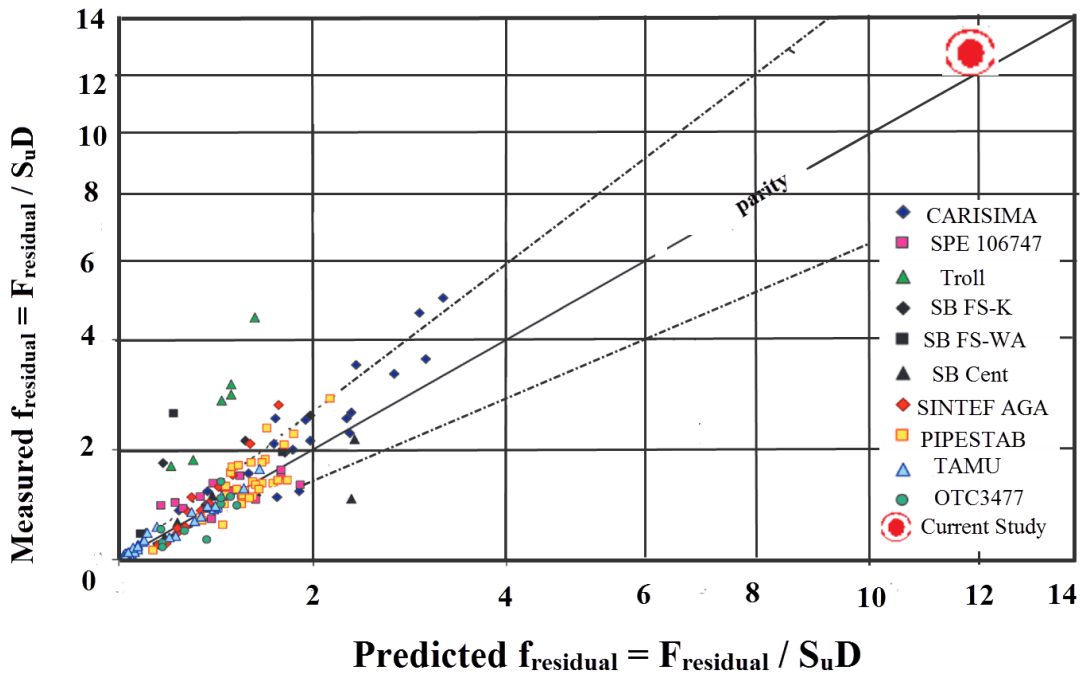


Figure 4.20: Comparison of the measured and predicted breakout resistance from different projects

4.1.2.2 Large Displacement Residual Resistance

The mobilization of break-out resistance occurs within a pipe movement of less than half of a diameter, while residual resistance occurs between 3 to 8 diameters of pipe. Horizontal resistance denoted by $f_{\text{residual}}=F_{\text{residual}}/S_u D$. Classical plasticity solutions for sliding failure of a surface foundation leads to a value of $F/W=0.39$. But this value overestimates the resistance for very soft soil range studied in here. Based on experimental analysis of more than 45 soil pipe test in full-scale tank, Equation is advised as:

$$\frac{F_{\text{res}}}{S_u \cdot D} = 14 + 0.1 \cdot \frac{W}{S_u \cdot D} + 7.2 \cdot \frac{\delta_{\text{in}}}{D} + 2.1 \cdot \frac{\lambda}{D} - 6.01 \cdot \frac{V_p}{D}, \quad (4.3)$$

In equation 4.3 the units are lb-force, inch, min and psi (pound per square inch), respectively, for force, length, time and stress. With V_{ref} is defined as the 1 in/min and the maximum value of $\frac{\lambda}{D}$ should not exceed 40 for any case.

Equation (4.3) gives good prediction of f_{residual} and as Figure 4.21 and Figure 4.22 shows there is no skew in the ratio of predicted to measured resistance.

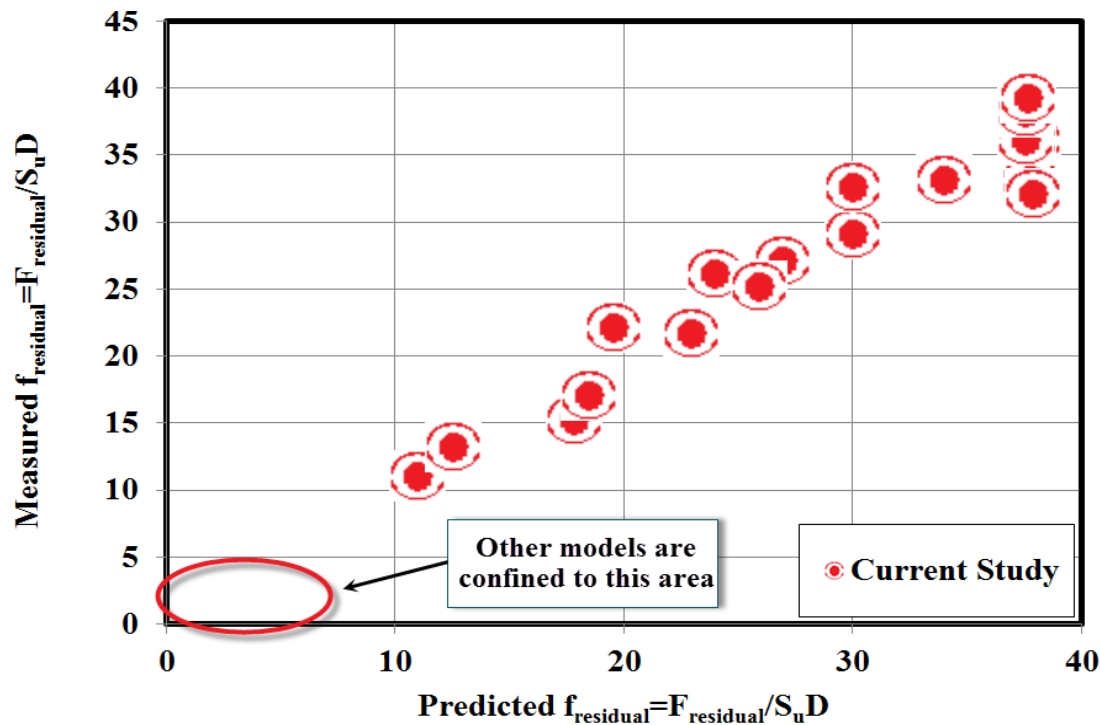


Figure 4.21: Comparison of the measured and predicted residual resistance calculated from equation 4-2

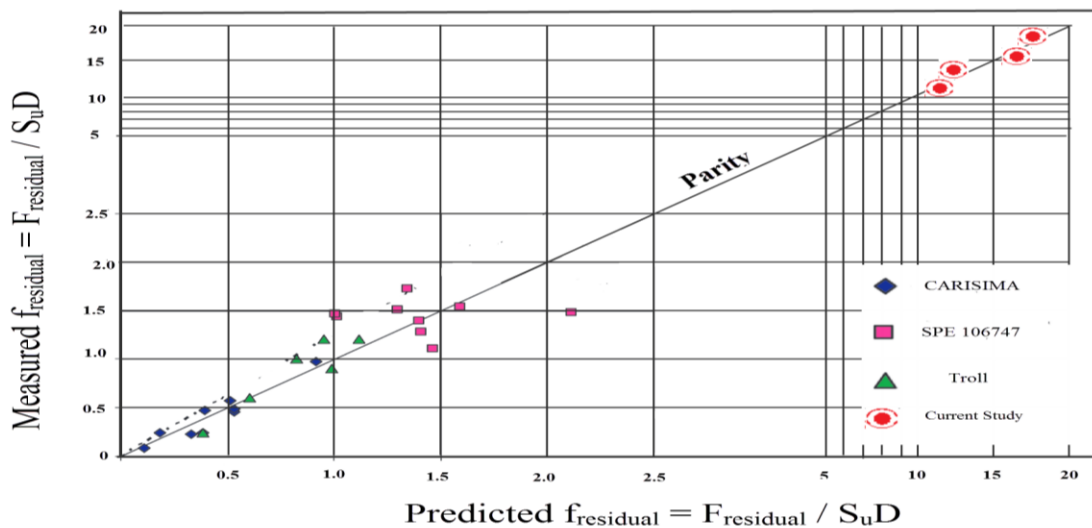


Figure 4.22: Comparison of the measured and predicted residual resistance from different projects

4.1.2.3 Full range Model

One of the objectives of pipe soil interaction testing was to come up with an empirical model to address axial resistance at every desired point within displacement range, from the onset of movement to breakout resistance and from break resistance to residual steady state resistance. In the following the main concepts of original p-q model are borrowed to advise a model that can fully predict the axial frictional behavior of pipe and soil. The modified p-q model which is called p-q-m, emulates the original model to a certain point call x_f or ε_f (inception of residual trend) and then m parameter deliver the slope of linear interpolation. For better understanding of the p-q-m model, the fundamental of original p-q model are explained.

4.1.2.3.1 Original p-q model

Original p-q model was introduced by Vipulanandan (1990) to model the stress-strain relationship of epoxy and polyester polymer concrete behavior in compression. It was presented as :

$$\sigma_i = \frac{\varepsilon_i / \varepsilon_y}{(1-p-q)+q(\varepsilon_i / \varepsilon_y) + p(\varepsilon_i / \varepsilon_y)^{\frac{1-q}{p}}} \sigma_y, \text{ then} \quad (4.4)$$

$$\frac{\varepsilon_i / \varepsilon_y}{\sigma_i / \sigma_y} = (1 - p - q) + q \left(\frac{\varepsilon_i}{\varepsilon_y} \right) + p \left(\frac{\varepsilon_i}{\varepsilon_y} \right)^{\frac{1-q}{p}}, \quad (4.5)$$

where ε_y is the yield strain, σ_y the yield strength, σ_i the uniaxial stress and ε_i uniaxial strain. The parameters p and q are functional variable of the material, different from the known hydrostatic pressure q and deviatoric stress p in constitutive modeling. They are function of the initial modulus E_i and the secant modulus at yield E_{sy} which in turn can be defined as:

$$E_i = f(\dot{\varepsilon}, T), \quad (4.6)$$

$$E_{sy} = f(\dot{\varepsilon}, T), \text{ and} \quad (4.7)$$

$$\sigma_y = f(\dot{\varepsilon}, T). \quad (4.8)$$

The model imposed at all time that

$$\sigma_i = f(\varepsilon_y) = \sigma_y \quad (4.9)$$

and

$$E_i = \frac{E_{sy}}{1-p-q}. \quad (4.10)$$

Normalizing the stress by yield stress and the strain by the yield strain,

$$\bar{\sigma} = \frac{\sigma}{\sigma_y} \text{ and} \quad (4.11)$$

$$\bar{\varepsilon} = \frac{\varepsilon}{\varepsilon_y}. \quad (4.12)$$

Equation (4-4) changes to

$$\frac{\bar{\varepsilon}}{\bar{\sigma}} = (1 - p - q) + q\bar{\varepsilon} + p\bar{\varepsilon}^{\frac{1-q}{p}}. \quad (4.13)$$

Mantrala (1995) presented a modified stress-strain model which provided the following relationship

$$\frac{\bar{\varepsilon}}{\bar{\sigma}} = q + (1 - p - q)\bar{\varepsilon} + p\bar{\varepsilon}^{\frac{p+q}{p}}, \quad (4.14)$$

in which q is defined as,

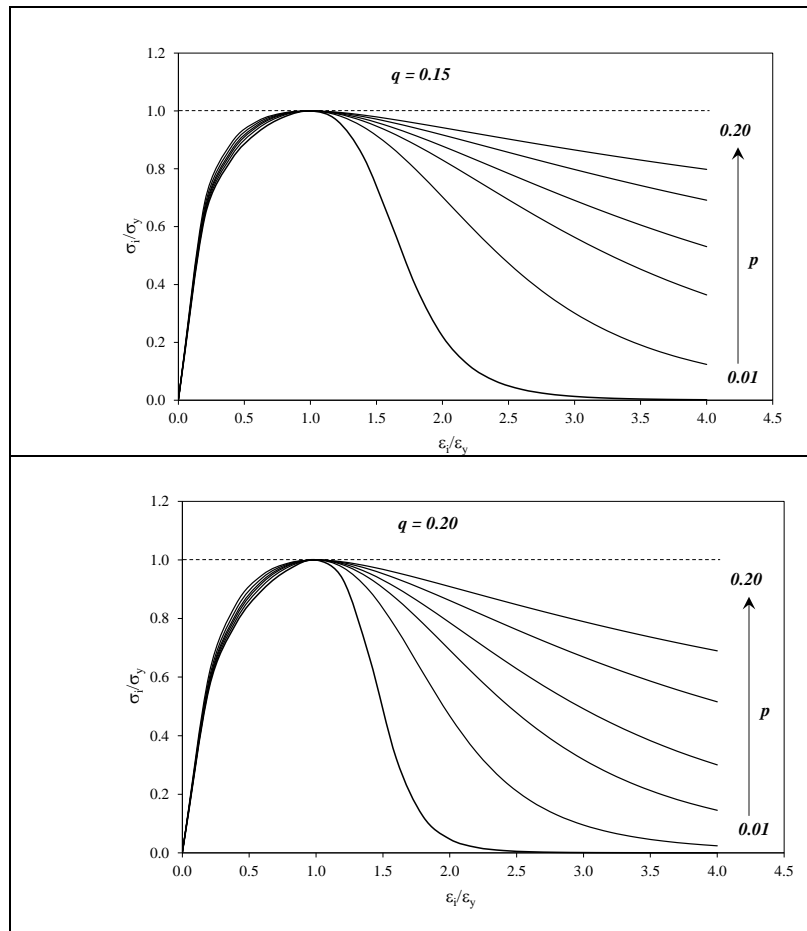
$$q = \frac{E_o}{E_i} \quad (4.15)$$

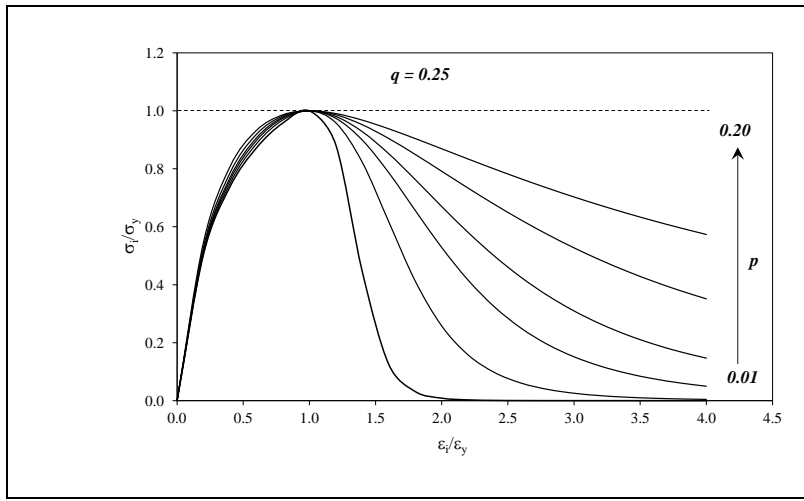
then $q \in [0 ; 1]$.

q is, therefore, a direct quantification of the material nonlinear elastic stress-strain behavior , and p is a material property. The condition in Equation (4.5) was satisfied. The normalized stress-

strain (or force-displacement) relationships, of the model prediction, are shown in Table 4.2 for values of q and range of p .

Table 4.2: Original model normalized stress-strain relationship prediction





4.1.2.3.2 p-q-m Model

According to experimental results, force displacement responses of axial tests consist of two stages. First the forces (F) reach a maximum value which is embodied as y_c (or σ_c) at displacement(u) of x_c (ε_c or u_c). And at the second stages, it declines to the limiting value of residual forces presented by y_f (σ_f or F_f). The start of limiting behavior is at displacement of x_f (ε_f or u_f). In equation (4.16) the symbol $\lfloor \quad \rfloor$ represent the floor function and $| \quad |$ represents absolute value function and p, q and m parameters are function of rate of loading V_p , undrained shear strength S_u , weight of pipe W , Pipe diameter D , initial embedment δ , Boundary length λ (not exceeding 96) and number of cycles N . The discrepancy in measured and predicted value for these three parameters was less than 10 %. It should be mentioned that for all the equations, the units are lb-force, inch, min and psi (pound per square inch) respectively for force, length, time and stress. The proposed p-q-m model is:

$$F = \frac{\frac{u}{u_c} - \lfloor (u - u_f) / (\max(2*u, u_f)) \rfloor}{\frac{p+q}{q + (1-p-q)*(\frac{u}{u_c}) + p*(\frac{u}{u_c})^p}} * f_c + \left| \frac{2*u - 0.99*u_f}{\max(u, u_f)} \right| * (f_f + m * (u - u_f)) \quad (4.16)$$

, where the parameters are as:

$$p = 0.375 * V^{-0.226} * S_u^{0.163} * W^{0.3933} * D^{-0.267} * \delta^{0.438} * \lambda^{1.552} * N^{0.1748}, \quad (4.17)$$

$$q = 2.69 * V^{0.1256} * S_u^{0.083} * W^{-0.3022} * D^{0.0046} * \delta^{-0.104} * \lambda^{0.0288} * N^{2.69}, \text{ and} \quad (4.18)$$

$$m = 1.19 * V^{0.0018} * S_u^{0.0647} * W^{0.0246} * D^{0.0246} * \delta^{0.057} * \lambda^{0.099} * N^{-0.234}. \quad (4.19)$$

Break out and residual displacement are

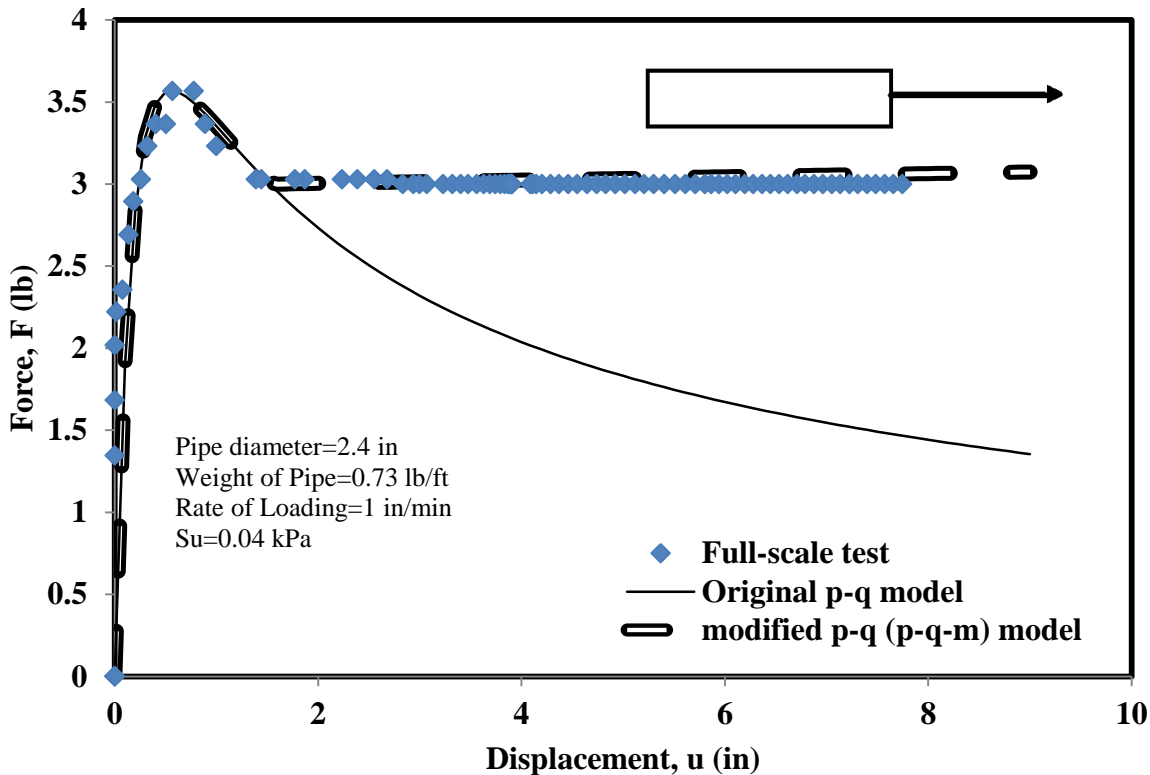
$$U_{\text{breakout}} = 11 + 0.1 * \frac{W}{S_u * D} + 3.2 * \frac{\delta_{\text{in}}}{D} + 2.0 * \frac{\lambda}{D} - 6 * \frac{V_p}{D} \quad (4.20)$$

and

$$U_{\text{residual}} = 17 + 0.12 * \frac{W}{S_u * D} + 2.9 * \frac{\delta_{\text{in}}}{D} + 3.5 * \frac{\lambda}{D} - 2.9 * \frac{V_p}{D}. \quad (4.21)$$

In Equation (4.16), f_c is equal to $f_{\text{break-out}}$ and f_f is equal to f_{residual} . These two values are calculated from Equation (4.2) and Equation (4.3) and $u_{\text{break-out}}$ and u_{residual} are calculated from Equation (4.20) and Equation (4.21).

Figure 4.22 shows the capability of p-q-m model in accurately following the trend of axial force-displacement responses of subsea pipe.



4.22: Test results are characterized by p-q and p-q-m model

4.2 Finite Element Analysis

4.2.1 Introduction

Offshore pipe embedment is a large deformation problem. Various techniques have been proposed in the past to overcome numerical difficulties in large strain finite element modeling, these techniques were explained in chapter 2.

The main focus of this part of our study is to conduct FEM analysis on pipe subjected to vertical loading (self-weight) and Axial cyclic loading due to thermal expansion and shut-down cycles. In this part of study, the analysis is divided into two stages. At the first stage, the vertical penetration of pipe on a very soft soil after lying is investigated. And in the second stage, dynamic axial force displacement responses of the subsea pipe (both wet coated and PIP) on a soft seabed is modeled. Lagrangian approach, ALE (Arbitrary Eulerian Lagrangian) adaptive

meshing, and CEL (Coupled Eulerian Lagrangian) approaches are extensively employed. Sixty-six numerical FEM models were developed in python syntax and five user-defined subroutines including UMAT (to modify constitutive models), SIGNI (to define initial stress field), DISP (to define prescribed boundary condition), DLOAD (to define non-uniform distributed loads) and UPOREP (to define initial pore pressure) programed in FORTRAN. Finally the python, which is the built-in scripting language of ABAQUS software and FORTRAN subroutines combined and executed in ABAQUS/CAE.

4.2.2 Finite element model

The large deformation finite element model developed for this study are based on “Lagrangian approach”, ”Coupled Eulerian Lagrangian approach” and ”Arbitrary Lagrangian Eulerian approach”. Geometry part, mesh and boundary conditions of each category are explained in the following.

4.2.2.1 Lagrangian model

Two dimensional plane strain model was defined in ABAQUS. The two side-edges of the model were confined horizontally but free to move vertically and the bottom edge was confined in both horizontal and vertical direction and for all cases, the pipe was modeled as rigid body. The two dimensional plane strain element CPE6 (which is the element with three vertex nodes and three mid-size nodes) was utilized. The optimized size of mesh density was determined after trying several options. For both vertical penetration (stage 1) and axial movement (stage 2) incremental displacement was taken as 1.5% of the diameter of pipe.

Contact between the pipe and the soft soil was modeled by defining the pipe surface as the master surface and the soil surface as the slave surface in interface module. The penalty method was used for the friction between pipe and soil. In penalty method setting, the maximum

shear stress at the interface, τ_{max} , was introduced as $\propto S_u$, where \propto is the interface roughness factor and S_u is the undrained shear strength of soil. Many researchers such as chaterjee reported as $\propto = \frac{1}{S_t}$, where S_t is soil sensitivity (S_t is relating the ratio of intact and remoulded value). In this study τ_{max} was calculated from the same methodology.

The analyses were executed by applying undrained total stress approach. Therefore, the Mohr-Coulomb soil model with no hardening cap was defined with zero friction angle and dilation angle (similar to Tresca model). The elastic part of soil model was defined with Poisson's ratio of 0.49 (almost no volume change (Nakshatrala 2008)) and with young's modulus of 430Su. To obtain optimal E=430Su several models with different E ranged from E=100Su to E=600Su was established and run in ABAQUS. Then the axial force displacement response compared to the experimental test. The E=430Su showed minimum discrepancy. On imperfection of ABAQUS is that, linear variation of undrained shear strength with depth cannot be defined as an input as mentioned by Dutt (2012). The undrained shear strength at any point and time increment is a non-linear function of strain rate, strain softening, Depth and etc. as:

$$S_u(x, t) = f(S_{u0}, S_t, \Delta\epsilon_{p1}, \Delta\epsilon_{p2}, \kappa, z, V_p, \Delta\epsilon_1, \Delta\epsilon_3, \dot{\gamma}_{max}, \mu) \quad (4.23)$$

The effect of soil strength non-homogeneity ($S_u = S_{u0} + \kappa Z$) and buoyancy on the vertical resistance of pipelines were evaluated. The effect of strain rate on shear strength was introduced after each time increment using part of Biscontin (2001) equation as:

$$S_u = \left[1 + \mu \log \left(\frac{\max(\dot{\gamma}_{max}, \dot{\gamma}_{ref})}{\dot{\gamma}_{ref}} \right) \right] S_{u0}, \quad (4.24)$$

where $\dot{\gamma}_{max} = \frac{(\Delta\epsilon_1 - \Delta\epsilon_3)}{\frac{\delta}{D}} * \frac{V_p}{D}$, $\dot{\gamma}_{ref} = 1 * 10^{-6} s^{-1}$, and

$\Delta\epsilon_1, \Delta\epsilon_3$ = Major and Minor Principal strain

V_p = Vertical velocity of pipe

δ = Displacement increment

$\dot{\gamma}_{\max}$ = Max shear Strain rate at a given location

μ = Rate of strain increase per decade strain rate

κ = Shear strain gradient

z = Depth

As Figure 4.23: The effect of strain rate on vertical penetration of pipe rested on soft soil shows, considering the effect of strain rate based on Equation 4.24 can markedly approach the numerical modeling to experimental results. In this case, the effect of strain rate on undrained shear strength after each increment resulted in more realistic penetration curve.

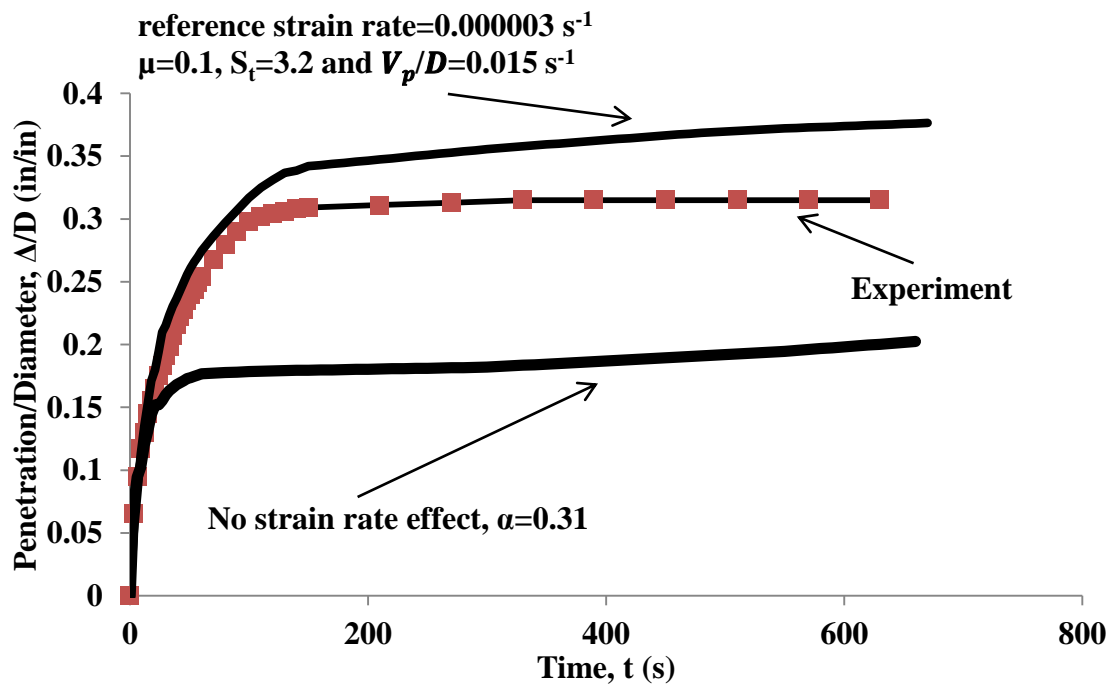


Figure 4.23: The effect of strain rate on vertical penetration of pipe rested on soft soil

The similar constitutive model was also used for all ALE and CEL analyses.

4.2.2.2 Coupled Eulerian Lagrangian (CEL)

For CEL analysis the pipe was modeled as Lagrangian part and rigid body and the soil was modeled as Eulerian part. The pipe simulated as three dimensional with shell element and element type of S4R (Which is general-purpose shell element) and the soil layer was modeled as three dimensional using Eulerian elements EC3D8R (which is an 8-noded linear brick, multi-material, reduced integration with hourglass control).

One of the critical characters of CEL model is to correctly define the space required to accommodate the displaced soil and berms. Since in ABAQUS only one Eulerian part could be defined, the void should be created inside the Eulerian part on top of soil by using Eulerian Volume Fraction (EVF) tool. The EVF determines the presence of material inside the element such that $\text{EVF}=0$ means void and $\text{EVF}=1$ means 100% presence of material and any number between 0 and 1 suggests an uncertainty in the presence of material. As a matter of fact, one of the drawbacks of CEL approach in ABAQUS is that, after analysis, in the contact area of soil and pipe EVF between 0 and 1 were observed and it was difficult to delineate the border of soil layer and void.

As shown in Figure 4.24 the bottom of the model is constrained from vertical movement and all the side are -edges constrained to move laterally. As for Eulerian boundaries, all components of velocity at the bottom and vertical faces are defined as zero to make sure that there is no in-flow or out-flow of Eulerian material outside the domain. For the top of the seabed no velocity boundary was defined to allow this surface move freely.

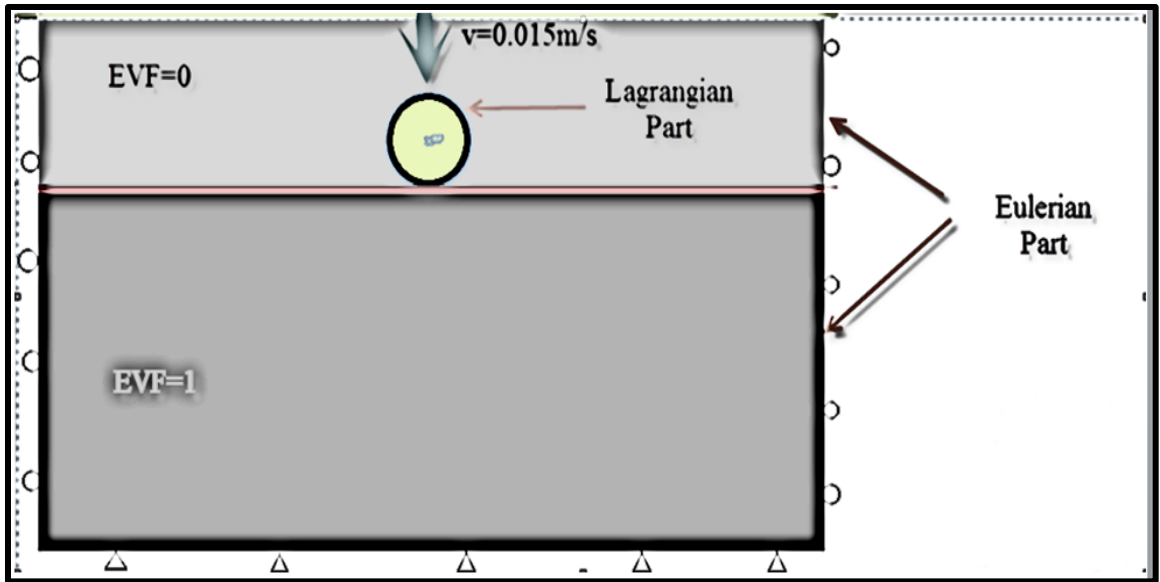


Figure 4.24: Coupled Eulerian Lagrangian (CEL) model used in ABAQUS

4.2.2.3 Arbitrary Lagrangian Eulerian (ALE)

As mentioned in chapter 2, ALE methods provide for the arbitrary motion of the computational mesh and provide a means of developing a continuous mesh between a fixed (Eulerian) and the deforming (Lagrangian) pipe. In the ALE method, the material point was separated from the computational mesh with a known movement. Mesh update was carried out in a given number of increments, typically 10-20 increments. A new mesh was generated and the quantities from the old mesh were mapped and interpolated to the newly generated mesh (Sun, 2013). In ABAQUS v.6.8 one of the recommended way to handle excessive mesh distortion is to use the built-in ALE method. The concept of the build-in-ALE in ABAQUS consists of five stages as:

- 1) The simulation is performed as usual
- 2) Re-meshing of the domain is executed at a prescribed frequency, usually every 10 increments

- 3) The domain is rediscertized to form a new mesh
- 4) An "advection" process is carried out to convey the variables from the old mesh to the new mesh
- 5) The simulation is continued and this process is repeated

The ALE model in ABAQUS first was modeled similar to pure Lagrangian model that discussed earlier with same boundary condition and element type. Then, the ALE adaptive mesh controls such as frequency and remeshing sweeps per increments should be defined in the step modulus.

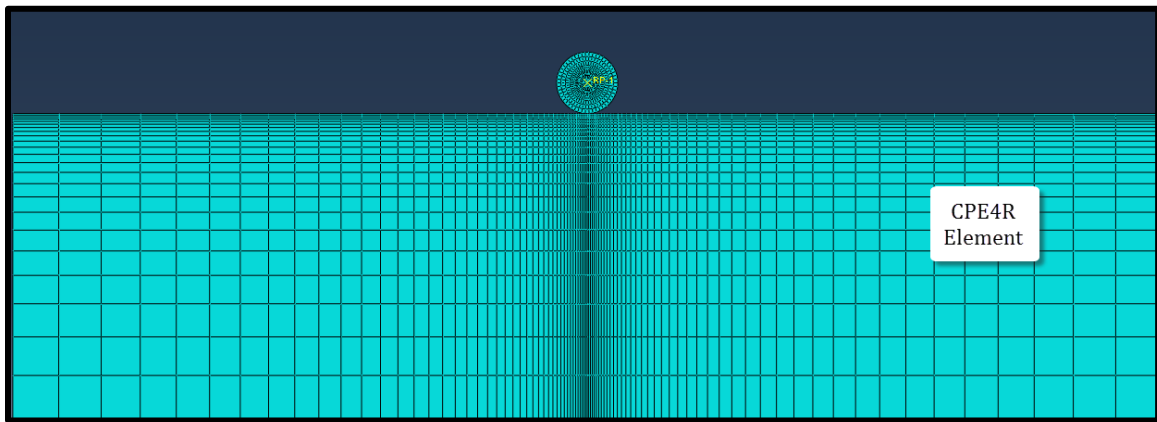


Figure 4.25: Arbitrary Lagrangian Eulerian (ALE) mesh configuration used for vertical penetration of pipe in very soft soil

4.2.3 Finite Element Procedures

The numerical study of axial pipe soil interaction is divided into two separate analyses of vertical penetration and axial sliding. After the completion of vertical penetration analysis, the coordination of the nodes of penetrated pipe, and also stresses at integration points and reaction forces of soil and pipe are transferred to the second analysis.

4.2.3.1 Vertical loading

The following steps are performed

Step1: geostatic (for Lagrangian, ALE and CEL)

ABAQUS software applies the initial stresses defined by the user as an initial guess or as a start in the process of getting a converged stresses for the start of the analysis. Nonconformity of the initial stress values from the actual would lead to incorrect higher soil displacements of the model which in turn leads to instabilities. In geostatic step, ABAQUS computes the stresses which are in equilibrium with the external loading and boundary conditions. The displacement that occur during the geostatic step is not because of the external loading but because of the difference between the user predicted initial stresses and the converged stresses calculated by ABAQUS, which is in equilibrium with the external loading. The best estimate of initial stresses is specified for every analysis to produce negligible displacement at the end of this step. During the geostatic step, pipe is kept outside the soil and the geostatic force is applied on soil to model initial confinement at different depth as shown in Figure 4.26.

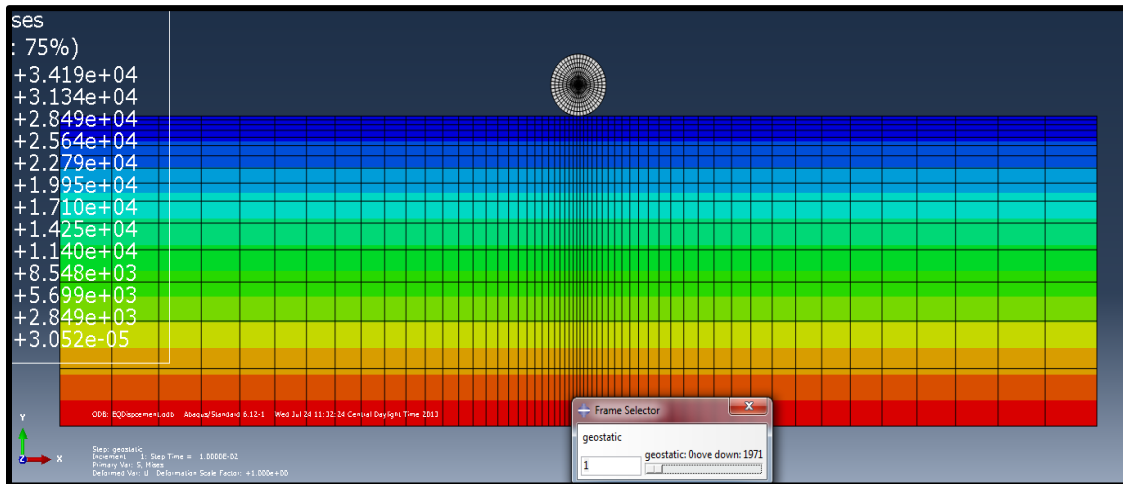


Figure 4.26: Application of geostatic step at ALE analysis

Step 2: penetration in voids (only for CEL)

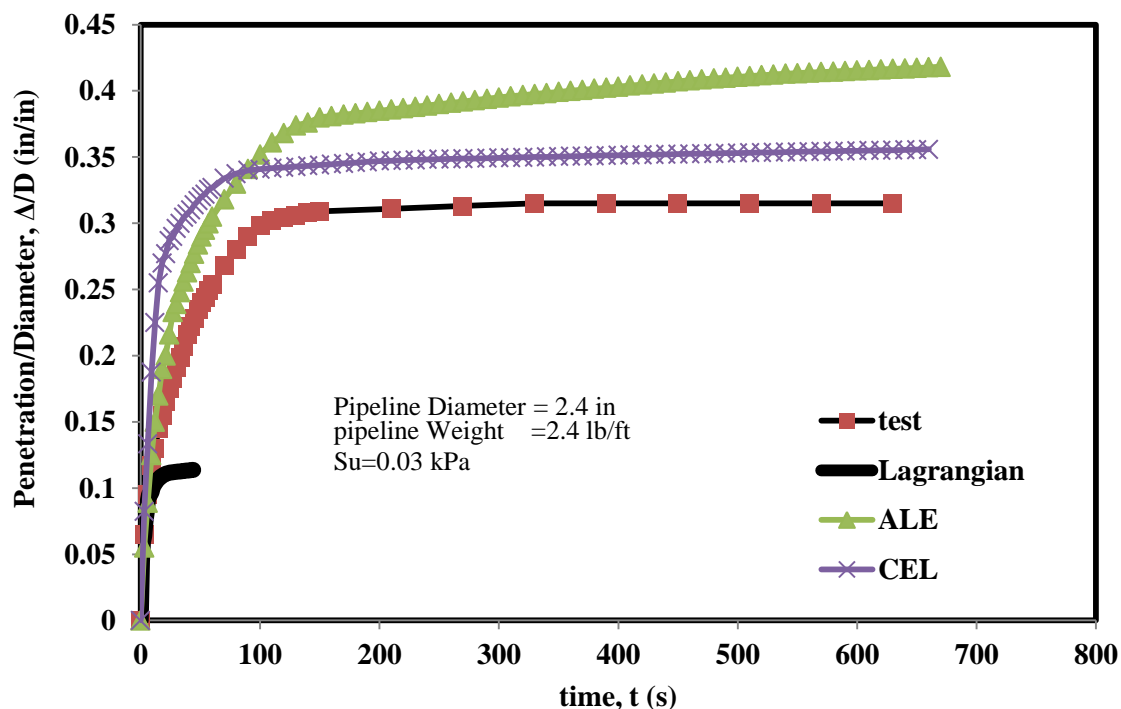
In this step, the pipe was moved downward at a selected displacement into Eulerian part.

Since this movement occurs only through the void, no reaction forces observed during this step.

Step 3: Penetration in soft clay (for Lagrangian, ALE, and CEL)

This step of analysis is force control and the pipe starts to penetrate into the seabed due to its self-weight. Figure 4.27 draws a comparison between experimental results and different finite element analyses during the vertical penetration of pipe on very soft soil with undrained shear strength of 0.03 kPa. As the results show, pure Lagrangian analysis provides very accurate responses only before the $\frac{\Delta}{D}$ (displacement/diameter) value reaches 0.1 where mesh entanglement occurs (

Figure 4.28). However, ALE and CEL provide acceptable results for larger displacement (Figure 4.29 and Figure 4.30).



At the start of penetration, ALE trend is more similar to experimental but CEL draws better results for the total penetration.

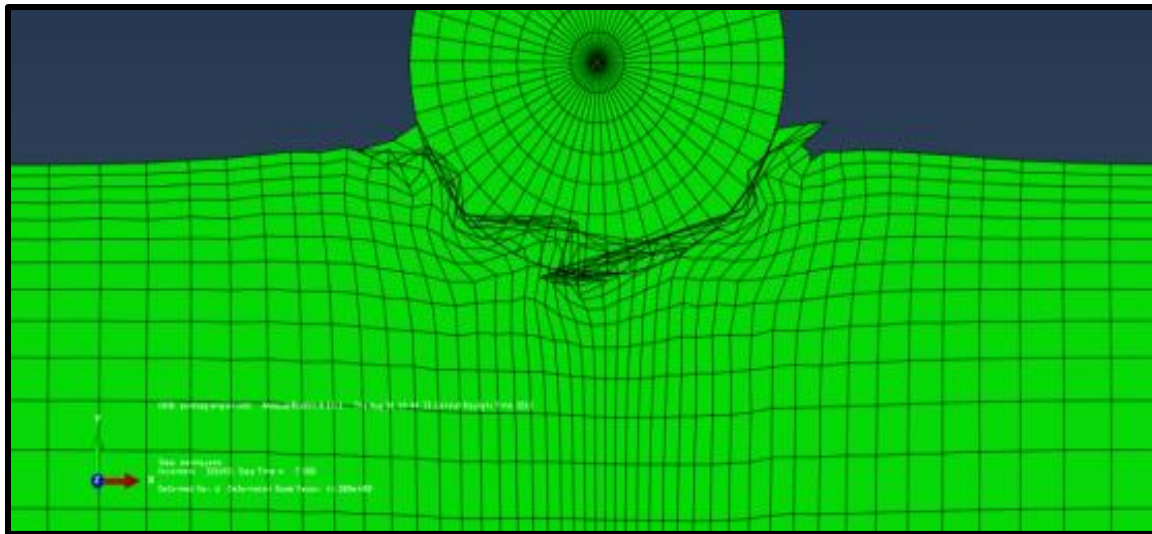


Figure 4.28: Severe mesh distortion by applying Pure Lagrangian approach in vertical penetration of Pipe in soft soil

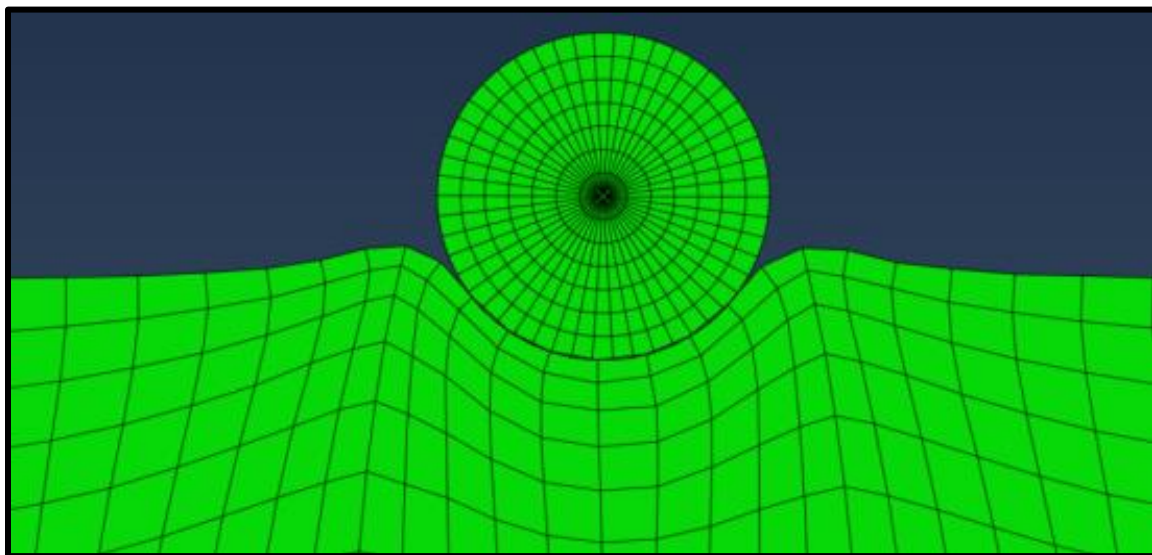


Figure 4.29: ALE approach was employed in vertical penetration of pipe on soft soil

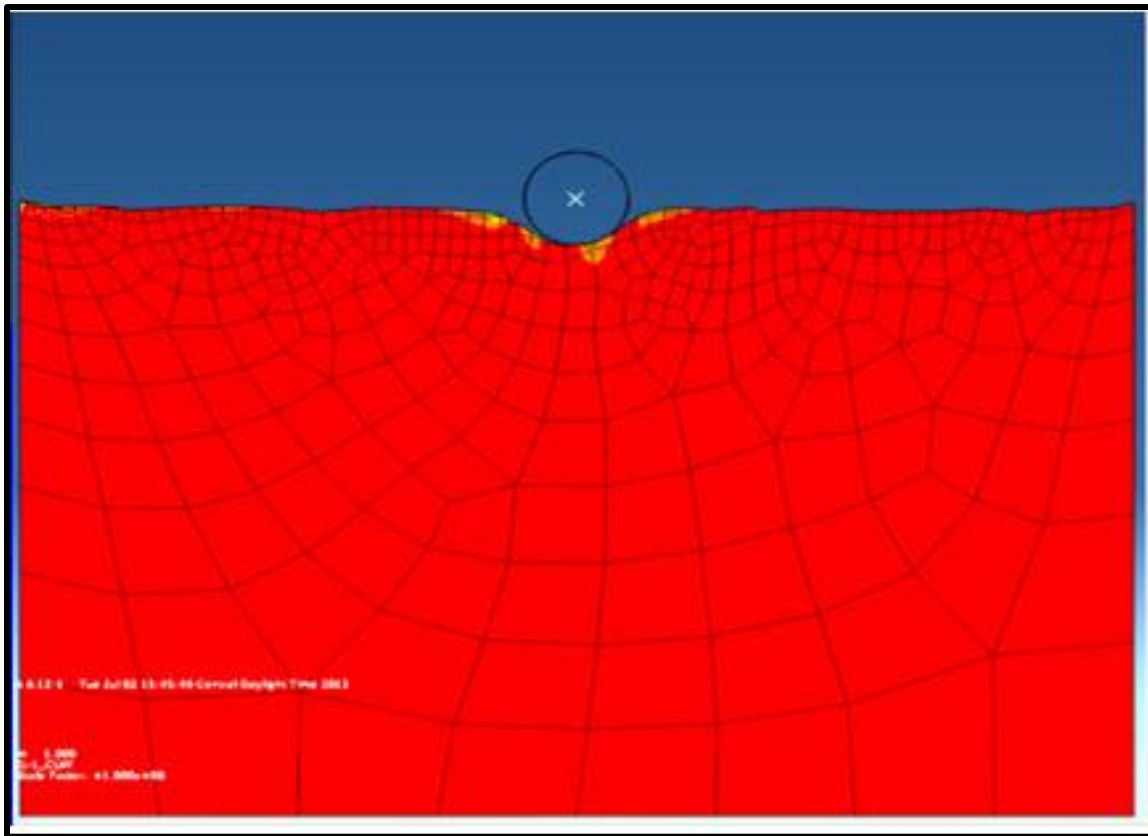


Figure 4.30: CEL approach was used in ABAQUS to model vertical penetration of pipe in soft soil

4.2.3.2 Axial sliding

Force-displacement responses and extra pipe penetration during axial cyclic sliding was recorded. New mesh configuration was defined and the coordination of the nodes of penetrated pipe, and a stresses at integration points and reaction forces of soil and pipe transferred to new meshes (Figure 4.31). In order to validate finite element models, initially set of parameters were chosen that matched those from our laboratory test. The results of different large displacement finite element approaches (in here pure Lagrangian, ALE, CEL) and experimental tests plotted in one graph for comparison reason (see Figure 4.32 and Figure 4.33). Lagrangian analyses due to mesh distortion were terminated at small displacement as predicted. Whereas, both CEL and

ALE successfully followed the trend of full scale tests. For all axial cases, the discrepancy of ALE and CEL from experimental results did not exceed 7.3 % and 12% respectively.

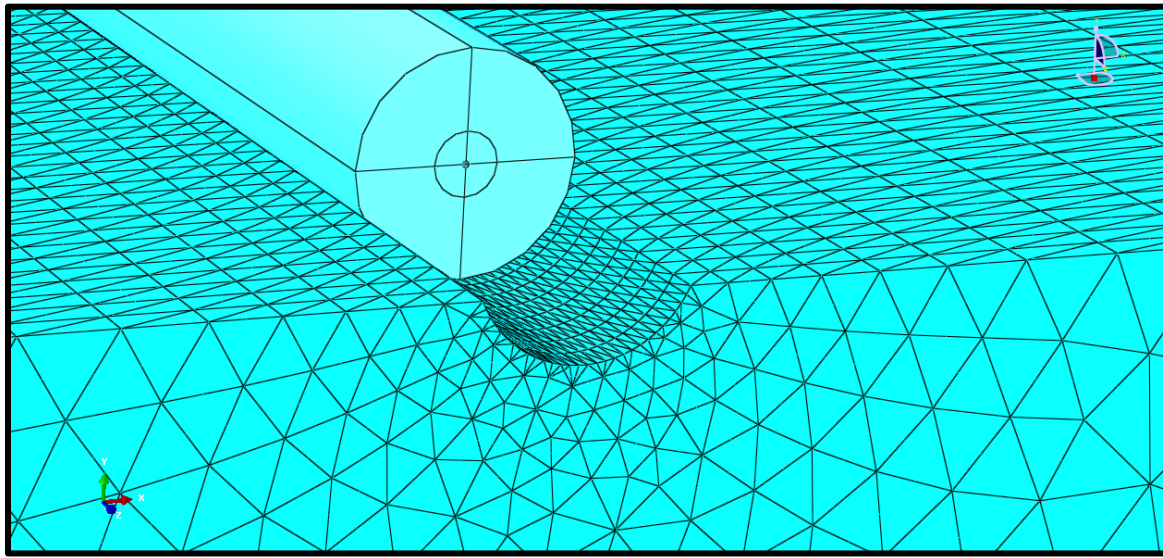


Figure 4.31: New mesh configuration formed for axial pipe sliding

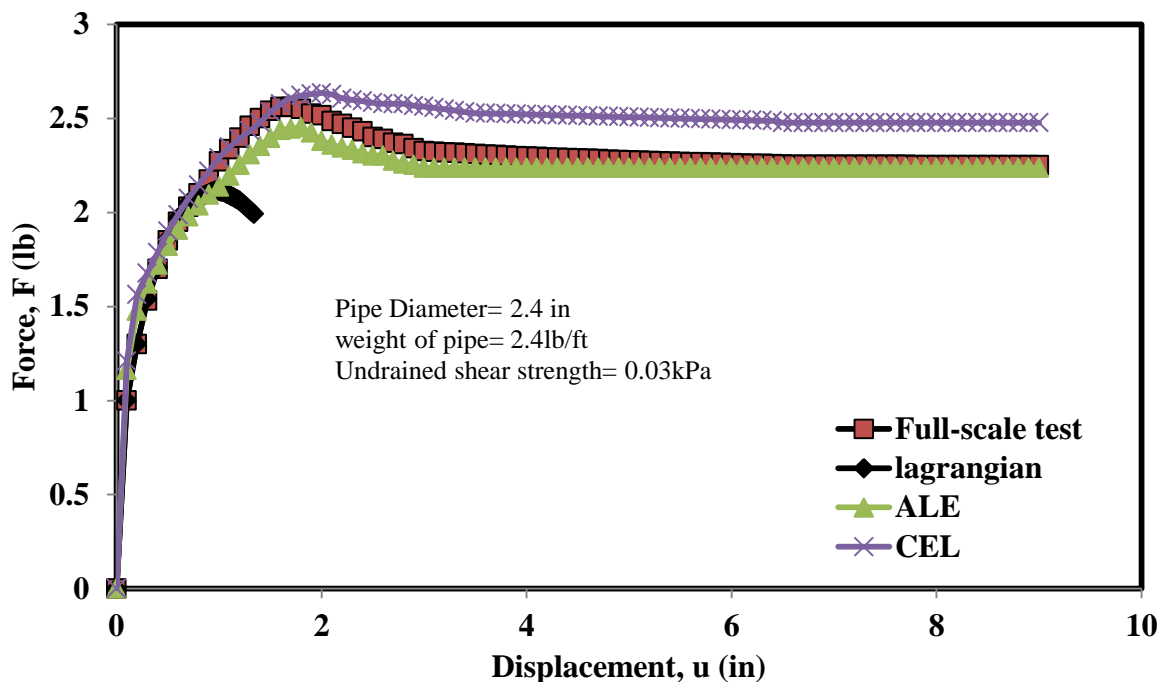


Figure 4.32: Axial force displacement responses for pipe sliding on soil with undrained shear strength of 0.11 kPa

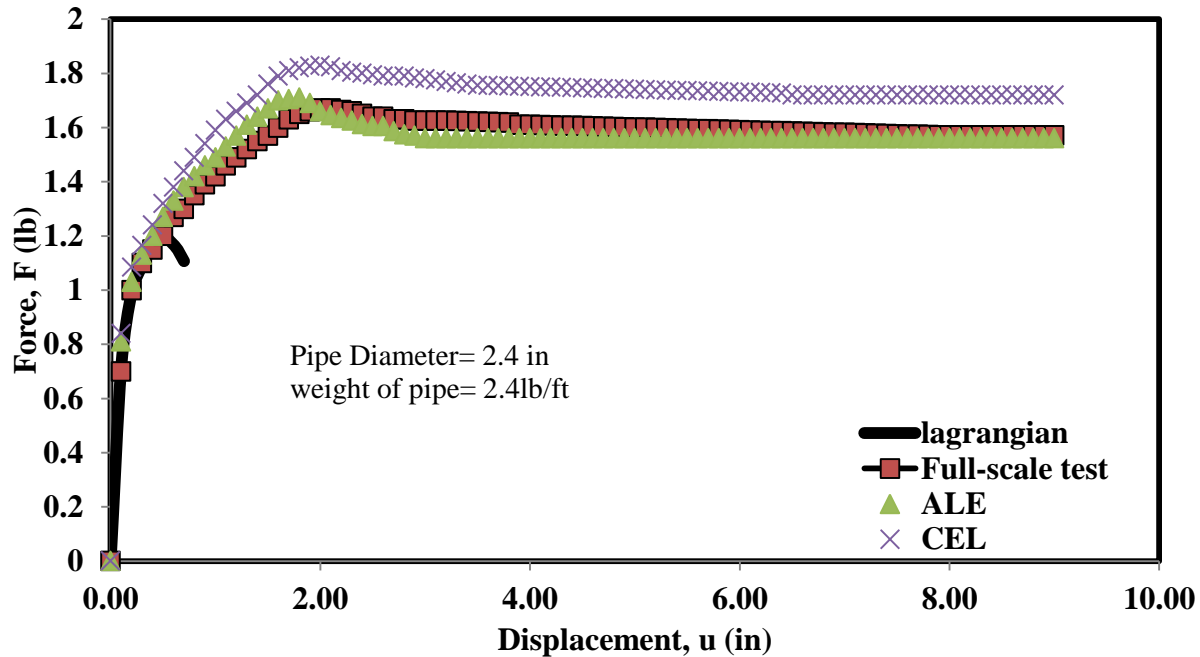


Figure 4.33: Axial force displacement responses for pipe sliding on soil with undrained shear strength of 0.03 kPa

4.2.4 Parametric study

In this part of study sixty-six numerical simulation were performed for vertical penetration and cyclic axial loading using Arbitrary Lagrangian Eulerian (ALE) approach. Details of the parameters chosen for this study are presented in Table 4-3. In table 4-3, the term no-over-penetration means that, the pipe was not manipulated during penetration but it moved down only by its own weight. The Horizontal reaction force during axial sliding, F was non-dimensionalised by DS_u and horizontal displacement was non-dimensionalised by pipe diameter D . Finally, the breakout resistance and residual resistance calculated from ALE finite element compared to empirical equations proposed earlier in this chapter (Equation (4.2) and Equation (4.3)). The results showed differentiating of only 7.2 % and 4.5 % for $f_{\text{break-out}}$ and f_{residual} respectively.

Table 4.3 : Parameter chosen for ALE analysis

| Material | Su(kPa(psi)) | D (in) | W (lb-force) | δ_{initial} (in) | Vp (in/min) | λ (in) |
|------------------------|------------------|--------------|--------------------|------------------------------------|-------------|----------------|
| Plastic | 0.01 (0.0015) | 1.35,2.4 | 0.73, 2.36 | No-over-penetration | 0.10 | 96 |
| Plastic | 0.03 (0.0044) | 2.4,8.5 | 0.73, 2.36, 7.5 | No-over-penetration | 0.1,1.05,5 | 96 |
| Plastic, Metal | 0.06 (0.0087) | 1.35,2.4,8.6 | 0.73, 2.36 | No-over-penetration,0.25,0.35,0.45 | 1.05 | 96 |
| Plastic | 0.08 (0.012) | 1.35 | 2.40 | No-over-penetration | 1.05 | 10,96,24 |
| Plastic | 0.1 (0.0145) | 2.40 | 2.40 | No-over-penetration | 0.10 | 96 |
| Plastic , Metal | 1 (0.145) | 2.4, 8.5 | 2.40 | No-over-penetration,0.55 | 0.10 | 96 |

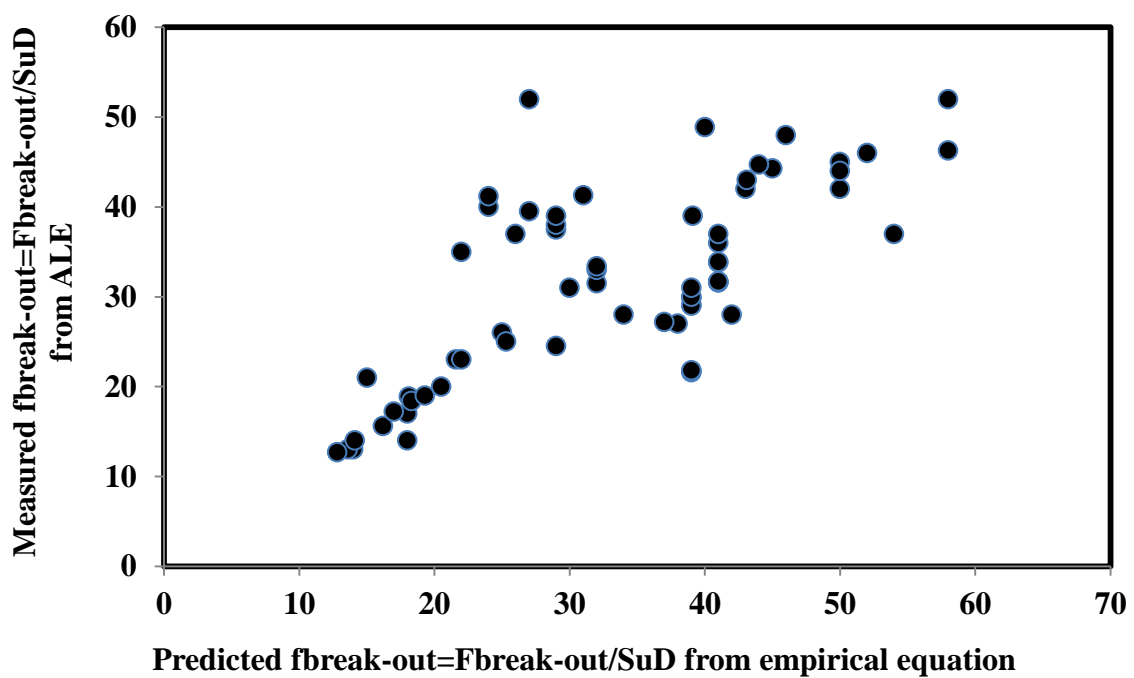


Figure 4.34: Comparison of the breakout resistance calculated from equation 4-2 and from ALE finite element analyses

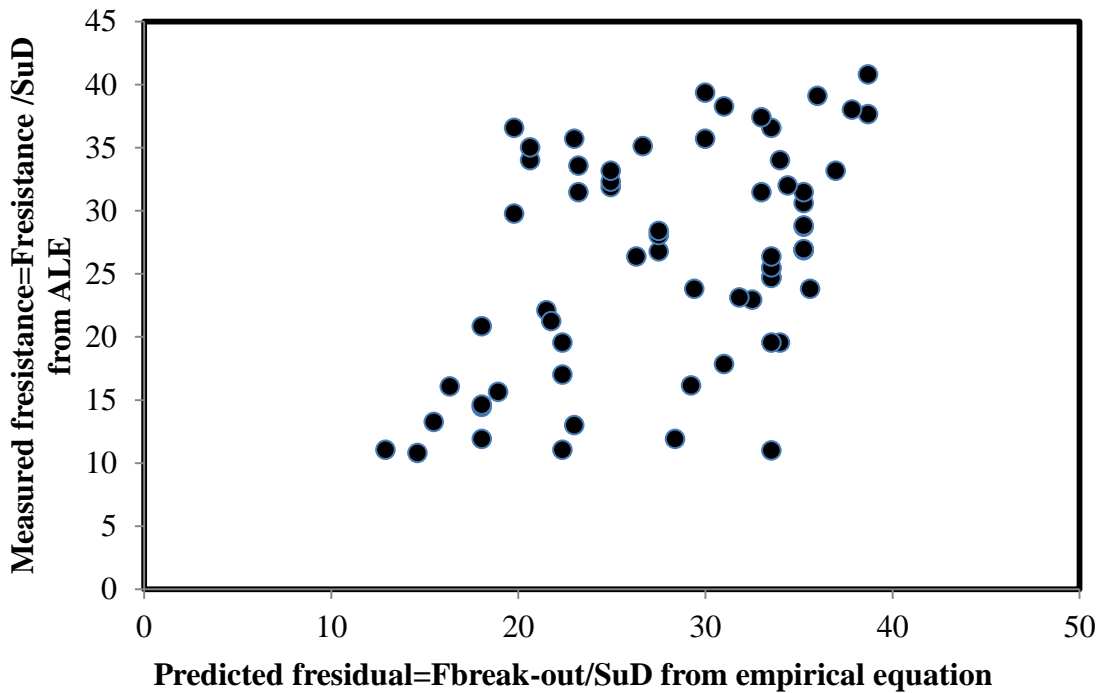


Figure 4.35: Comparison of the residual resistance calculated from equation 4-3 and from ALE finite element analyses

4.3 Summary

The objective of this chapter was to investigate pipe soil interaction during axial movement of subsea pipeline on very soft soil using both testing facilities and large displacement finite element methods. Based on the analyses of the results from our large scale model tests, following observations are advanced:

- (1) Maximum axial resistances (break out resistance) were reached after relatively short movement of the pipe. For the axial tests, the average residual frictional factor was about 15 % lower than Maximum frictional factor for the same rate of displacement, same undrained shear strength and same weight of pipeline.
- (2) Axial resistance was affected by the pipe material, the pipe weight, the rate of displacement and soil strength. Using plastic pipe (wet coating) instead of steel pipe (Pipe-In -

Pipe) increased the axial residual frictional factor. Increasing the rate of displacement and undrained shear strength of soft soil, decreased and increased the residual friction factor respectively. However, the axial frictional factor was not affected by the pipe weight.

(3) Both axial break out resistance and residual resistance were noticeably affected by dictating initial penetration of pipe and changing boundary length of soil sample.

(4) Modifying original p-q model, reliable empirical solutions were offered for predicting axial break out resistance, axial residual resistance and full range prediction of axial force displacement responses for soil with undrained shear strength in order of 0.02 kPa to 0.11 kPa.

Also the axial pipe-soil behavior was numerically modeled using the Coupled Eulerian Lagrangian (CEL) and Arbitrary-Lagrangian-Eulerian (ALE) formulations. Based on finite element analyses, following points were realized:

(1) Pure Lagrangian analysis provides very accurate responses only before very small displacement, where mesh entanglement occurs. However, ALE and CEL provide acceptable results for larger displacement in both vertical penetration and axial sliding.

(2) At the start of penetration, ALE trend is more similar to experimental but CEL draws better results for the total vertical penetration.

(3) A numerical parametric study of sixty-six different cases of axial pipe soil interaction based on ALE approach were performed for both vertical penetration and then axial sliding. The breakout resistance and residual resistance calculated from ALE finite element compared to empirical equations proposed earlier in this chapter. The results showed differentiating of only 7.2 % and 4.5 % for $f_{\text{break-out}}$ and f_{residual} respectively.

Chapter 5. LATERAL PIPE SOIL INTERACTION

5.1 Introduction

This chapter addresses lateral pipe/soil interaction behavior at the large displacements that occur with lateral buckling of a pipeline. The lateral behavior of deepwater pipeline is divided into two categories of fixed-end and free-end boundaries. In the latter, during the lateral loading the pipe is free to slide or rotate along longitudinal axis of pipe. In addition, the effect of pipeline material, rate of loading, pipe size and pipe weight on lateral force displacement responses will be discussed. It should be noted that lateral movement of short length pipe simulates the lateral displacement of a limited section of long pipeline at the crown of lateral bucking due to axial feed-in.

5.2 Fix-End and Free-End Lateral Loading

The lateral loads were transferred to the pipeline via solid loading frame (The frame dimension was adjustable according to pipe size and length). The pipe was rested inside an aluminum rectangular frame which was capable of inducing two different modes for frame-pipe boundaries as:

- 1) Free-end boundary, and
- 2) Fixed end boundary

Figure 5.1 illustrates that in the free end boundary mode, the pipe is free to rotate along y axis (longitudinal axis of pipe) and both rotation and sliding behavior are predictable during lateral movement. However, the fixed end boundary confines the lateral movement only to sliding without any rotation.

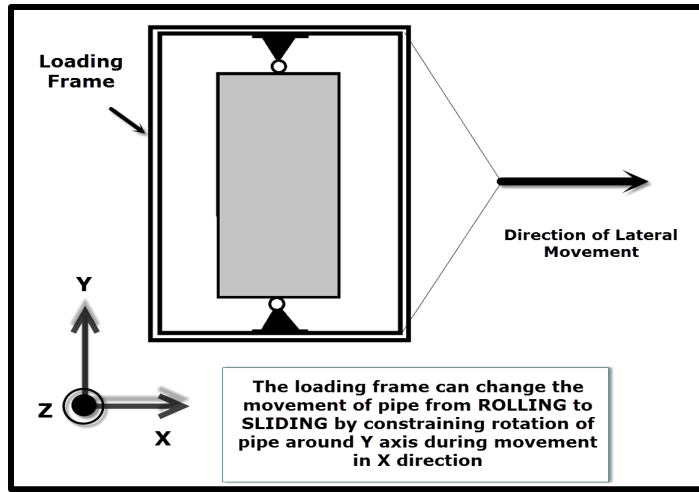


Figure 5.1: Specific lateral loading frame was implemented which is capable of controlling pipe ends fixity

A plastic pipe with a length of 4 ft and diameter of 8.5 in (Type: AL 102) with a dead load of 8.25 lb/ft and displacement rates of 0.8 in/min was instrumented for lateral loading. The test was performed in one half cycles using lateral loading frame with specific adjustment for two cases of free-end and fixed-end boundaries. For both cases, the pipe slowly laid on the soil and due to self-weight first, the pipe penetrated 2.35 in (28% of pipe diameter) within 5 minutes and after 24 hours, the pipe kept penetrating for 4 in (47% of pipe diameter). The first stage of penetration is called primary and the long-term penetration is called secondary penetration (Figure 5.2 and Figure 5.3). After the vertical penetration of laid pipe, the lateral test was performed. For fixed-end case, the pipe continuously penetrated for more 2.1 in (25% of pipe diameter). However, for free-end case, the pipe showed different penetration pattern as first the pipe smoothly penetrated to a maximum value and subsequently the pipe elevation raised. As shown in Figure 5.4, while the pipe is moved laterally, the vertical penetration of free-end pipe includes a discontinuity point.

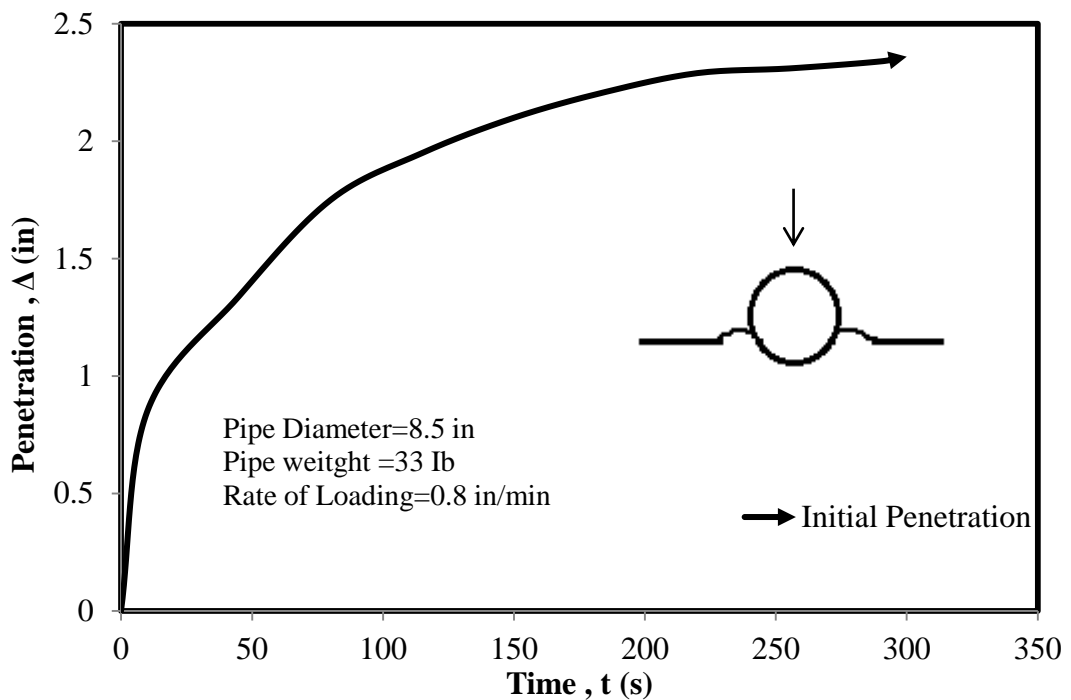


Figure 5.2: Primary penetration of plastic pipe after laying

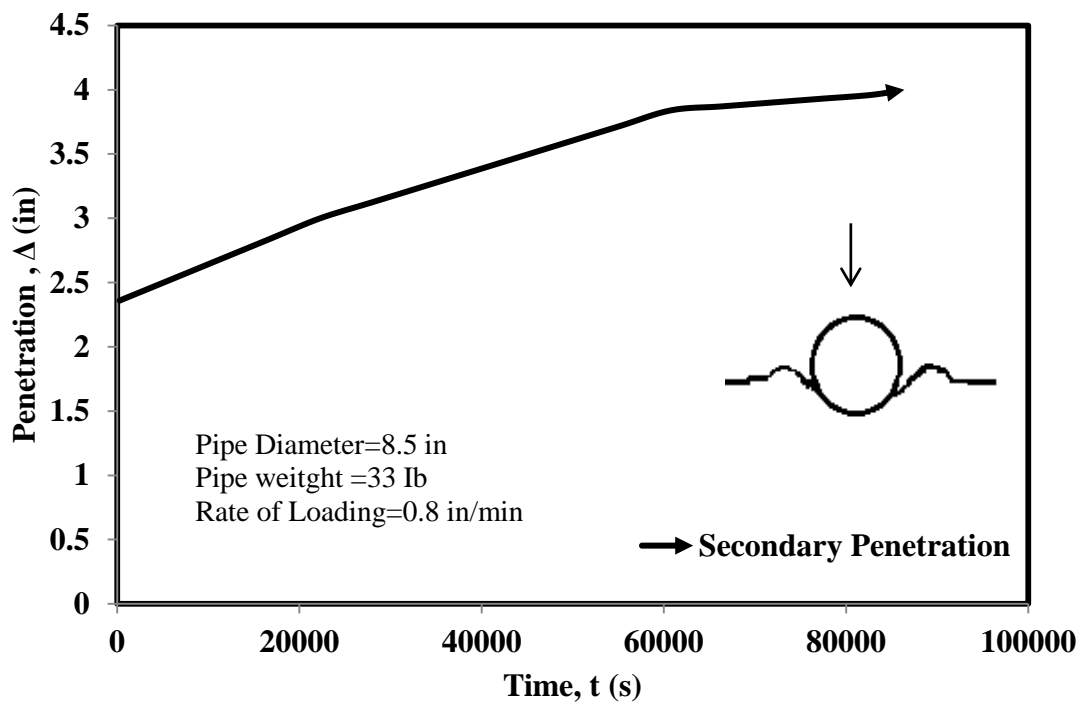


Figure 5.3: Secondary (long-term) penetration of plastic pipe

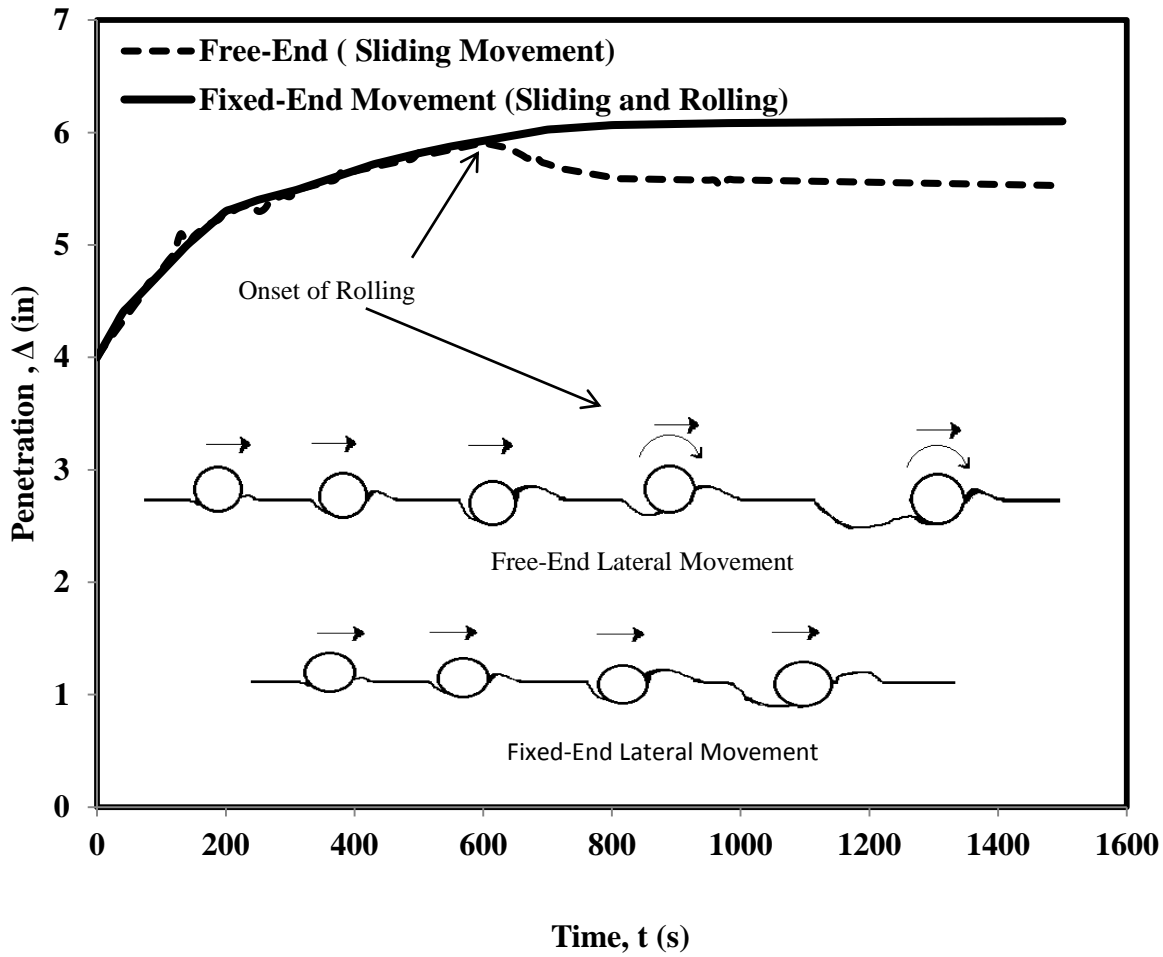


Figure 5.4: Vertical penetration of plastic pipe during lateral loading for both cases of fixed-end and free-end boundaries

Lateral pipe soil interaction results for both cases of free-end and fixed-end boundaries are shown in Figure 5.5. For this study, the fixed-end boundaries in comparison to the free-end boundaries developed more resistance of 39% against lateral displacement. On contrary to similar studies performed in other institutes, the lateral resistance smoothly reached a steady state (residual) without break-out behavior at any point. As for free end boundary, the lateral resistance initially increased for displacement of 6.8 in, then no increase was captured for 1.7 in and then the resistance again increased yet with slower rate. The start of this lag phase in resistance buildup predictably matched the discontinuity point observed in vertical penetration of

free-end lateral loading. RGS analysis later cleared that the aforementioned point is the onset of pipe rotation (rolling), that is, in free-end case the pipe initially slides and after the pipe mobilized, it simultaneously slides and rotates. In-depth analysis of pipe mechanics during lateral loading could rationalize the pipe behavior. When the pipe moves laterally, the berms accumulate in front of pipe and plausibly more force is required to mobilize both berm and pipe. In the meanwhile, the skin friction of pipe and soil increases and finally there would be no sliding between pipe surface and soil. At this point the pipe rotates and passes over the generated berms. As a result, the lateral resistance and skin friction significantly drops and the pipe can slide again. The new berms begin to form on top of old berms and sliding-rolling cycles repeat.

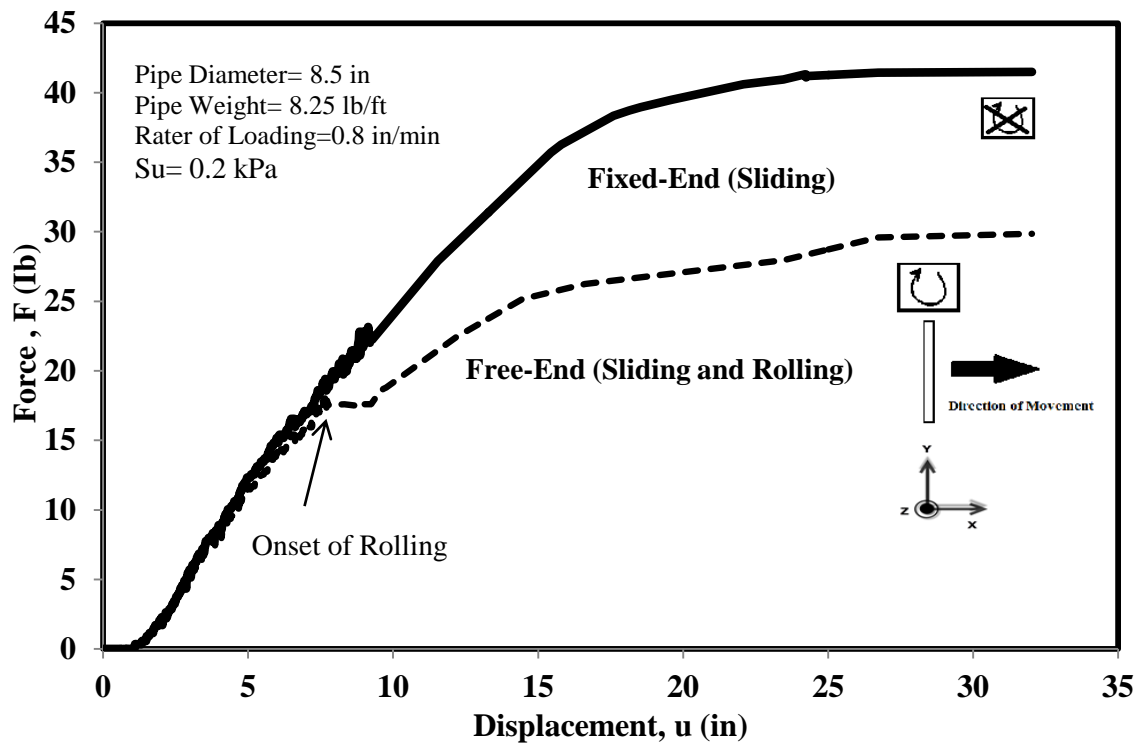


Figure 5.5: Effect of boundary condition on lateral pipe soil interaction

5.3 Effect of Pipeline Material

A plastic pipe with a length of 4 ft and diameter of 3.5 in with a dead load of 4.75 lb/ft and a steel pipe of same diameter and length with the dead load of 4.75lb/ft were used for this study. For both pipes, the boundaries were considered as free-end and the undrained shear strength of soil was 0.08 kPa (0.0116 psi) which measured before during and after each test to ensure soil consistency. As shown in Figure 5.6, the plastic pipe reached a steady state resistance of 17.48 lb at a displacement of 23.9 in or 680% of diameter without any breakout resistance. While, the metal pipe smoothly reached to the maximum steady state resistance of 10.2 lb at a displacement of 26.2 in or 750% of diameter without any breakout resistance. The steady state resistance for plastic pipe was 42% more than steel pipe as the soil in the plastic interface tends to adhere more rigorously to pipe. In addition, discontinuity in resistance increase was observed faster for plastic pipe than for metal pipe.

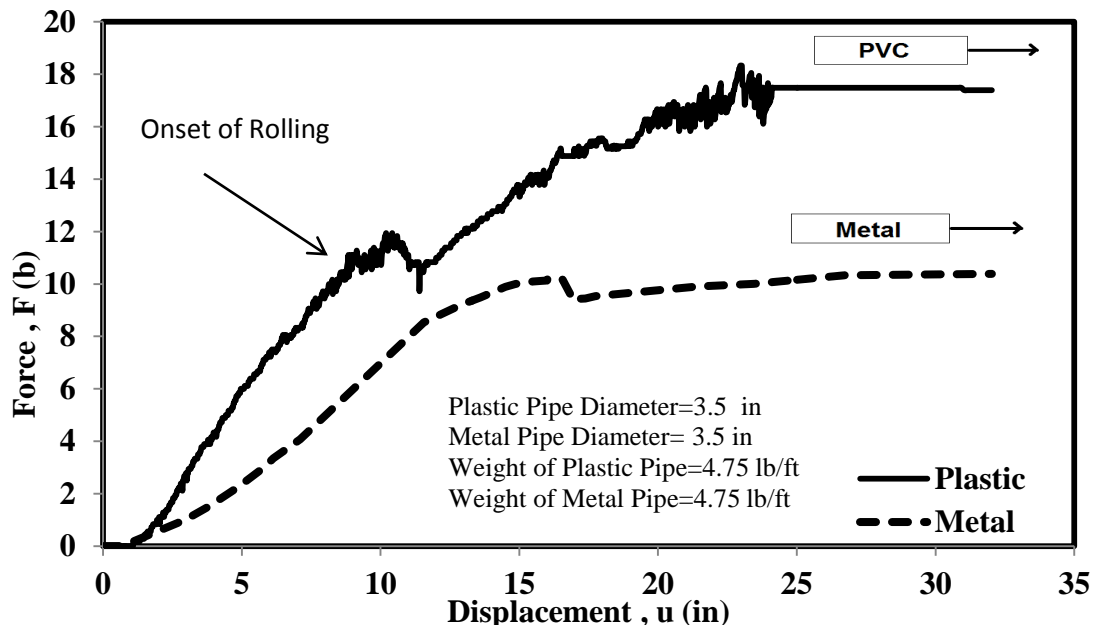


Figure 5.6: Effect of pipeline material on lateral pipe soil interaction of plastic pipe

5.4 Soil strength

To study the effect of undrained shear strength on lateral responses, for both cases of free-end and fixed-end boundaries, a plastic pipe with a length of 4 ft and diameter of 8.5 in with a dead load of 8.25 lb/ft (Type: AL 102) was laid first on soil with undrained shear strength of 0.02 kPa for 24 hours to study vertical penetration. Then, the lateral test was performed with the constant rate of 0.08 in/min. Later, the same test was repeated for soils with shear strength of 0.08 kPa and 0.09 kPa. Continuous measurement of undrained shear strength before, after and during the test with reasonable time interval performed in five area of soil box to ensure soil homogeneity.

In free-end boundary case, the pipe laid on first soil sample ($S_u=0.02$ kPa) and the vertical penetration of 4.2 in was observed after 24 hours. The pipe demonstrated maximum penetration of 6.56 in, after lateral displacement of 7.3 in. For the second soil sample ($S_u=0.08$ kPa) and third soil sample ($S_u=0.2$ kPa), vertical penetration of 4 in and 3.67 in was respectively captured 24 hours after laying. Then, the pipe laterally moved and for the second soil sample, maximum vertical penetration of 5.84 in observed after displacement of 8.52 in and for the third soil sample, the maximum vertical penetration of 5.1 in observed after displacement of 9.9 in. With increase in soil undrained shear strength both initial and final penetration of plastic pipe reduced and the maximum penetration (discontinuity point) shifted slightly to the right.

In fixed-end case, no discontinuity point was detected and for all three soil samples the penetration gradually increased during lateral movement

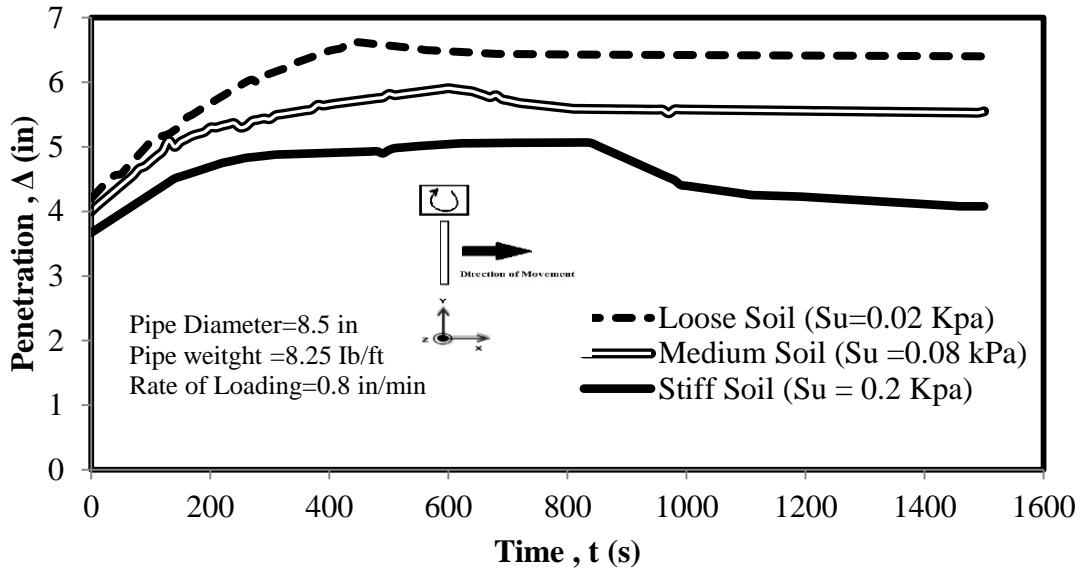


Figure 5.7: Vertical penetration of plastic pipe during lateral loading with free-end

. The ultimate penetration of fix-end boundary case was only 4.6% more than free-end boundary in loose soil ($S_u=0.02$). However, in stiff soil with undrained shear strength of 0.2 kPa, the ultimate penetration of fix-end boundary case was 36% more than free-end boundary case (Figure 5.8).

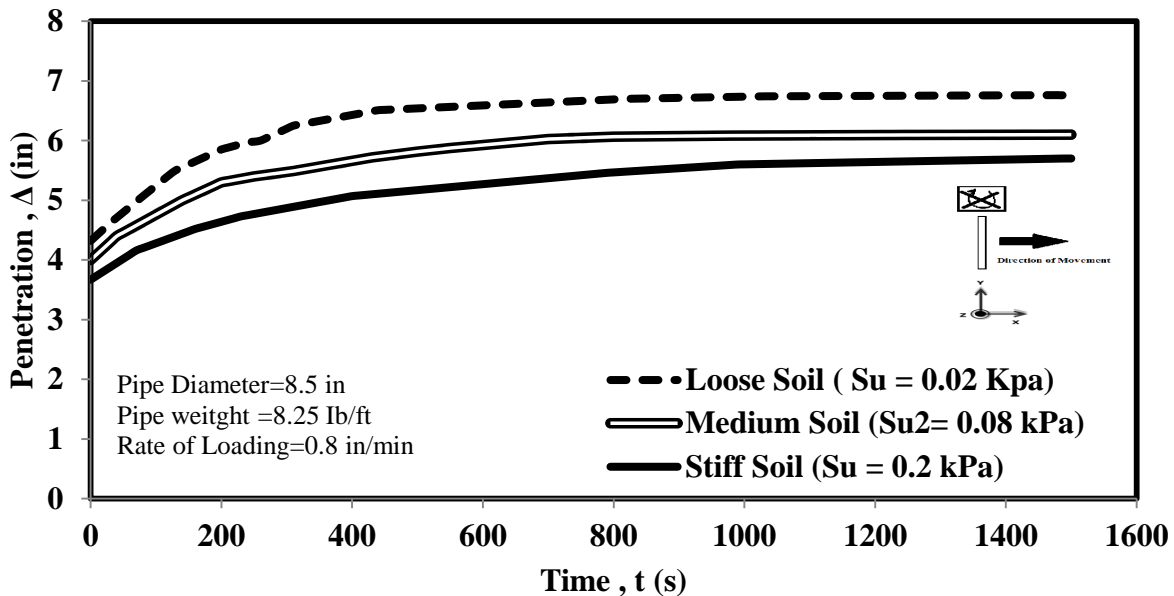


Figure 5.8: Vertical penetration of plastic pipe during lateral loading with fixed-end boundaries

Figure 5.9 demonstrates the effect of soil undrained shear strength on force displacement responses of laterally loaded pipe using free-end boundaries. For three cases of loose soil ($S_u=0.02$ kPa), medium soil ($S_u=0.08$ kPa) and stiff soil ($S_u=0.2$ kPa) after displacement of 32 in (3.76 D), the pipe respectively reached steady state resistance of 18.7 lb, 23.8 lb and 29.8 lb. In addition, resistance increase lag observed faster for stiffer soil.

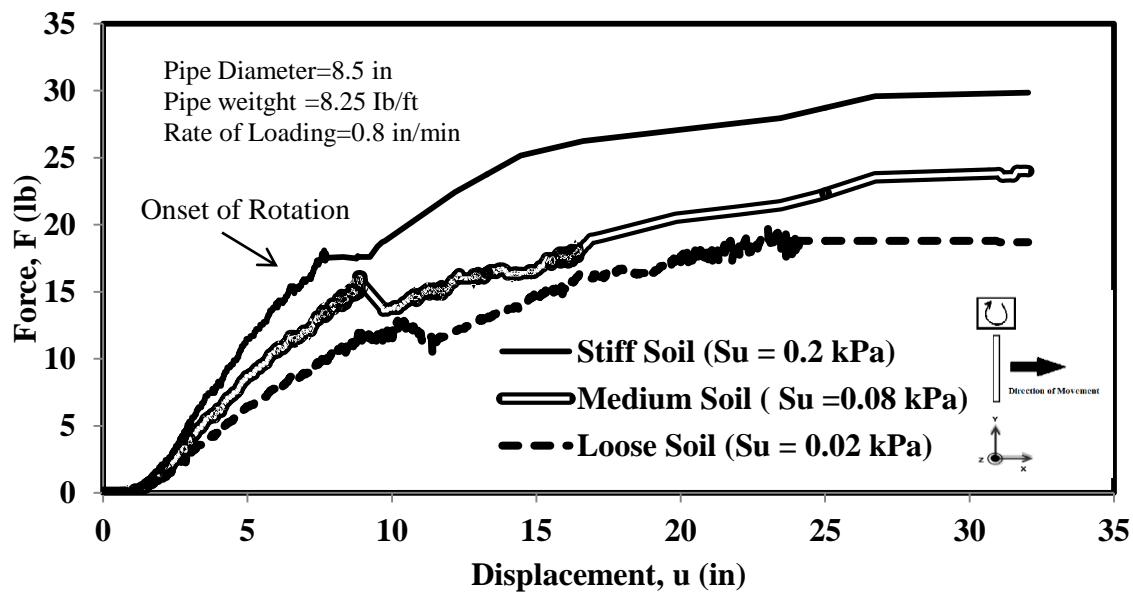


Figure 5.9 : Effect soil shear strength on lateral pipe soil interaction with free end boundaries

The results of lateral pipe soil interaction on three different soil samples and considering fixed end boundary case is graphed in Figure 5.10. With increase in soil shear strength for each axial test, the steady state of lateral resistance notably increased by 63% for medium soil (4 times increase in shear strength) and 108 % for stiff soil (10 times increase in shear strength). By changing free-end boundary to fixed-end boundary, the lateral resistance of stiff soil drastically increased by 41%, while this increase was 32% for medium soil and barely 5 % for loose soil.

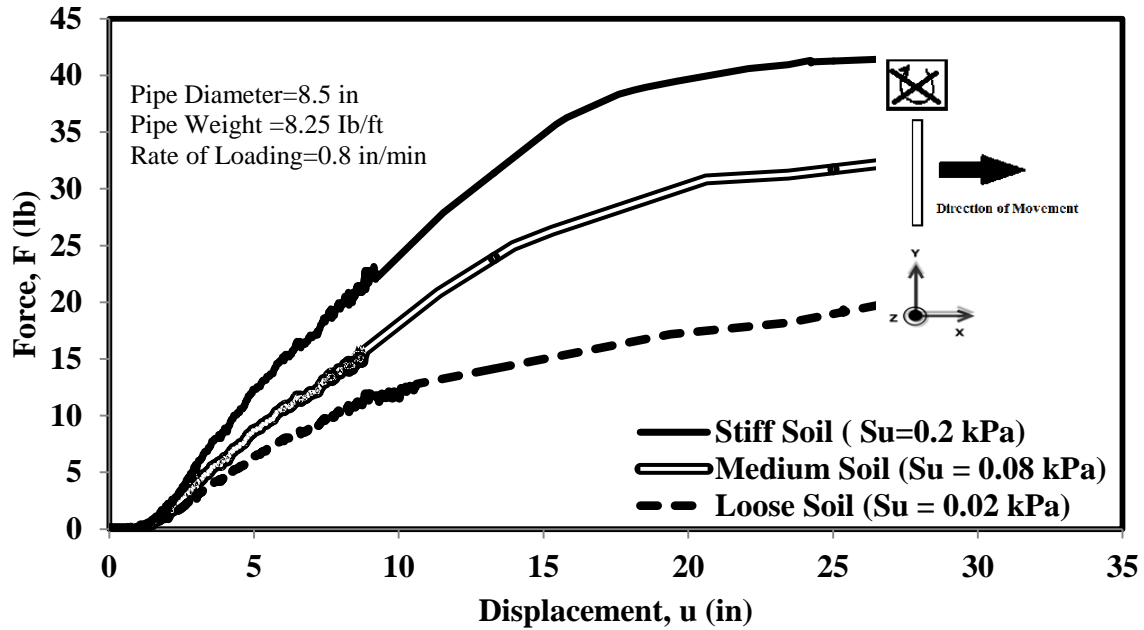


Figure 5.10: Effect of soil shear strength on lateral pipe soil interaction with fixed end boundaries

5.5 Rate of Loading

A plastic pipe with a length of 4 ft and diameter of 8.5 in with a dead load of 12 lb/ft and displacement rates of 2.54mm/min (0.1 in/min), 26mm/min (1.01 in/min) and 127 mm/min (5 in/min) was used in this study. With increase in the rate of displacement the steady state resistance increased respectively by 17% and 24%. One of the important results of this study was that by increasing the speed of lateral movement in very soft soil (order of 0.08 kPa), the breakout resistance could happen. As Figure 5.11 shows, the breakout resistance of 32.7 took place at displacement of 4.34 inch with rate of loading of 5 in/min.

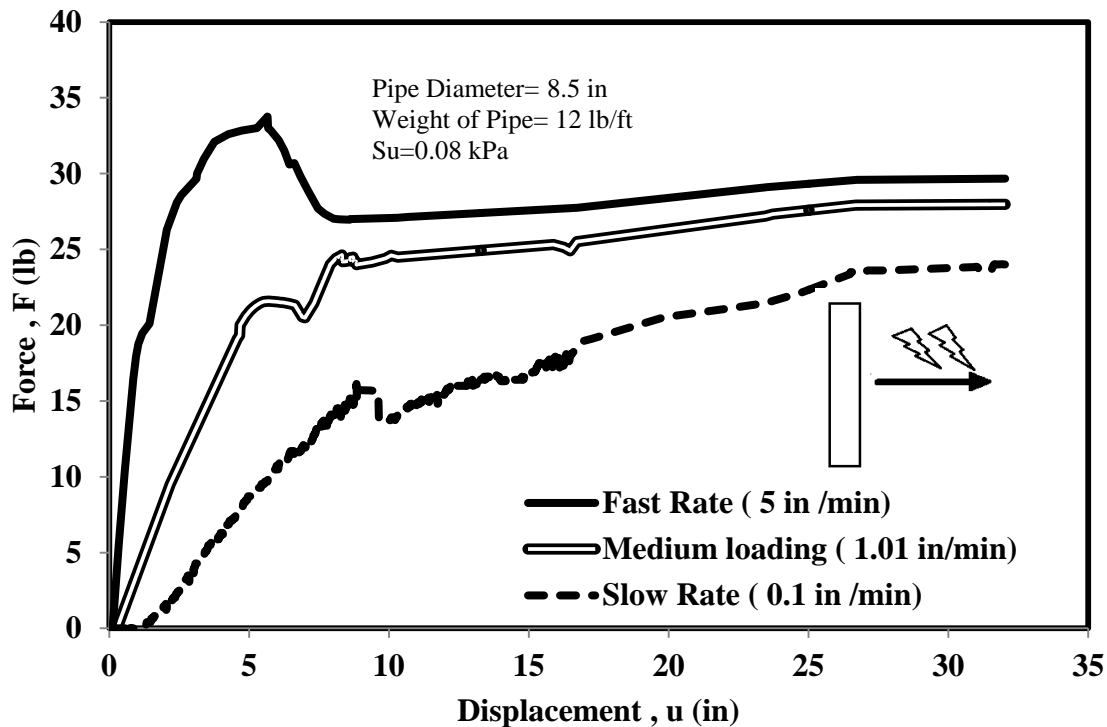


Figure 5.11: Effect of rate of loading on lateral pipe soil interaction with free end boundaries

The main reason for significant increase in lateral steady state resistance after increase in rate of loading could be justified only by analyzing the history of excess pore water pressure below the pipe (in here 1 D beneath the pipe invert). Figure 5.12 exhibits that by movement of pipe, the excess pore water pressure instantly increases and reaches plateau but the faster the pipe is dragged; less excess pore water pressure is generated. On the other hand, the resistance stresses at the interface of pipe is reversely related to pore water pressure, which is very similar to effective stress when decreases by the growth of pore water pressure. So that increase in rate of loading will also increase the steady state (residual) resistance.

Pore Water Pressure and Rate of Loading

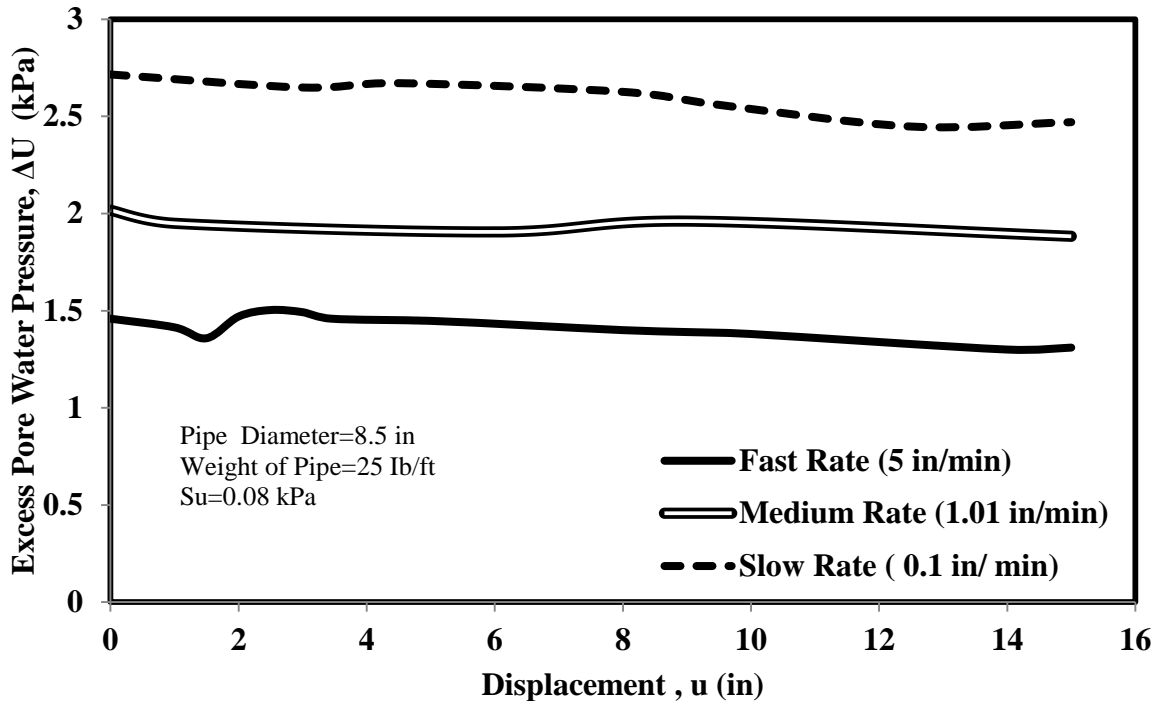


Figure 5.12: Variation of excess pore water pressure during lateral movement with different rate of loading

5.6 Effect of Pipe Size

Two plastic pipes with length of 4 ft and diameter of 2.4 in as “small pipe” (Type: AL 101 B) and 8.5 in as “big pipe” (Type: AL 102) was used for this part of study. The lateral test was performed with the constant rate of 0.3 in/min for both small and big pipe. The undrained shear strength was 0.2 kPa and continuous measurement of undrained shear strength before, after and during the test with reasonable time interval performed to ensure soil homogeneity. The small pipe reached a steady state resistance of 5.9 in at a small displacement of 3.3 in and with break out resistance of 6.4 lb at displacement of 1.02 in.

However big pipe gradually reached a steady state resistance of 29.6 at displacement of 26.6 in or 312 % of diameter (3.12 D) and no break out resistance was observed. The results suggested that the size of the pipe is a key factor in formation of breakout resistance.

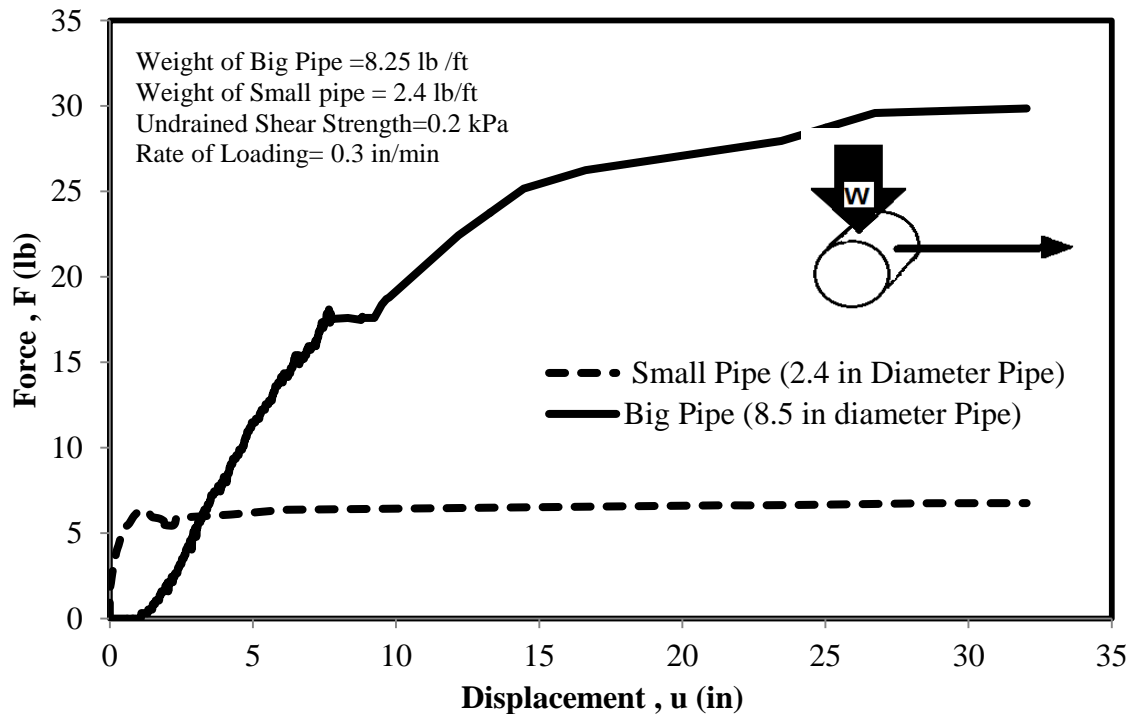


Figure 5.13: Effect of pipe size on lateral pipe soil interaction with free end boundaries

5.7 Influenced Area of Soil

A plastic pipe with a length of 4 ft and diameter of 8.5 in (Type: AL 102) with a dead load of 8.25 lb/ft and displacement rates of 0.3 in/min was instrumented. The test was performed in three full cycles (each full cycle included one Forward and one backward movement) and by employing RGS, surface displacement field of soil particles was achieved as shown Table 5.1. At the first cycle, the direction of particle movement is almost perpendicular to the direction of pipe movement. However, at second and third cycles, soil particles shows reveals complicated behavior and the area of disturbed soil increases (Figure 5.14)

Table 5.1: Surface displacement of Soil particles during cyclic lateral loading

| | |
|-----------------------------|------------------------------|
| | |
| <p>First Cycle Forward</p> | <p>First Cycle Backward</p> |
| <p>Second Cycle Forward</p> | <p>Second Cycle Backward</p> |
| <p>Third Cycle Forward</p> | <p>Third Cycle Backward</p> |

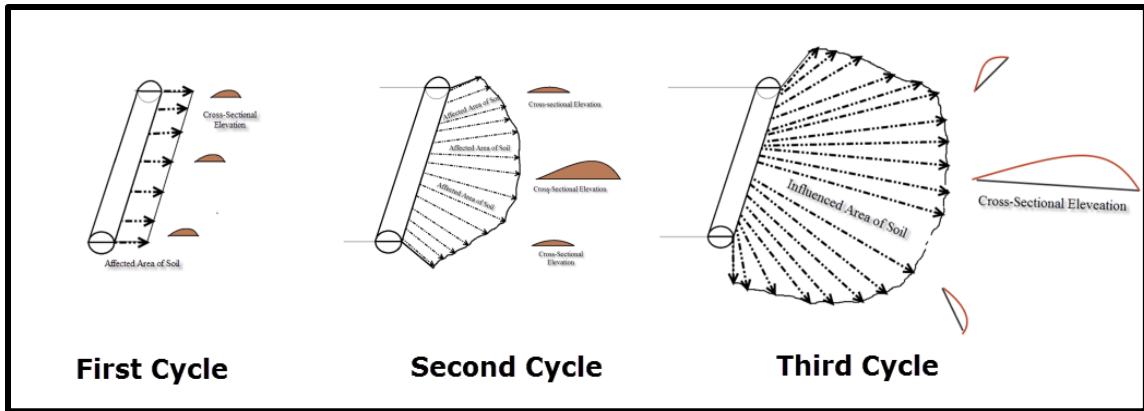


Figure 5.14: Gradual increase in the area of influenced (disturbed) soil during lateral loading of pipe

5.8 Summary

The objective of this chapter was to investigate pipe soil interaction during Lateral movement of subsea pipeline on very soft soil using both full scale testing and medium-size facilities. Based on the experiments, following observations are realized:

- (1) In free end boundary case, the vertical penetration during lateral loading and lateral force displacement responses both show a discontinuity point or a lag phase where the pipe starts to rotate. The lateral resistance was significantly increased by changing free end boundary to fixed end boundary case.
- (2) Lateral resistance was affected by the pipe material, the pipe weight, the rate of displacement and soil strength. Using plastic pipe instead of steel pipe increased the lateral residual resistance. Increasing the rate of displacement and undrained shear strength of soft soil, increased the residual resistance.
- (3) For the studied range of undrained shear strength, break out behavior was not common and the resistance gradually increased to steady state in absence of peak resistance.

Chapter 6. MITIGATION METHODS

6.1 Introduction

When the internal pressure and temperature increase to operating conditions, the pipeline tends to expand but this expansion is resisted by axial resistance between the pipe and the seabed. This restraint causes an axial compressive force to develop in pipeline (Burton, 2008).

Figure 6.1 shows the effective axial forces along the pipeline length for a typical pipeline with upper bound estimate of $\mu_{axial} = 0.58$ and lower bound estimate of $\mu_{axial} = 0.10$ for axial friction factor. This lower bound and upper bound correspond to drained and undrained axial friction respectively. The effective axial force is the force in pipe wall which depends on the operating condition of the pipeline and the axial friction. The fully constrained force is the maximum effective axial force that is possible to happen for pipeline with zero slenderness. The slow increase in effective axial force from zero to full-constraint is because of cumulative axial restraint of the soil. The slope of this line is equal to the axial resistance force ($F_{axial} = W_{pipe} * \mu_{axila}$). In case of high axial friction, the effective axial force reaches the fully constrained force. If the compressive force is sufficiently large, then the pipeline is vulnerable to lateral buckling (The buckling happens when the compressive force goes above the critical buckling force). Figure 6.2 confirms that buckling can drastically decrease the axial forces. In the case of lower bound friction ($\mu_{axial}=0.10$) the pipeline undergoes a significantly greater end expansion and will be susceptible to pipe-walking. However, the upper bound friction ($\mu_{axial}=0.58$) conveys that the pipeline will become fully-constrained over some of its length. As a result this section will not move in the axial direction (no pipe walking) but it releases the axial effective forces through lateral buckling.

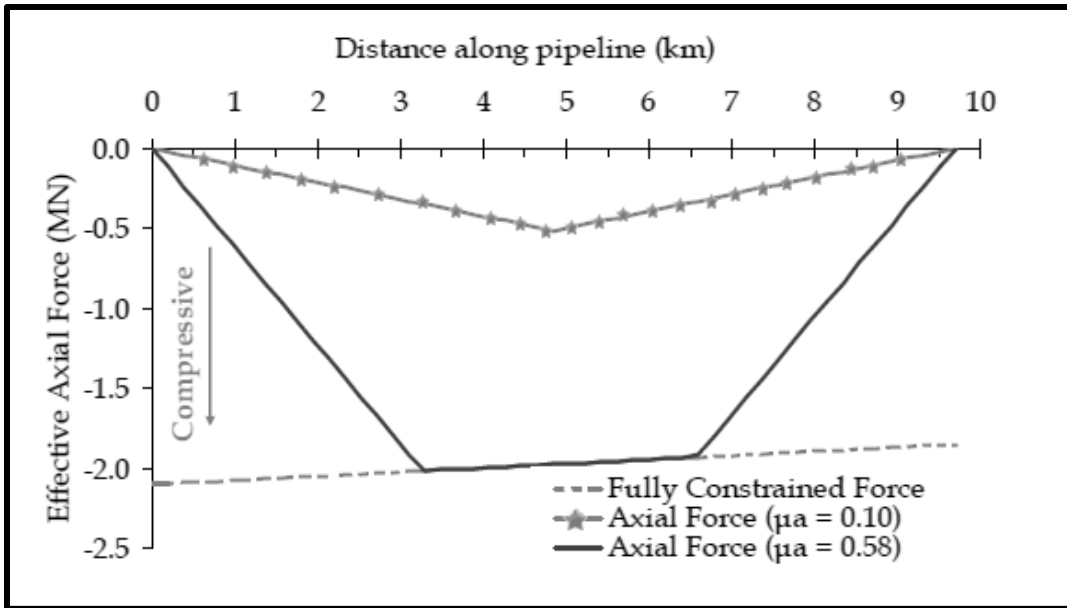


Figure 6.1: Effective axial force for a range of friction in a straight pipeline
(Burton, 2008)

According to Burton (2008) study, the design challenge in the low axial friction condition is controlling the extreme end expansion and its susceptibility to walking. However, for the high axial friction condition, the pipe is susceptible to buckling over most of its length and the design challenge is controlling the intensity of lateral buckling throughout the flowline and axial walking only near the free ends. For this part of study several full scale and medium-size tests are performed to advise mitigation approaches for both pipeline walking and lateral buckling.

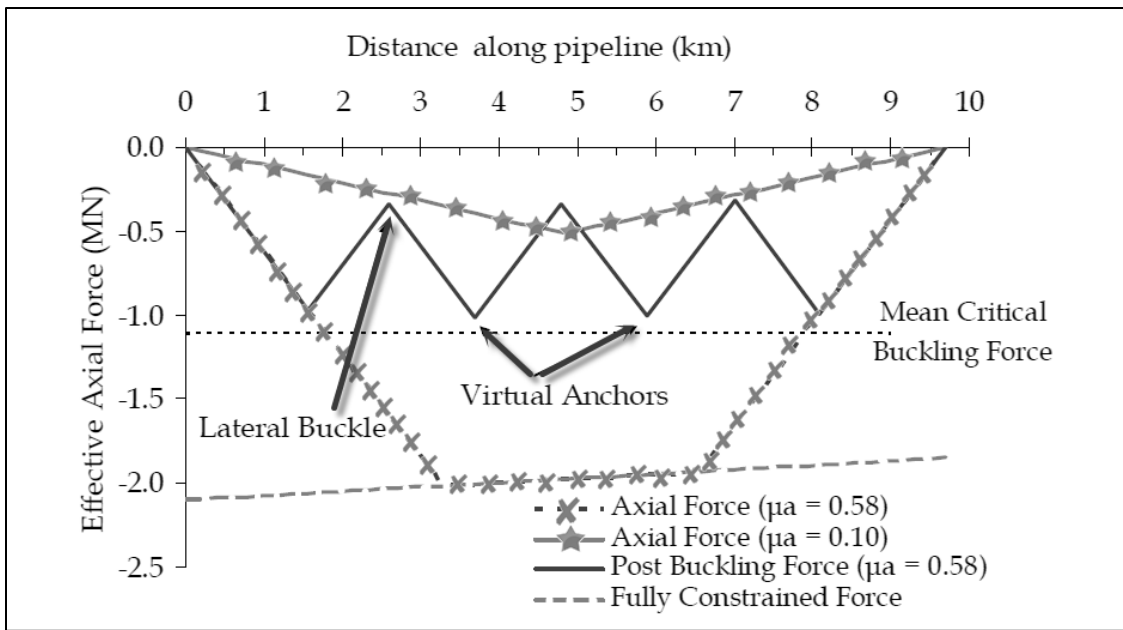


Figure 6.2: Effective axial force in a short pipeline with lateral buckles (Burton, 2008)

6.2 Axial mitigation

6.2.1 Application of Axial Resistors

The term “resistors” for the first time used in this study to refer to a proposed mechanical solution that could significantly increase axial resistance of subsea pipeline. Resistors are thin disk-shape apparatus installed around the pipe at prescribed distances. Spaces between resistors and radius of resistors are two key parameters in design methodology. Both medium-size and full scale soil boxes were employed to investigate the effect of different systems of resistors on axial pipe soil interaction. Three types of resistors system include solid resistors, spring-solid resistors and perforated resistors. The prototype of the first two types of resistors were first built and then tested in medium-size soil box and the axial responses compared with pre-snaked and no-mitigated pipes. As a benchmark, A plastic pipe with a length of 22 in and diameter of 3.5 in with a dead load of 1.53 lb/ft (Type: A 102) were used for this study. The undrained shear strength of soil for all tests were 0.07 kPa which measured before during and after each test to

ensure soil consistency. With the constant rate of horizontal displacement of 0.3 in/min, the sliding pipe reached a steady state of frictional resistance ($\tan(\phi)$) of 0.23 at a displacement of 0.84 in or 24% of diameter. As shown in Figure 6.3, no-mitigated pipe (benchmark pipe) at a relative displacement of 0.1 D, reached a frictional resistance (factor) of 0.26, whereas none of the mitigated pipes developed any break-out resistance. The axial frictional resistance of the pipe equipped with double resistors (Type: MA104) gradually increase to the maximum value of 0.74 after horizontal displacement of 10.5 in. Subsequently, the other type of axial resistors systems that are composed of three parts (fixed resistor, moving resistor and connecting springs) tested. Imagine the pipe is moving to the right direction, if the moving resistor is located in the right side of fixed resistor the connecting springs show compressive behavior, but if the moving resistor is the one in the left side, the springs will be in tension. Both mechanisms significantly escalated frictional resistance between sliding pipe and soft soil. For the resistors with compressive springs (Type: MA 105) the normalized force reached the limiting value of 0.76, which is 216% increase in axial resistance in comparison to benchmark test , at horizontal displacement of 5.9 in. The sliding pipe armed with resistors working in tension (Type: MA 106) smoothly reached to the maximum steady state of frictional resistance ($\tan(\phi)$) of 0.71 at a displacement of 8.26 in or 236% of diameter without any break out resistance.

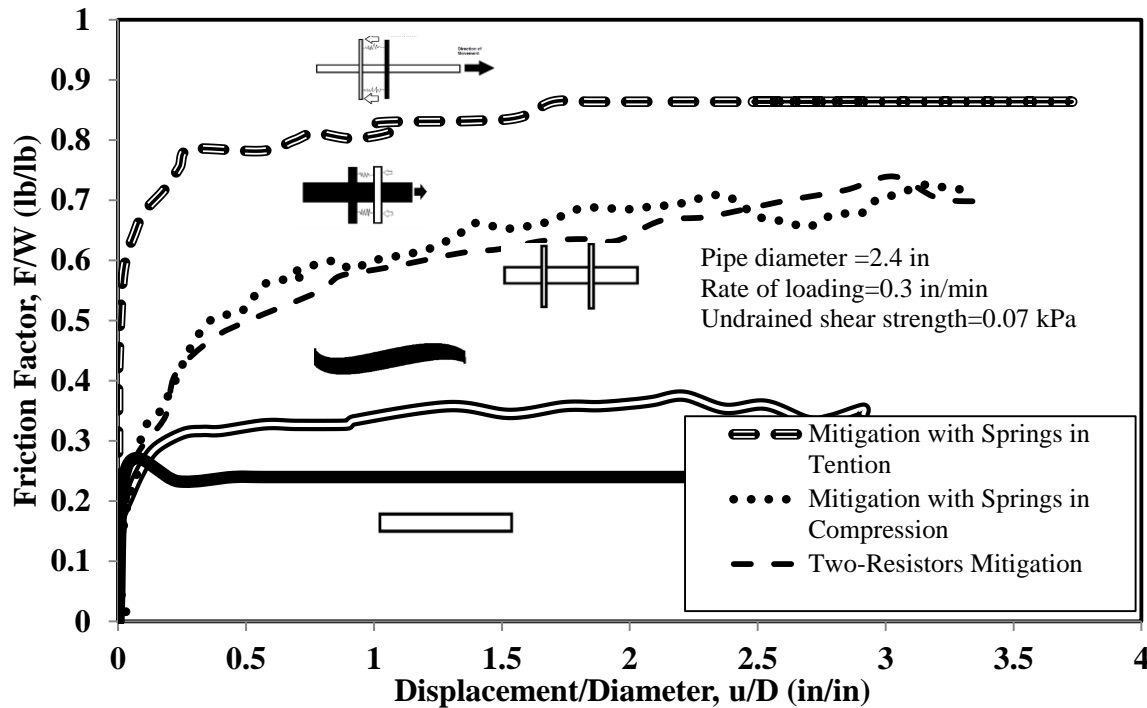


Figure 6.3: Axial mitigation methods in medium-sized soil box

Table 6.1: Axial mitigation solutions tested in medium-sized soil box

| | | |
|----------------------------------|--|--|
| | | |
| Axial sliding with no mitigation | Pre-snaked pipe | |
| | | |
| Double-resistors | Double-resistors with springs in compression | Double-resistors with springs in tension |

6.2.1.1 One Resistor or Two Resistors

Series of tests were performed in full scale soil box to study the effects of axial resistors on pipe soil interaction. The main challenge was to correlate the increase in frictional resistance to the spacing between resistors (or number of resistors per length). Accordingly, two plastic pipes with length of 4 ft and diameter of 2.4 in were tested on very soft soil with undrained shear strength of not more than 0.04 kPa. The first pipe geared with one single resistor with diameter of 6 in (Type: MA 102) and the second pipe was prepared with two fixed resistors installed at one-third and two-third of the pipe length (Type: MA 103 B) (see Figure 6.5 and Figure 6.6). With the constant rate of horizontal displacement of 0.5 in/min, the one resistor pipe reached a steady state of frictional resistance ($\tan(\phi)$) of 0.43 at a displacement of 2.16 inch or 90% of pipe diameter and a trivial break out resistance observed at displacement of 1.88 in. During the reverse loading (or backward loading) for single resistor mitigation method, the frictional resistance slowly increased to a limiting value without any break-out force development. However, a residual (steady state) resistance of 0.1 was observed at the end of first cycle (see Figure 6.4). In other words, the soil strength in the vicinity of pipe is remoulded. So that, the pipe moves easier with less resistance in the second half-cycle. The vane shear test confirmed 13% decrease in undrained shear strength at the center of soil box just after the second cycle.

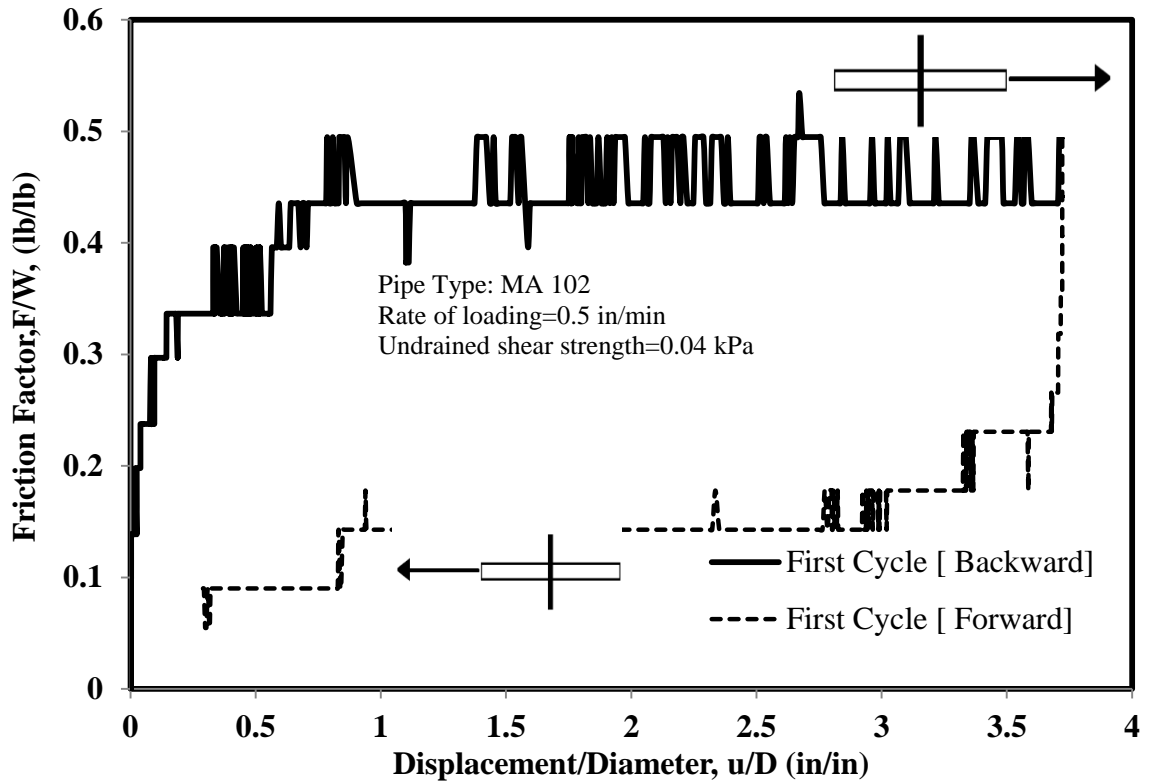


Figure 6.4: Single-resistor mitigation for the first cycle the axial sliding

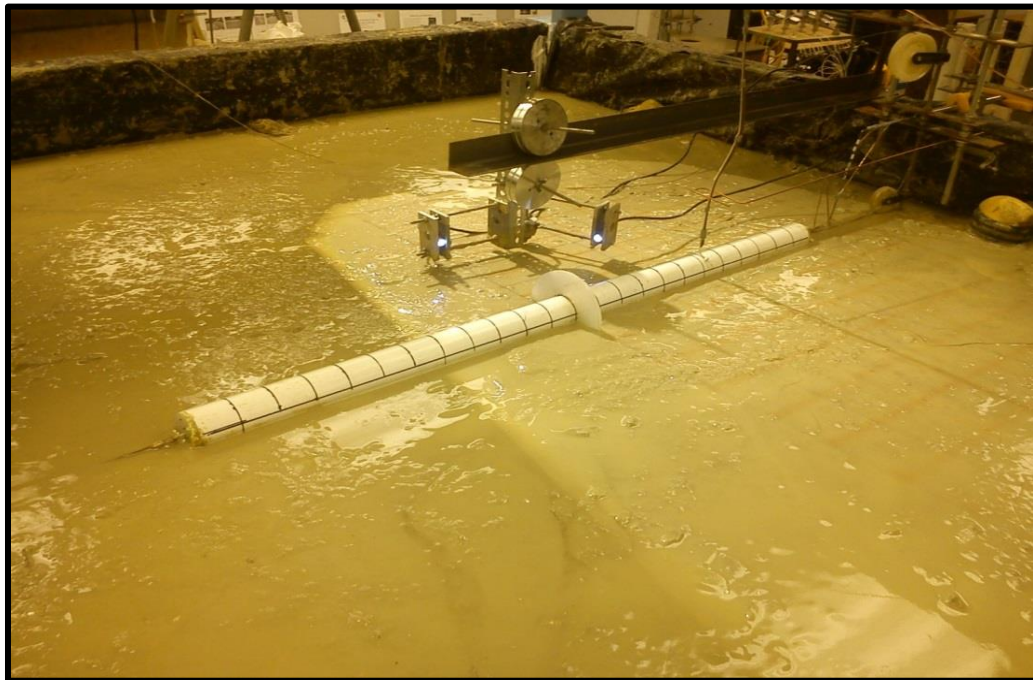


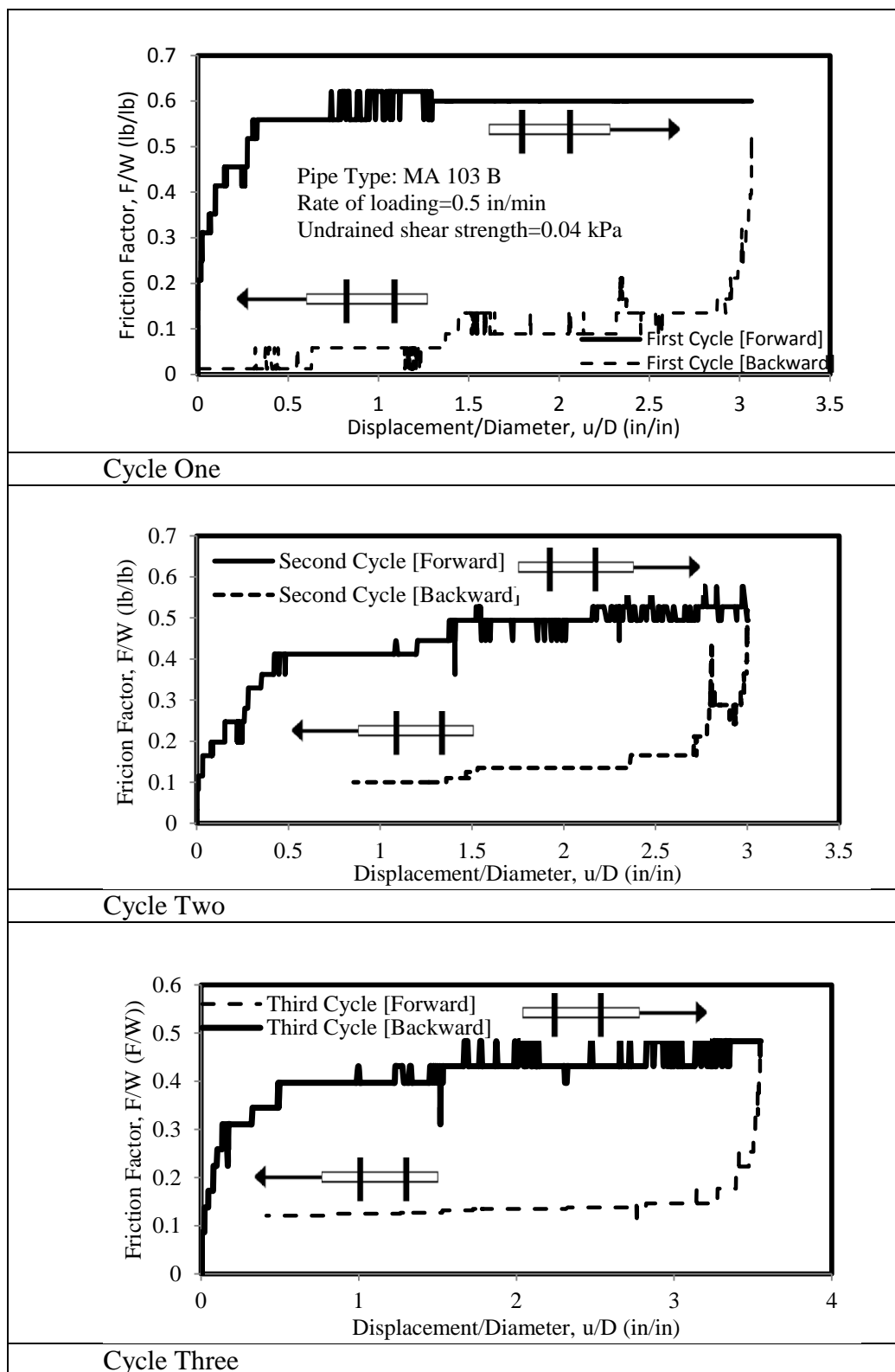
Figure 6.5: Single resistor mitigation method was tested in full-scale soil box

The cyclic loading was carried out for both one resistor and double resistors pipe. The axial results of the second pipe (with double resistors) for the first three cycles (each full cycle included one forward and one backward movement) are presented in Table 6.2. For the first cycle, With the constant rate of horizontal displacement of 0.5 in/min, the pipe reached a steady state of frictional resistance ($\tan(\phi)$) of 0.61 at a displacement of 2.76 in and a trivial break out resistance observed at displacement of 1.9 in. For the reverse loading of the first cycle, gradual mount in resistance was perceived to the limiting point almost equal to the steady state of first half-cycle. The trend of the second and the third cycles were similar to the first cycle with one concerning differences. For the second and third cycles, the gap between residual resistance of forward and backward half-cycles increased to the value of 0.11 and 0.13 respectively.



Figure 6.6: Double resistors mitigation method was tested in full-scale soil box

Table 6.2: Normalized force-displacement responses for the first three cycles of axial sliding when double resistors mitigation was employed



As debated earlier, the design focus in the low axial friction condition is controlling the extreme end expansion and its proneness to walking. The axial resistors are proposed in order to prevent pipeline walking in small displacement. Correspondingly, the best resistors system is the one that develop more resistance force within less displacement. For the purpose of comparison, the resistance force F , is normalized as F/W , where W is the total weight of system ($F/W=\tan(\phi)$) and displacement u , is normalized as u/D , where D is pipe diameter. Figure 6.7 investigates the effect of single and double resistors on normalized force displacement responses. When single resistor system devoted, the steady state resistance reached to the value of 0.43, which is 138% increase and when double resistors system employed, the steady state resistance reached to the value of 0.61 which is 240% increase in axial resistance In comparison to no-mitigated pipe.

After applying resistors system, the peak value (break out resistance) shifted slightly to the right. For example, the peak value for no-mitigated pipe detected at the displacement of 0.504 in, whereas the pick value for the double resistors system observed at the displacement of 2.1 in, which is equivalent to approximately 85 % of the pipe diameter.

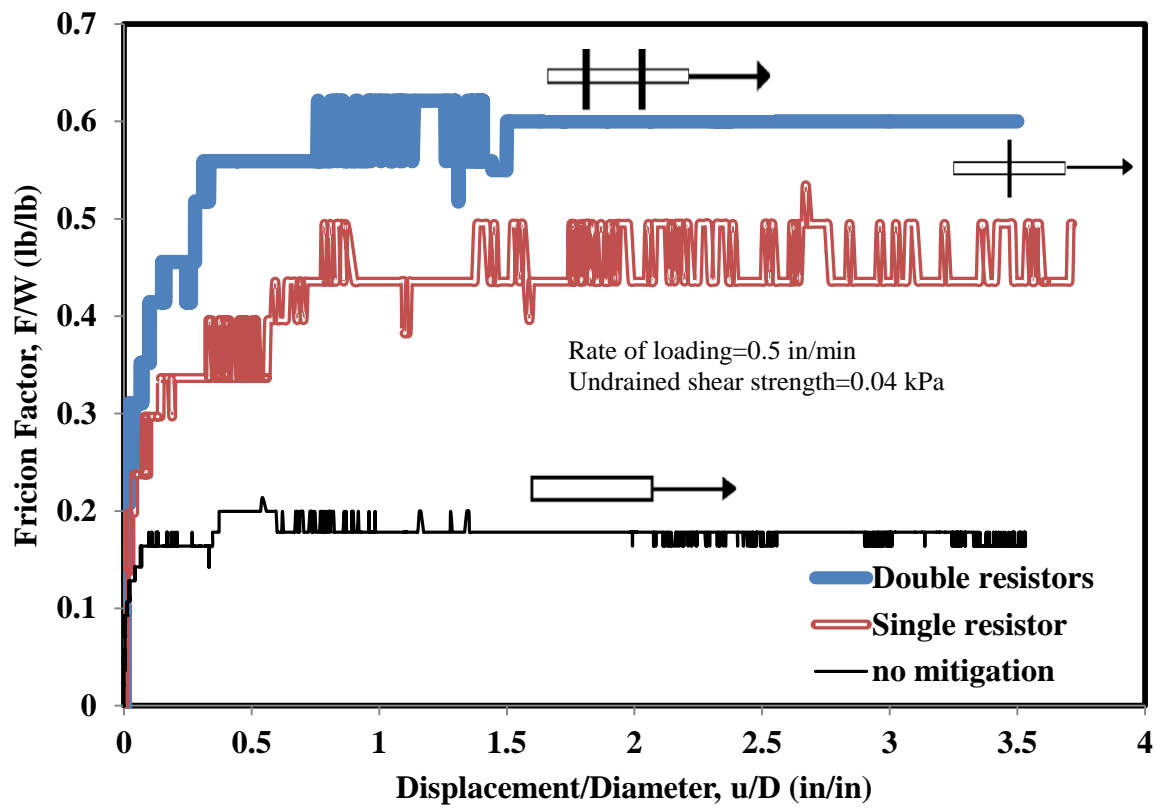


Figure 6.7: Effect of different axial mitigations on normalized force-displacement responses

6.2.1.2 15 % and 25 % Perforated Resistors

The third group of axial resistors (perforated resistors) is proposed with the purpose of achieving high frictional resistance $\frac{F}{W}$, but with lighter sections. In future, economic analysis should be performed to investigate whether the perforation cost justifies corresponding increase in the frictional resistance between subsea pipe and seabed. Two sets of plastic pipe with length of 4 ft and diameter of 2.4 in, one with 15% perforation (Type: MA101B) and another with 25% perforation (MA 101 A) were tested on very soft soil with undrained shear strength of 0.04 kPa (Table 6.3). With constant rate of 0.5 in/min, the 15% and 25 % perforated-resistors respectively increased the steady state resistance ($\frac{F_{residual}}{W}$) by 5.1 % and 7.9 %. Another detectable

phenomenon was relocation of the break out resistance ($\frac{F_{break-out}}{W}$) slightly to the right after employing perforated double resistors (Figure 6.8).

Table 6.3: Types of double resistors

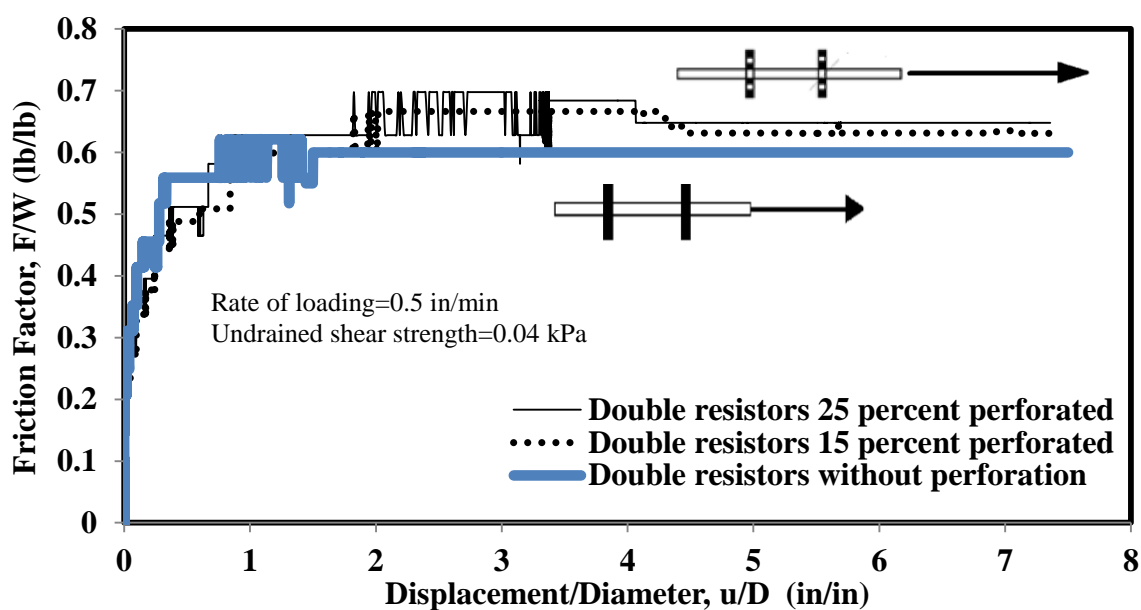
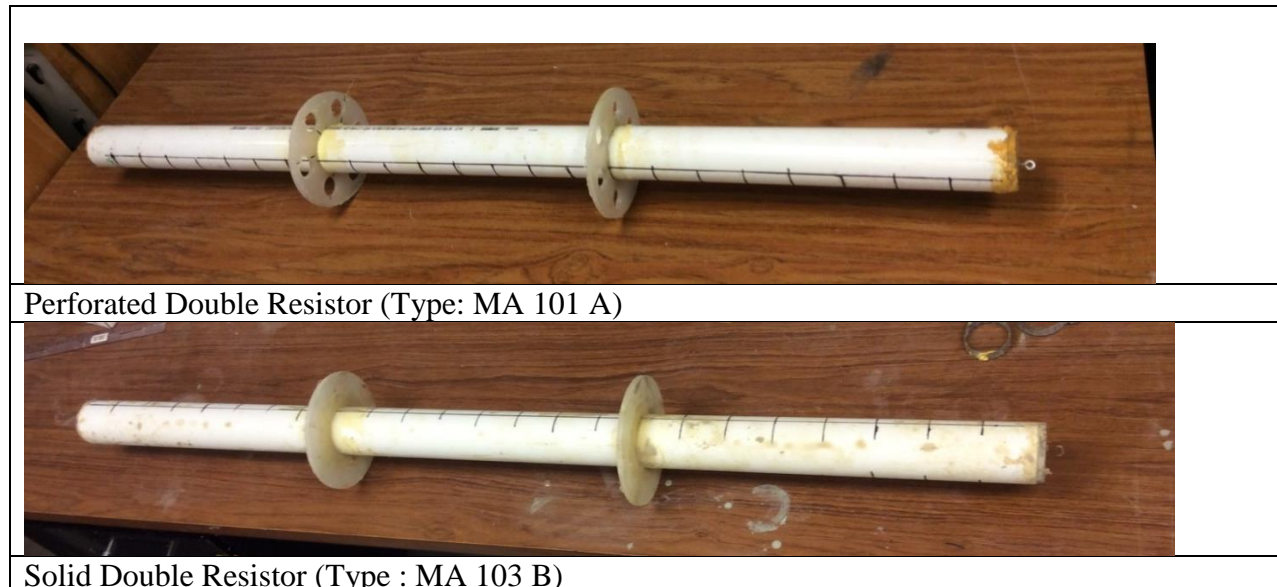


Figure 6.8: Normalized force-displacement responses for different type of double resistors during axial sliding

6.3 Pre-Snaking

The idea of snake lay is to provide an over length of the pipeline within the deliberate curves developed during pipe laying, which will absorb the expansion of the pipeline. Snake laying or pre-snaking is a common solution to mitigate the lateral buckling. However, this part of study examines the ensuing effect of snake laying (pre-snaking) on axial pipe soil interaction. Two types of pre-snaked pipe with length of 23.5 in and diameter of 1.325 in (type: MAL 303) and 3.5 in (Type: MAL 302) were built and tested in medium-size soil box (see Figure 6.4).

Table 6.4: snaked lay (pre-snaked) pipe tested in medium-size soil box

| | |
|---|--|
|  |  |
| Small diameter ($D=1.325$ in) snaked lay pipe | Small diameter ($D=1.325$ in) straight pipe |
|  |  |
| Big diameter ($D=3.5$ in) snaked lay pipe | Big diameter ($d=3.5$ in) straight pipe |

Figure 6.9 illustrates the effects of pre-snaking mitigation on axial pipe soil interaction. To make the results comparable, The axial force F, is normalized by pipeline weight W, and the displacement u, is normalized by Diameter D. Using pre-snaked mitigation method, the breakout frictional resistance ($\frac{F_{Break-out}}{W}$) was vanished and the corresponding resistance at displacement of 1.45 D exceeded the steady state (residual) resistance ($\frac{F_{residual}}{W}$) of no-mitigated pipe (straight pipe). The axial sliding test was also performed on the pre-snaked pipe with larger diameter (D=3.5) and the results plotted on Figure 6.10. On the contrary to the smaller pre-snaked pipe, the frictional resistance of pre-snaked pipe exceeded that of no-mitigated pipe (straight pipe) at very short displacement. In addition, the pre-snaked pipe mitigation resulted in higher residual resistance by 43 % in absence of any break-out resistance.

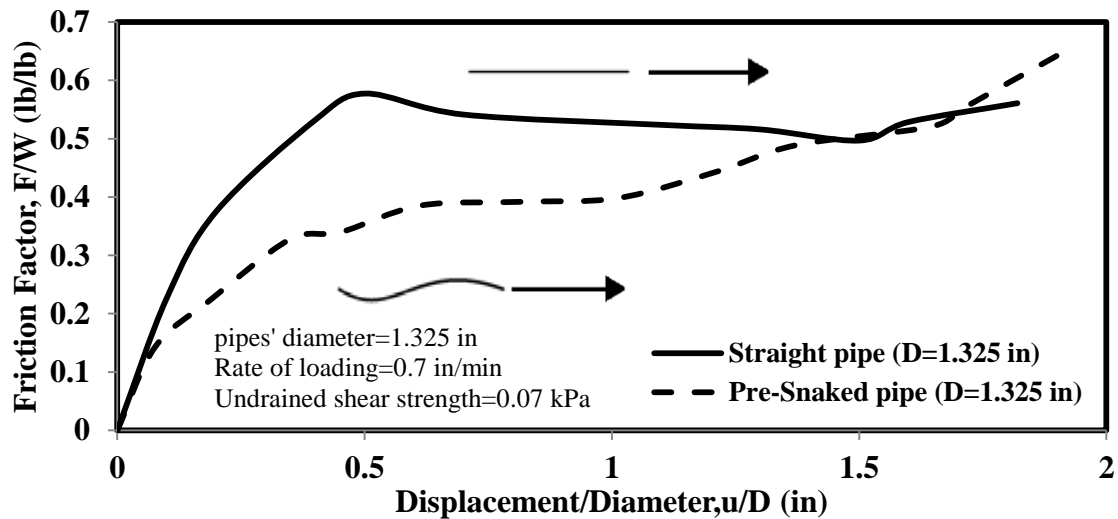


Figure 6.9: Comparison in axial responses of pre-snaked (Snaked Lay) and straight pipe (small pipe)

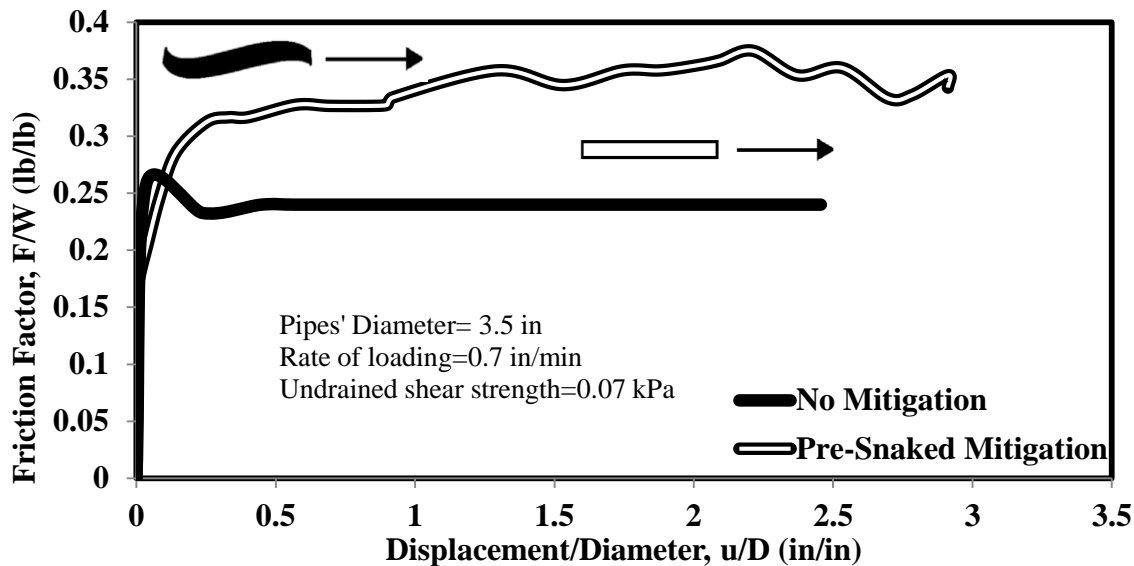


Figure 6.10: Comparison in axial responses of pre-snaked (Snaked Lay) and straight pipe (big pipe)

6.4 Lateral Mitigation

Different approaches such as sleepers, snake lay and buoyancy sections are widely used in subsea developments to mitigate lateral buckling of pipelines. The mechanisms are to trigger the lateral buckling in multiple locations by reducing the pipeline section submerged weight. This triggering is happening due to corresponding decrease in lateral pipe soil interaction. As a result, the most efficient buoyancy section is the one that extensively reduces the lateral pipe soil interaction. Two key design parameters for any buoyancy sections are buoyancy section length and buoyant force.

6.4.1 Application of Buoyancy Sections

At CIGMAT laboratory both medium-size and full scale soil boxes were used to investigate the effects of single buoyancy section and multiple buoyancy sections on the lateral force displacement responses. In the section, efficiency of different buoyancy sections considering rolling and fixed cases are studied.

6.4.1.1 Medium-size

As Figure 6.11 shows a pipe with length of 15.5 in and dead load of 3.95 lb was equipped with single rolling buoyancy section with length of 5 in and diameter of 6.5 in (Type: M203 B). The reduced submerged weight for 1 ft length of this buoyancy section was 295%. The mentioned pipe was laterally tested with displacement rate of 0.4 in/min on a very soft soil with undrained shear strength of 0.05 kPa, and the results were compared with the same pipe with no mitigation (see Figure 6.11).



Figure 6.11: Pipe equipped with single buoyancy section tested in medium-sized soil box

Figure 6.12 shows the lateral responses of a mitigated pipe in the first cycle (including forward and backward half-cycles). In order to make responses more comparable, resistance force F , is normalized with weight of pipe W , and displacement u , is normalized with diameter of pipe D . For no-mitigated pipe (benchmark pipe), the frictional resistance $\frac{F}{W}$ is divided into

four steps. First sharp increase to a maximum value (break out resistance), Second, abrupt decrease ,third, steady state (residual) resistance and four, gradual increase due to berm formation in front of pipe. According to Remote Gridding System (RGS), in soft soil with undrained shear strength of 0.01 kPa to 0.15 kPa, at the start of lateral displacement the pipe penetrates and laterally slides without any rotation but at a certain point the pipe starts to rotate and slide simultaneously and moves upward. Hence, the sudden drop in resistance is the result of change in the nature of pipe movement from sliding to rolling and the result of shear surface failure. With application of single buoyancy section, the steady state of frictional resistance $\frac{F_{residual}}{W}$ reduced by 39% and no break-out resistance was detected. It should be noted that for this particular test, the lateral resistance of second half-cycle was more than that of first half-cycle (which led to negative value of frictional resistance $\frac{F}{W}$) due to extensive penetration of pipe at the end of first cycle.

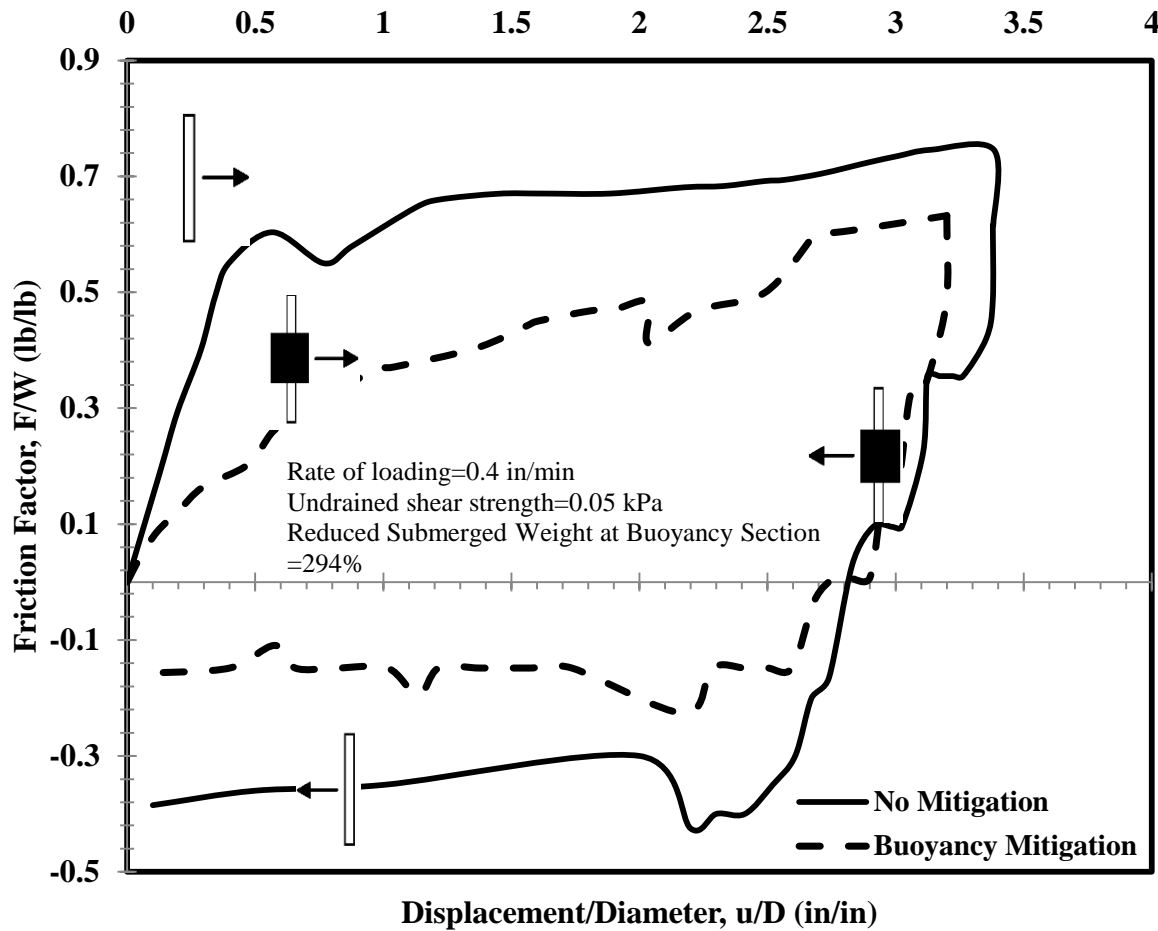


Figure 6.12: Application of buoyancy section significantly decreased lateral resistance

6.4.1.2 Full scale box

A pipe with length of 5 ft and dead load of 15 lb was equipped with single rolling buoyancy section with length of 17 inch and diameter of 6.5 in (Type: ML204 B). The reduced submerged weight for 1 ft length of this buoyancy section was 435%. The mentioned pipe was laterally tested with displacement rate of 0.3 in/min on a very soft soil with undrained shear strength of 0.05 kPa, and the results were compared with the same pipe with no mitigation (see Figure 6.13). As Figure 6.14 shows, when lateral buoyancy used, the residual resistance $\frac{F_{residual}}{W}$

dramatically declined by 73 % and the breakout resistance $\frac{F_{break-out}}{W}$ vanished. According to a series of similar tests it could be concluded that, the competence of lateral buoyancy sections is directly associated to the ensuing reduced submerged weight.

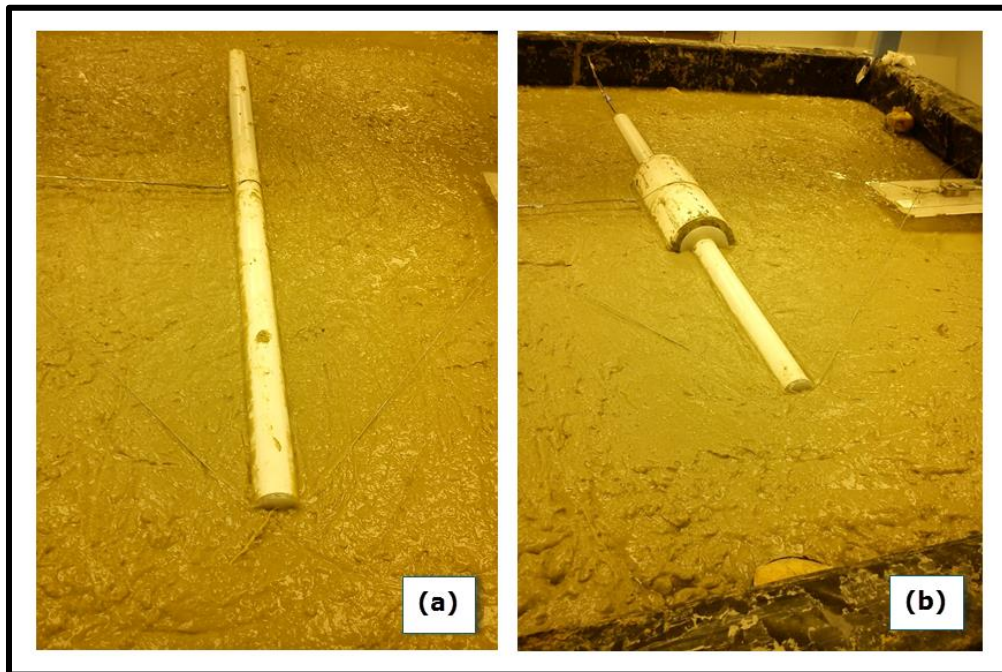


Figure 6.13: Lateral movement of plastic in full-scale soil box: (a) no mitigation, (b) single buoyancy section

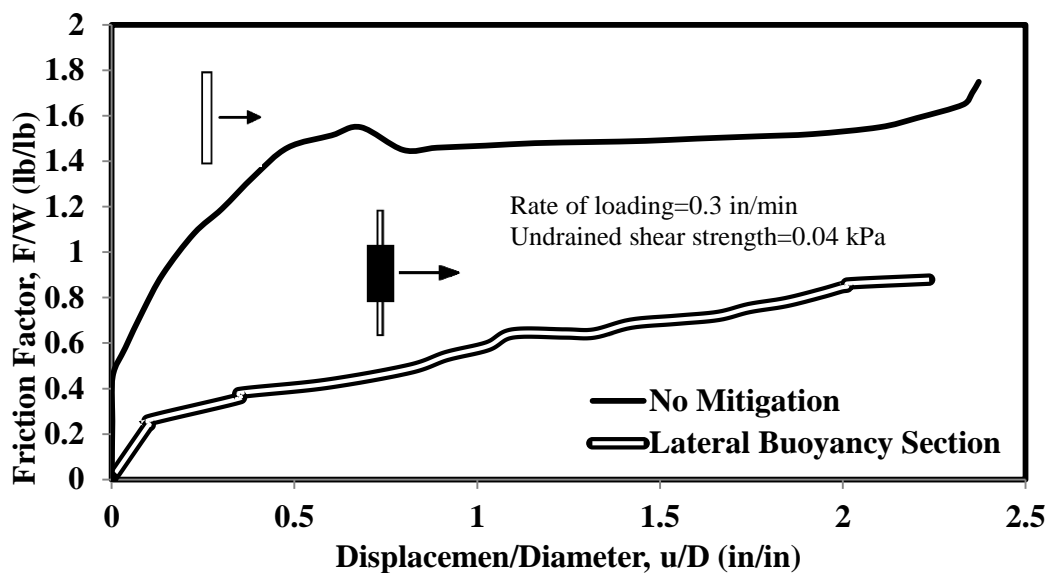


Figure 6.14: Effect of single buoyancy section in lateral pipe soil interaction

6.4.1.3 Rolling Buoyancy and Fixed Buoyancies

For any buoyancy section, two conditions could be assumed. First, the buoyancy section cannot rotate around the pipe longitudinal axis and second, the buoyancy section is allowed to rotate around the longitudinal axis of pipe. Both cases of fixed and rotating (rolling) buoyancy sections were tested in full scale soil box (Figure 6.15).

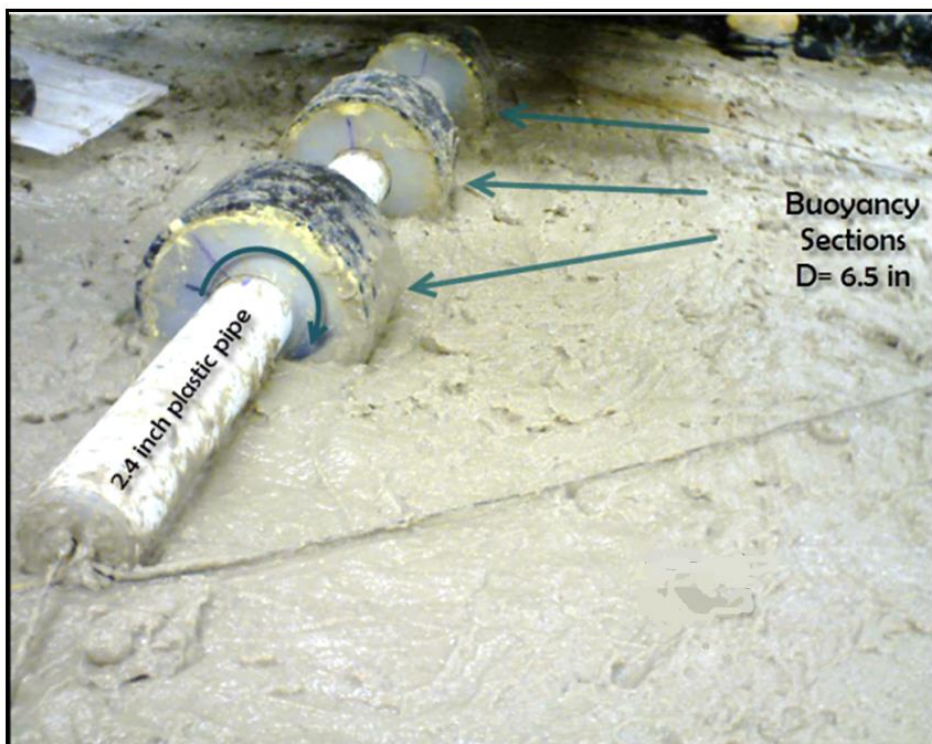


Figure 6.15: Lateral buoyancy sections were tested in full-scale soil box for cases of fixed and rolling sections

The lateral frictional resistance ($\frac{F}{W}$) between the interface of pipe and soil was very sensitive to the fixity of buoyancy sections. By fixing the rotation of separated buoyancy sections, the trend of resistance did not change (similar to rotating buoyancy sections, the resistance gradually increased at the absence of break-out resistance) yet the residual resistance $\frac{f_{residual}}{w}$ notably increased by 41 %. By comparing Figure 6.15 and Figure 6.16, it was cleared

that the effect of concentration of buoyancy sections within the pipe length is negligible. In other words, separated buoyancy sections with short spacing or one long buoyancy section with length equal to the total length of separated buoyancy sections provides same lateral force-displacement responses.

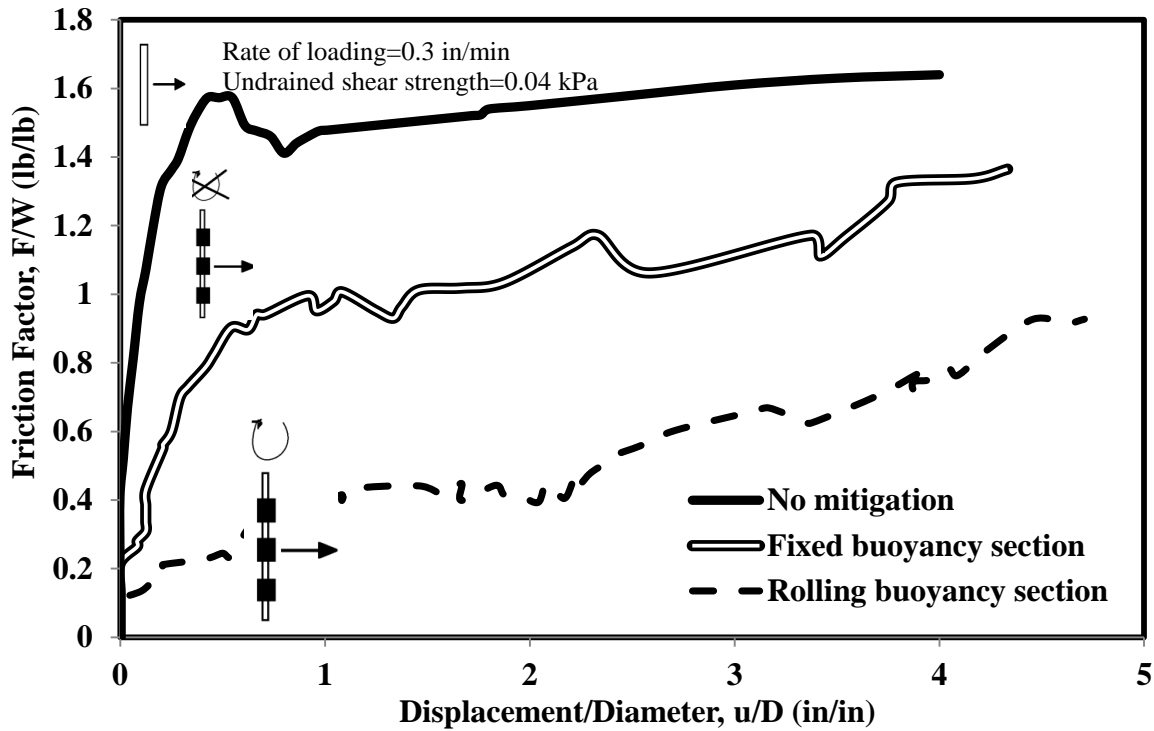


Figure 6.16: Effect of fixed and rolling buoyancy sections on the lateral pipe soil interaction

6.4.1.4 Numerical model of fixed and rolling buoyancy systems on lateral pipe movement

The main focus of this section of study was to investigate the pipe-soil interaction of fixed buoyancy and rolling buoyancy using model tests in the soft clay with undrained shear strength of 0.1 kPa to represent the seabed. A PVC pipe of 2.4 in diameter (D) equipped with three evenly spaced buoyancy sections of 6.5 in \times 5 in (outer diameter \times length). To model the soil an Eulerian domain of 8ft \times 8 ft \times 0.04 m (width \times height \times thickness) was used and the soil was modeled as an elastic perfectly plastic material. $E_u=430S_u$ and Poisson's ration was assumed

to be 0.49 with a unit weight of 1620 kg/m^3 for clay. In this study for both case of fixed and rolling buoyancy sections,

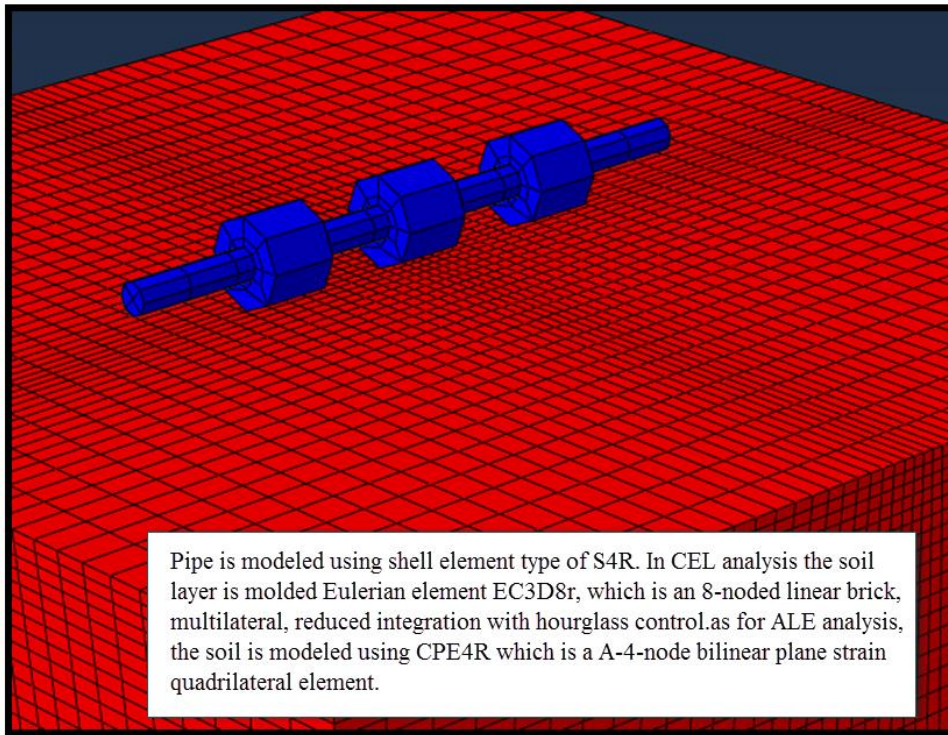


Figure 6.17: Separated buoyancy sections was modeled using finite element analysis

6.4.1.4.1 FEM Formulation and Parameter Selection

the numerical analyses was divided into four steps. The first step is the geostatic step. During the geostatic step pipe is kept outside the Eulerian part and the gravity and geostatic force applied to pipe. In the second step, the pipe is moved downward. During the third step, pipe starts to penetrate into the seabed due to only gravity load. And the analyses shifts from displacement controlled to force controlled. In the fourth step, during lateral loading, a fully displacement controlled analyses was conducted to measure force displacement response of pipe over subsea seabed. As Figure 6.18 and Figure 6.19 show, Coupled Eulerian Lagrangian (CEL) finite element approach was completely capable of modeling fixed and rolling buoyancy

sections. The FE results were close to experimental analyses with 6.9 % and 7.4% discrepancy, respectively for fixed and rolling buoyancy sections.

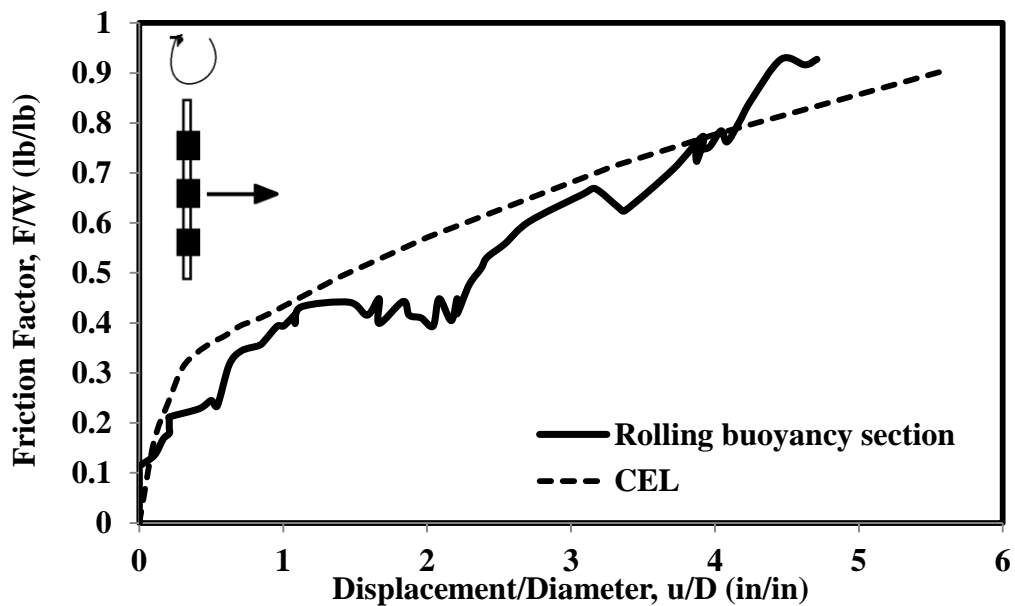


Figure 6.18: Lateral responses of a pipe employed rolling buoyancy sections

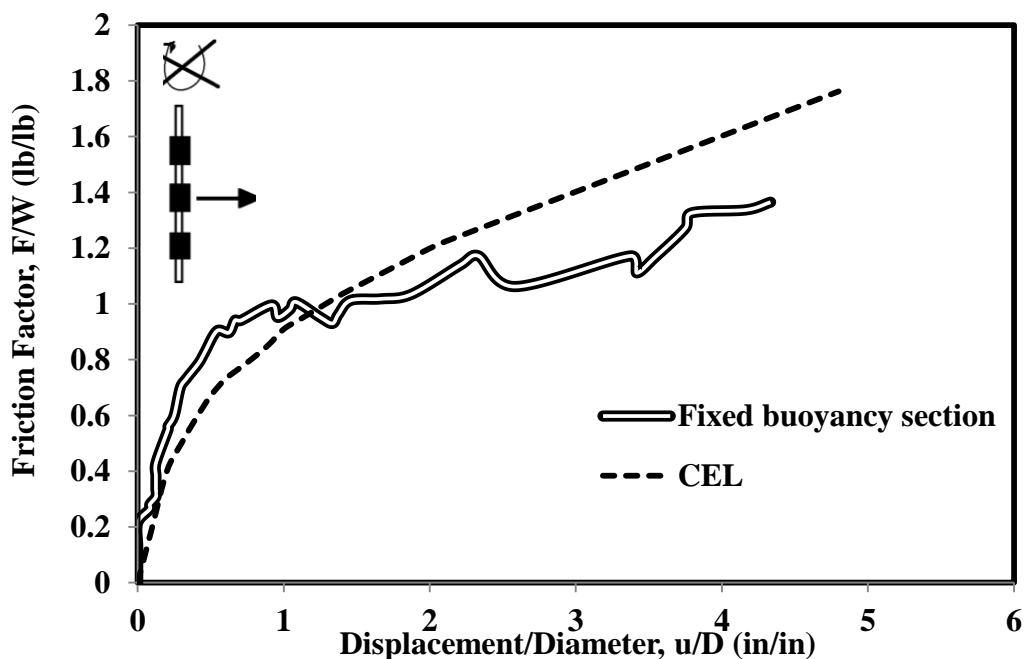


Figure 6.19: Lateral responses of a pipe employed fixed buoyancy sections

6.5 Summary

The objective of this chapter was to investigate the efficiency of different axial and lateral mitigation methods against pipeline walking and lateral buckling. Based on experiments, the following points were realized:

- (1) Application of axial resistors meaningfully increases the resistance of pipe on soft soil. Double resistors shows the most promising results However, perforated resistors did not show satisfying results.
- (2) The lateral frictional resistance ($\frac{F}{W}$) between the interface of pipe and soil was very sensitive to the fixity of buoyancy sections. By fixing the rotation of separated buoyancy sections, the residual resistance $\frac{f_{residual}}{w}$ notably increased
- (3) The effect of concentration of buoyancy sections within the pipe length is negligible. In other words, separated buoyancy sections with short spacing or one long buoyancy section with length equal to the length of separated buoyancy sections provides same lateral force-displacement responses.

Chapter 7. CONCLUSIONS AND RECOMMENDATIONS

In this study, several full-scale models have been designed and constructed to investigate the behavior of various types of pipes (steel, plastic) on the simulated clayey sea bed (undrained shear strength ranged from 0.01 kPa to 0.11 kPa). Axial and lateral pipe soil interactions have been characterized, and appropriate mitigation solutions for axial walking and lateral buckling have been proposed. On the numerical modeling front, the pipe-soil behavior is simulated using the Coupled Eulerian Lagrangian (CEL) and Arbitrary-Lagrangian-Eulerian (ALE) formulations.

In this research the following observations were realized:

- (1) Maximum axial resistances (break out resistance) were reached after relatively short movement of the pipe. For the axial tests, the average residual frictional factor was about 15 % lower than Maximum frictional factor for the same rate of displacement, same undrained shear strength and same weight of pipeline.
- (2) Axial resistance was affected by the pipe material, the pipe weight, the rate of displacement and soil strength. Using plastic pipe (wet coating) instead of steel pipe (Pipe-In-Pipe) increased the axial residual frictional factor. Increasing the rate of displacement and undrained shear strength of soft soil, decreased and increased the residual friction factor respectively. However, the axial frictional factor was not affected by the pipe weight.
- (3) Both axial break out resistance and residual resistance were noticeably affected by dictating initial penetration of pipe and changing boundary length of soil sample.
- (4) Modifying original p-q model, reliable empirical solutions were offered for predicting axial break out resistance, axial residual resistance and full range prediction of axial force displacement responses for soil with undrained shear strength in order of 0.02 kPa to 0.11 kPa.

(5) Pure Lagrangian analysis provides very accurate responses only before very small displacement, where mesh entanglement occurs. However, ALE and CEL provide acceptable results for larger displacement in both vertical penetration and axial sliding.

(6) At the start of penetration, ALE trend is more similar to experimental but CEL draws better results for the total vertical penetration.

(7) A numerical parametric study of sixty-six different cases of axial pipe soil interaction based on ALE approach were performed for both vertical penetration and then axial sliding. The breakout resistance and residual resistance calculated from ALE finite element compared to empirical equations. The results showed differentiating of only 7.2% and 4.5 % for $f_{\text{break-out}}$ and f_{residual} respectively.

(8) In free end boundary case, the vertical penetration during lateral loading and lateral force displacement responses both show a discontinuity point or a lag phase where the pipe starts to rotate. The lateral resistance was significantly increased by changing free end boundary to fixed end boundary case.

(9) Lateral resistance was affected by the pipe material, the pipe weight, the rate of displacement and soil strength. Using plastic pipe instead of steel pipe increased the lateral residual resistance. Increasing the rate of displacement and undrained shear strength of soft soil, increased the residual resistance.

(10) For the studied range of undrained shear strength, break out behavior was not common and the resistance gradually increased to steady state in absence of peak resistance.

(11) Application of axial resistors meaningfully increases the resistance of pipe on soft soil. Double resistors shows the most promising results However, perforated resistors did not show satisfying results.

(12) The lateral frictional resistance ($\frac{F}{W}$) between the interface of pipe and soil was very sensitive to the fixity of buoyancy sections. By fixing the rotation of separated buoyancy sections, the residual resistance $\frac{f_{residual}}{w}$ notably increased

(13) The effect of concentration of buoyancy sections within the pipe length is negligible. In other words, separated buoyancy sections with short spacing or one long buoyancy section with equal length provides same lateral force-displacement responses.

This study opened the door to future work on soil structure interaction. Mainly, Pipe laid on very soft soil susceptible to axial walking and lateral buckling. The developed constitutive equations can be parametrically updated for soil with higher shear strength and more rigorous numerical study and code development could be performed on lateral pipe soil interaction and mitigation methods.

REFERENCE

- Abdalla, B., Pike, K., Eltaher, A., Jukes, P. "A Coupled Eulerian Lagrangian Finite Element Model of Ice Soil Pipe Interaction" Osaka: *International offshore and Polar Engineering Conference*, 2009.
- Anderson, C.E. "Overview of The Theory of Hydro Codes" *International Journal of Impact Engineering* 1-4, no. 5 (1987): 33-59.
- Aubeny, C. P., Shi, H. and Murff, J.D. "Collapsed Load for Cylinder Embedded in Trench in Cohesive Soil" *International journal of Geomechanics* 5, no. 4 (2005): 320-325.
- Baligh, M. M., Azzouz, A.S., Wissa, A. Z. E., Martin, R. T. and Morison, M. H. "The Piezocone Penetrometer: Cone Penetration Testing and Experience" St. Louis Session: *ASCE National Convention*, 1981.
- Ballard, J.C., Barier, C., Stassen, K. and Jewell, R.A. "Observations of Pipe-Soil Response From in Situ Measurements" Houston: *Offshore Technology Conference*, OPT 24154, 2013.
- Bath, K. J. "Finite Element Procedure" Prentice Hall, New Jersey, 1996.
- Benson, D. J. "Computational Methods in Lagrangian and Eulerian Hydrocodes." *Computer Methods in Applied Mechanics and Engineering*, no. 99 (1992): 235-394.
- Borel, D., Puech, A., Dendani, H. and Ruijter, M. "High Quality Sampling for Deepwater Engineering: The STARCORE® Experience" Berest, France: *Conference of Ultra Deep Engineering and Technology (UDET)*, 2002.
- Brown, K.H., Burns, S.P., Christon, M.A. "Coupled Lagrangian Eulerian Methods for Earth Penetrating Weapon Applications" Albuquerque: Sandia National Laboratories, 2002.

Buckley, D. E., Mackinnon, W. G., Cranston, R.E. and Christan, H.A. "Problems With Piston Core Sampling: Mechanical and Geotechnical Diagnosis" *Marine Geology*, no. 117 (1994): 95-106.

Burton, D. A. S., White, D. J., Carr, M. and Cheuk, C.Y. "Pipe-Soil Interaction during Axial Lateral Buckling and Pipeline Walking- The SAFEBCUCK JIP" *Offshore Technology conference*, OTC 19589, 2008.

Campanula, R.G. and Davis. M. P. "The Seismic Piezocene: A Practical Site Investigation Too" *Geophysical characterization of sites*, Volume prepared by ISSMFE; Technical Committee no 10, 1994.

Cardoso, C.O., and Silveira, R.M.S. "Pipe Soil Interaction Behavior for Pipelines under Large Displacements on Clay Soils- A model for Lateral Residual Friction Factor" Houston: *Offshore Technology Conference*, OTC 20767, 2010.

Carr, Sinclair, F. and Burton, D. "Pipeline Walking-Understanding The Field Layout Challenges, and Analytical Solutions Developed for SAFEBCUCK JIP" Houston: *Offshore Technology Conference*, 2006.

Carter, J. P., Daies, P. J. and Kransnostein, P. "The Future of Offshore Site Investigation-Robotic Drilling on The Seabed" *Australian Geomechanics* 3, no. 43 (1999): 77-84.

Chatterjee, S. "Numerical Modelling of Pipe-Soil Interactions" *University of Western Australia*, 2012.

Cheuk, C.Y., White, D.J. and Dingle, H.R.C. "Upper Bound Plasticity Analysis of a Partially-Embedded Pipe under Combined Vertical and Horizontal Loading" *Soils and Foundations* 1, no. 48 (2008): 133-140.

Cheuk, C.Y., White, D.J. "Modeling the Dynamic Embedment of Seabed Pipelines"

Geotechnique 61, no. 1 (2011): 39-57.

Cheuk, C. Y., White, D. J., Bolton, M. D. "Large-Scale Modeling of Soil-Pipe Interaction during

Large Amplitude Cyclic Movements of Partially Embedded Pipelines" *Canadian Geotechnical Journal* 44, no. 8 (2007): 977-996.

Dendani, H. and Jaeck, C. "Flowline and Riser: Soil Interaction in Plastic Clays" Houston:

Offshore Technology Conference. OTC 19261, 2008.

Dingle, H. R., White, D. J. and Guadin, C. "Mechanisms of Pipe Embedment and Lateral

Breakout on Soft Clay" *Canadian Geotechnical Journal* 5, no. 45 (2008): 635-652.

Dutt, R. N., Rainey, W. S., Hamilton, T. K., Pelletier, J. H. and Doyle, E.H. "Recent Advances in

Deepwater Gulf of Mexico Geotechnical Investigation" Houston: *Offshore Technology*

Conference, OTC 8303, 1997.

Einav, I. and Randolph, M. F. "Combining Upper Bound and Strain Path Methods for Evaluating

Penetration Resistance" *International Journal of Numerical Methods of Engineering* 14,

no. 63 (2005): 1991-2006.

Frank, R. M. and Lazarus, R. B. "Mixed Eulerian -Lagrangian Method" *Fundamental Methods in*

Hydrodynamics, Academic Press, New York, 1964: 47-67.

Geise, J. M., Hooke, J. and May, R.J. "Design and Offshore Experience with an In Situ Vane.

Vane Shear Strength Testing in Soil: Field and Laboratory Studies." *ASTM STP* 1014,

1988: 318-388.

Ghosh, S. and Kikuchi, N. "Finite Element Formulation for the Simulation of Hot Sheet Metal

Forming Process" *International Journal of Engineering Science*, no. 26 (1988): 143-161.

- Harrison, G. E. Burner, M. S., Burton, D. A. S. "King Flowlines-Thermal Expansion Design and Implementation." Houston: *Offshore Technology Conference*, OTC 15310, 2003.
- Height, D. W., Boese, R. Butcher, A. P., Clayton, C. R. I. and Smith, P. R. "Disturbance of Bothkennar Clay Prior to Laboratory Testing." *Geotechnique* 2, no. 42 (1992): 199-217.
- High, D.W. "Sampling Effect in Soft Clay: An Update on Ladd and Lambe (1963)" *Soil Behavior and Soft Ground Construction*, no. 119 (2001): 86-121.
- Hossain, M. S. "New Mechanism-Based Design Approaches for Spudcan Foundations on Clays" *The University of Western Australia*, 2008.
- Hu, Y. and Randolph, MF "A Practical Numerical Approach for Large Deformation Problems in Soil" *International Journal of Numerical Analysis* 22, no. 5 (1998): 327-350.
- Jung, J., Personal Communication, 2001.
- Kelleher, P. and Hull, T. "Quality Assessment of Marine Sediments Recovered with a Hydraulically Tethered Piston Corer" Houston: *Offshore Technology Conference*, 2008.
- Kenny, S., Barrett, J., Philips, R. and Popescu, R. "Integrating Geohazard Demand and Structural Capacity Modeling within a Probabilistic Design Framework for Offshore Arctic Pipelines" Lisbon: *International Offshore and Polar Engineering Conference*, 2007.
- Kulkarni, S. P. and Vipulanandan, C. "Hot Wire Method to Characterize the Thermal Conductivity of Particle-Filled Polymer Grouts Used in Pipe-In-Pipe Application" *Journal of Testing and Evaluation*, 2006: 224-232.
- Long, M. "Sample Disturbance Effects on Medium Plasticity Clay/Silt" *The Institution of Civil Engineers, Geotechnical Engineering*, 2006.

Long, M., Hadj, N. E. and Hanberg, K. "Quality of Conventional Fixed Piston Samples of Norwegian Soft Clay" *Geotechnical and Geoenvironmental Engineering* 135, no. 2 (2009): 185-195.

Lune, T. and long, M. "Review of Long Seabed Samplers and Criteria for New Sampler Design" *Marine Geology* 226 (2006): 145-165.

Lunne, T. and Anderson, K. H. "Key Note Lecture: Soft Clay Shear Strength Parameters for Deepwater Geotechnical Design" London, UK: *Proceeding of 6th international Offshore Site Investigation and Geomechanics Conference*, 2007.

Lunne, T. Tajelta, T.I., Walta, a. and Barwise, A. "Design and Testing Out of Deepwater Seabed Sampler." Houston: *Offshore Technology Conference*, OTC 19290, 2008.

Lunne, T., Berre, T. and Strandvik, K. "Sample Disturbance Effects in Soft Low Plastic Norwegian Clay" Brazil: *International Conference on Recent Developments in Soil and Pavement Mechanics*, 1997.

Lunne, T., Berre, T., Strandivik, S., Andersen, K. H. and Tjelta, T. I. "Deepwater Sample Disturbance Due to Stress Relied" *International conference on Geotechnical, Geological and Geophysical Properties of Deepwater Sediments*, 2001.

Martin, C. M. and Randolph, M. F. "Upper Bound Analysis of Lateral Pile Capacity in Cohesive Soil" *Geotechnique* 56, no. 2 (2006): 141-145.

McCarran, W. O. "Deepwater Foundations and Pipeline Geomechanics" *First. J. Ross Publication*, 2011.

Mebarkia, S. "Effect Of High Pressure/High Temperature Flowlines and Soil Interaction on Subsea Development." Houston: *Offshore Technology Conference*, OTC 18107, 2006.

- Merifield, R. S., White, D. J. and Randolph, M. F. "The Ultimate Undrained Resistance of Partially Embedded Pipelines" *Geotechnique* 6, no. 58 (2008): 461-470.
- Murff, J. D., Wange, D. A. and Randolph, M. F. "Pipe Penetration in Cohesive Soil" *Geotechnique* 2, no. 39 (1989): 213-229.
- Nakshatrala, K.B., Masud, A. and Hjelmstad, K.D. "On Finite Element Formulations for Nearly Incompressible Linear Elastic" *Computational Mechanics* 41 (2008): 574-561.
- Noh, W.F. "A Time-Dependent Two-Space-Dimensional Coupled Eulerian Lagrangian Code." *Methods in Computational Physics*, no. 3 (1964): 117-179.
- Parker, W.R. and Sills, G.C. "Observation of Corer Penetration and Sample Entry During Gravity Coring" *Marine Geotechnical Researchers*, no. 12 (1990): 101-107.
- Prinet, D., and Frazer, I. A. "Mitigation Methods for Deepwater Pipeline Instability Induced by Pressure and Temperature Variations" Houston: *Offshore Technology Conference*, OTC 17815, 2006.
- Randolph, M.F. and Houlsby, G.T. "The Limiting Pressure on a Circular Pile Loaded Laterally in Cohesive Soil" *Geotechnique* 4, no. 623 (1984): 613-623.
- Randolph, M.F. "Keynote Lecture: Characterization of Soft Sediments for Offshore Applications" Porto, Portugal: *Geotechnical and Geophysical Site Characterization, Offshore Geotechnical Engineering*. First. Spon Press, 2011.
- Randolph, M. F. White, D. J. "Pipeline Embedment in Deep Water: Process and Quantitative Assessment" Houston: *Offshore Technology Conference*, OTC 19128, 2008.

Randolph, M. F., Low, H. E. and Zhou, H. "Key Note Lecture: In Situ Testing for Design of Pipeline and Anchoring Systems" London, UK: *6th International Conference On Offshore Site Investigation And Geomechanics Conference*, 2007.

Randolph, M. F. and White, D. J. "Upper-Bound Yield Envelopes for Pipelines at Shallow Embedment in Clay" *Geotechnique* 4, no. 58 (2008): 297-301.

Randolph, M. F. and White, D. J. "Upper-Bound Yield Envelopes for Pipelines at Shallow Embedment in Clay" *Geotechnique* 4, no. 58 (2008): 297-301.

"Recommended Practice DNV-RP-F110, Global Buckling of Submarine Pipeline" *Det Norske Veritas*, 2007.

"Recommended Practice DNV-RP-F105, Free Spanning Pipelines." *Det Norske Veritas*, 2006.

"Recommended Practice DNV-RP-F109, On-Bottom Stability Design of Submarine Pipeline" *Det Norske Veritas*, 2010.

Roy, M., Tremblay, M. M., Tanvena, F. and LaRochelle, P. "Induced Pore Pressures in Static Penetration Tests in Sensitive Clay" Calgary: *Canadian Geotechnical Conference*, 1980.

Sarraf, M. J., Vipulanandan, C. "Axial And Lateral Sliding Of Pipe On Simulated Seabed Soft Soil" Houston: *Center for Innovative Grouting Material and Technologies (CIGMAT)*, 2013.

Sarraf, M. J., Vipulanandan, C. "Numerical Simulation of Subsea Pipeline Response during Installation and Earthquake" Houston: *Texas Hurricane Center for Innovative technology*, 2013.

Silling, S. A. "Simulation of Penetration and Perforation with CTH: Advances in Numerical Simulation Techniques for Penetration of Solids" *AMD, American Society of Mechanical Engineering, Applied Mechanics Division*, 1993: 57-66.

silva, A. J. and Hollister, C. D. "Geotechnical Properties Of Ocean Sediments Recovered With A Giant Piston Corer: Gulf of Marine." *Journal of Geophysics Researchers* 2, no. 122 (1973): 99-108.

Silva, A.J., Baxter, C., Bryant, W.R., Bradshaw, A. and LaRosa, P. "stress-Strain Behavior and Stress State of Gulf Of Mexico Clays in Relation to Slope Processes." Houston: *Offshore Technology Conference*, OTC 12091, 2000.

Solano, R., Azevedo, F., Carr, M., Tindall, L., Dolinski, A. and Valer, C. "Thermo-Mechanical Design of CANAPU PIP System" *Offshore Mechanics and Arctic Engineering Conference*, OMAE 2009-79713, 2009.

Steward, D. P. and Randolph, M. F. "T-Bar Penetration Testing in Soft Clay" *Geotechnical Engineering*, ASCE 2, no. 120 (1994): 2230-2235.

Sun, J., Jukes, P., and Shi, H. "Thermal Expansion /Global Buckling Mitigation of HPHT Deepwater Pipelines, Sleeper or Buoyancy" Rhodes: *International Offshore and Polar Engineering Conference*, 2012.

Sun, T.K. "Numerical Modeling of Skin Friction and Penetration Problems in Geotechnical Engineering" PhD thesis, *University of Hong Kong*, 2013.

Van den Berg, P., Teunissen, J. A. M. and Huetink, J. "Cone Penetration in Layered Media, an ALE Element Formulation" *International Conference of Computer Methods and Advances in Geomechanics*, 1991.

Vipulanandan, C. Yahouide, J. A., Sarraf, M. J. "Deepwater Axial And Lateral Sliding Pipe Soil Interaction" Forth Worth, Texas: ASCE, *Pipeline section*, 2013.

Wang, D., White, D.J., and Randolph, M. F. "Large Deformation Finite Element Analysis of Pipe Penetration and Large-Amplitude Lateral Displacement" Canadian Geotechnical Journal 8, no. 47 (2010): 842-856.

Weaver, P. P. E. and Schultheiss, P. J. "Current Methods for Obtaining, Logging and Splitting Marine Sediment Cores" *Marine Geotechnical Researchers*, no. 12 (1990): 85-100.

Westgate, Z. W., White, D. J., Randolph, M.F. and Brunning, P. "Pipeline Laying and Embedment in Soft Fine-Grained Soils: Field Observations and Numerical Simulations" Houston: *Offshore Technology Conference*, OTC 20407, 2010.

Wingate, C.A., Stellingwerf, R.F., "Smooth Partial Hydrodynamics: The SPHINX and SPHC Codes. Advances in Numerical Simulation Techniques for Penetration and Perforation of Solids" AMD, *American Society of Mechanical Engineers*, Applied Mechanics Division 171 (1993): 75-94.

Wong, P. C., Taylor, B. B., Jean, M. E. "Differences in Shear Strength Between Jumbo Piston Core and Conventional Rotary Core Samples" Houston: *Offshore Technology Conference*, OTC 19683, 2008.

Young, A.G., McClelland, B. and Quiroz, G.W. "In Situ Vane Shear Strength Testing of Soils: Field and Laboratory Studies" ASTM STP 1014 (A), 1988: 46-67.

Young, A.G., Honegan, C.D., Silva, A.J, and Bryant, W. R. "Compression of Geotechnical Properties from Large Diameter Long Cores and Borings In Deep Water Gulf of Mexico" Houston: *Offshore Technology Conference*, OTC 12089, 2000.

APPENDIX I

Part of FORTRAN subroutines used for axial soil pipe interaction modeling in ABAQUS is presented in the following.

```
C
      subroutine dload(f,kstep,kinc,time,noel,npt,layer,kspt,
$      coords,jltyp,sname)
C
      include 'aba_param.inc'
C
      dimension time(2),coords(3)
      character*45 sname
      if (coords(3).ge.-3345.d0) then
         f = 3809.d0 - (23.1d0*coords(3))
      else if (coords(3).ge.-3317) then
         f = 22770 - (21.3d0*coords(3))
      else
         f = 3310.d0 - (21.3d0*coords(3))
      end if
C
      return
      end
C
      subroutine disp(u,kstep,kinc,time,node,noel,jdof,coords)
C
      include 'aba_param.inc'
C
      dimension u(3),time(2),coords(3)
```

```

C
    u(1) = -17.2d0*coords(3)

C
    return
end

C
C
subroutine uporep(uw0,coords,node)
C
include 'aba_param.inc'
C
dimension coords(3)
C
uw0 = -17.23d0 * coords(3)

C
return
end

C
C
subroutine voidri(ezero,coords,noel)
C
include 'aba_param.inc'
C
dimension coords(3)
C
if(      coords(3) .ge. -3105) then
    ezero = 0.2
else if(coords(3) .ge. -3110) then
    ezero = 0.3

```

```

else if(coords(3) .ge. -3112) then
    ezero = 0.31
else if(coords(3) .ge. -3114) then
    ezero = 0.32
else if(coords(3) .ge. -3116) then
    ezero = 0.34
else if(coords(3) .ge. -3118) then
    ezero = 0.37
else if(coords(3) .ge. -3120) then
    ezero = 0.39
else if(coords(3) .ge. -3122) then
    ezero = 0.401
else if(coords(3) .ge. -3124) then
    ezero = 0.403
else if(coords(3) .ge. -3126) then
    ezero = 0.41
else if(coords(3) .ge. -3128) then
    ezero = 0.43
else if(coords(3) .ge. -3130) then
    ezero = 0.435
else
    ezero = 0.167
end if

C
return
end

C
subroutine ufluidleakoff (perm,pgrad,dn,p_int,p_bot,p_top,

```

```

$      anm,tang,time,dtime,temp,dtemp,predef,dpred,c_bot,c_top,
$      dc_bot,dc_top,svar,mstvax,noel,npt,kstep,kinc)

C

C

include 'aba_param.inc'

C

if (kstep.ne.4) then

c_bot = 6.3423E-10

c_top = 6.8757E-10

else

c_bot = 2.1.E-3

c_top = 2.1.E-3

end if

C

return

end

C

subroutine sigini(sigma,coords,ntens,ncrds,noel,npt,layer,
$      kspt,lrebar,rebarn)

C

include 'aba_param.inc'

C

dimension sigma(ntens),coords(ncrds)

character*45 rebarn

C

buoy = -23.5d0*coords(3)

if(noe7.le.5120) then

ratio = 0.99d0

```

```

if (coords(3).ge.-2110.d0) then
    sigma(1) = -(33.d0 + (16.25d0*coords(3)) - buoy)
    sigma(2) = sigma(1) * ratio
else if (coords(3).ge.-3492) then
    sigma(1) = -(34920.d0 + (16.25d0*coords(3)) - buoy)
    sigma(2) = sigma(1) * ratio
else
    sigma(1) = -(3524.d0 + (16.25d0*coords(3)) - buoy)
    sigma(2) = sigma(1) * ratio
end if
sigma(3) = coords(3) * 44.0d0 + porep
else
    sigma(1) = coords(3) * 44.0d0 + porep
end if
C
return
end

```

